DAMPING IN CARBON NANOTUBE NANOCOMPOSITES BY INTERFACIAL SLIPPAGE AND THERMALLY AUGMENTED POLYMER RELAXATION

A Dissertation

by

FRANK GARDEA

Submitted to the Office of Graduate and Professional Studies of
Texas A&M University
in partial fulfillment of the requirements for the degree of

DOCTOR OF PHILOSOPHY

Chair of Committee,	Mohammad Naraghi
Co-Chair of Commitee,	Dimitris C. Lagoudas
Committee Members,	John Whitcomb
	Philip Park
Head of Department,	Rodney Bowersox

August 2015

Major Subject: Aerospace Engineering

ABSTRACT

The present work investigates the damping potential of carbon nanotube (CNT) reinforced polymer matrix composites through integrated experiments and continuum modeling techniques. Both “passive" and “active” damping are studied. The passive damping here refers to the inherent capability of a composite to damp vibrations in the absence of external stimuli, such as electrical signals, by exploiting different damping mechanisms introduced by the presence of the nanoscale reinforcements. Among the targeted passive damping mechanisms in nanocomposites is a ‘slip-stick’ mechanism in which the interactions between the filler and polymer results in energy dissipation in a frictional mode along the interface. Microstructural design of nanocomposites, such as the development of CNT alignment, was pursued here to enhance the contribution of interfacial sliding to damping, relative to other mechanisms such as stress concentrations within the matrix and matrix plasticity. A micromechanics model was used to provide additional insight into the experimental observations by showing that the nonlinear variation of damping with dynamic strain can be attributed to slip-stick behavior. The dependence of the interfacial load-transfer reversibility on the dynamic strain history and characteristic time scale was experimentally investigated to demonstrate the relative significance of van der Waals (vdW) interactions, mechanical interlocking, and covalent bonding on shear interactions.

In this effort, we also studied the controllability of energy dissipation capability in nanocomposites via electrical signals, referred to as active damping. This mechanism

benefits from the electrically conductive network of CNTs, as well as their high surface to volume ratio, to thermally enhance viscous phenomena, such as chain relaxation in polymers. For active damping, the thermomechanical response of the polymer is targeted and studied as a potential damping source within the nanocomposite. By taking advantage of the polymer relaxation resulting from an increase in temperature, the composite shows the potential for damping enhancement. However, the non-uniform temperature distribution in the composite sample has a large effect on the overall damping enhancement. The non-uniformity of the temperature distribution, both locally and globally, was studied via experiments and multi-resolution models to further shed light on this phenomenon.

This effort clearly points to the significance of interface phenomena, both friction between filler and matrix and energy transfer from the fillers to the matrix, in controlling the damping mechanisms in nanocomposites and presents insights, both qualitative and quantitative, into the origins of these effects.

DEDICATION

To my loved ones

ACKNOWLEDGEMENTS

I would like to thank my committee chairs and advisors, Dr. Dimitris C. Lagoudas and Dr. Mohammad Naraghi for all of their guidance and support throughout the course of this research. Not only did they provide me with the knowledge and guidance I needed to be successful during my graduate studies but they also motivated me to always strive to become superior. For that, I am personally grateful. I would also like to thank my committee members, Dr. John Whitcomb and Dr. Philip Park for all of their input and time. I would like to extend my gratitude to Dr. Micah Green for being involved as a substitute at my defense and providing all the great feedback, not only in this work but also in my future plans.

I would like to thank the United States Army Research Laboratory (USARL) for providing me the opportunity to work on this research and I acknowledge their support under the award No. W911NF-14-2-0080. Specifically, I would like to thank Dr. Jaret Riddick and Dr. Bryan Glaz at USARL for their great input and guidance throughout this research.

The use of the TAMU Materials Characterization Facility is also acknowledged. I personally would like to extend my gratitude to Dr. Amanda Young for her continued support and technical help during my graduate studies.

I had the privilege of working with some great scientists and researchers throughout my studies, some of which I consider my dear friends. I would like to express my gratitude to Antonino Parrinello, Majid Tabesh, Brian Lester, and Seokjin Hong. Not

only could I go to them for technical help but I could rely on them on a personal level. In my eyes, having to go through the same trials and tribulations gave more meaning to our friendship. I cherish their invaluable friendship greatly.

One of the greatest motivations continues to come from my siblings. My personal growth stems from giving them the motivation and guidance to improve not only intellectually but also on a spiritual and emotional level. I thank them for all of their encouragement and support. In addition, I hope someday my nieces and nephews see me as an inspiration to pursue a great career and become successful in life.

I owe everything to my mother and father. They have always pushed me to excel at everything I set my mind to, with failure never being an acceptable option. They kept me humble and focused by always reminding me to not compare myself to others, for there will always be greater and lesser persons than myself. As this chapter in my life comes to an end, I can now understand and appreciate the road they paved for me as a child. My sole purpose is to make them proud and I hope I have accomplished that with this achievement.

Lastly, to all those left unmentioned that have influenced my life, either in a positive or negative way, I am forever indebted. Even though I always welcomed the positive motivation to feel a sense of comfort, the negative has had a larger impact on my life. This negative influence has not been a deterrence in my life, but a growth mechanism, since I strive to become superior from the discouragement of others.

TABLE OF CONTENTS

Page

LIST OF FIGURES

Page

LIST OF TABLES

Page

CHAPTER I

INTRODUCTION AND LITERATURE REVIEW

Nanoparticle reinforced polymer composites have the potential for widespread use in many fields, such as aerospace, biomedical, and military [1]. The introduction of nanoparticles to polymer matrices is often to enhance properties such as strength and toughness and to develop multifunctional materials. One of the main factors for increased interest in nanocomposites is the remarkable and often unique properties of the nanoparticles, such as the high strength and modulus of carbon nanotubes. Moreover, due to their large surface to volume ratio, the addition of nanoparticles to polymers may introduce unique interfacial characteristics between the filler and matrix, significantly influencing the properties of the composite [2]. The nanofillers allow for the development of high-performance multifunctional composites that can address many issues that are still of significant research interest. One of the topics of interest is the mechanical energy dissipation in structural components during oscillatory loads, which is the main focus of this research.

I.A. Background and Literature Review

Structural integrity and safe operation of many structures, such as rotary-wings [1]

Part of this chapter is reprinted with permission from "Effect of thermal interface on heat flow in carbon nanofiber composites." by Gardea F., Naraghi M., Lagoudas D. ACS Appl Mater Interfaces. 2013;6(2):1061–72 and “Energy Dissipation due to Interfacial Slip in Nanocomposites Reinforced with Aligned Carbon Nanotubes." by Gardea, F., Glaz B., Riddick J, Lagoudas D, Naraghi M. ACS Appl Mater Interfaces. 2015;7(18):9725–35.

and radar antennas [3], relies on their ability to damp vibrations and dynamic instabilities. Undesired vibrations may severely compromise structural performance by inducing fatigue damages and/or high strains. In addition, in cases such as rotorcraft, rotary-wing damping and stability can potentially enable advanced concepts that are currently infeasible, with potential benefits including damperless and bearingless rotors, soft-in-plane tiltrotors, and reduced operating and maintenance costs [1, 4]. Traditional approaches to suppress vibration in structures often includes the incorporation of auxiliary dampers (i.e. polymer-tapes [5]) which leads to increased weight and footprint of the component. A potential alternative to auxiliary dampers is to take advantage of the inherent damping capability in structural materials, such as polymer composites, which is the focus of this study. Significant attention and research interest has focused on the use of polymers due to their low density and high processability [6-8]. One downfall however, is the limited inherent damping capability of polymers. In addition, typically, a tradeoff between loss modulus and stiffness is inevitable [9]. While polymers show the largest damping capability near the glass transition temperature, the polymer stiffness (e.g., storage modulus) is often significantly reduced [10]. With the addition of nanoscale fillers, the damping capability of the nanocomposite can be *passively* and *actively* augmented. The passive damping here refers to the inherent capability of the composite to damp vibrations in the absence of external stimuli, such as electrical signals, by exploiting damping mechanisms in the nanocomposite. Moreover, augmenting energy dissipation capability in nanocomposites via electrical signals is referred to herein as active damping.

I.A.1. Passive Damping in Nanocomposites

One approach to improve the energy dissipation in polymers, without compromising effective stiffness and strength, is embedding nanoparticles into polymers. The large surface to volume ratio and high aspect ratio of carbon nanotubes (CNTs) and carbon nanofibers (CNFs), rooted in their sub-micron diameter relative to many other types of reinforcements (Figure 1), such as carbon fibers, offers a great opportunity to dissipate energy and damp vibrations in composites via interfacial sliding. In addition, due to their remarkable intrinsic properties, such as high strength and modulus, these graphitic nanoparticles can effectively enhance the strength and stiffness of the composite materials [11-13].

Even though nanoscale reinforcements have the potential to increase the effective composite properties, this ability is highly dependent on the mechanics of the reinforcement-polymer interface. In general, enhancing the strength and stiffness of a polymer by adding nanoscale fillers, e.g., CNTs, requires efficient load transfer between the filler and matrix, with limited or no sliding. On the other hand, relative sliding of the filler and matrix along their interface can lead to strain energy dissipation due to frictional sliding. This mode of energy dissipation is augmented by the large surface to volume ratio of the nanoscale reinforcements, as shown in Figure 1. A large interfacial contact area - and thus substantial interfacial strain energy dissipation - can be introduced when embedding nanoscale fillers into the matrix, with minimal increase in weight. This mechanism, sliding between filler and matrix, would be in addition to any existing inherent structural damping capability of the matrix.

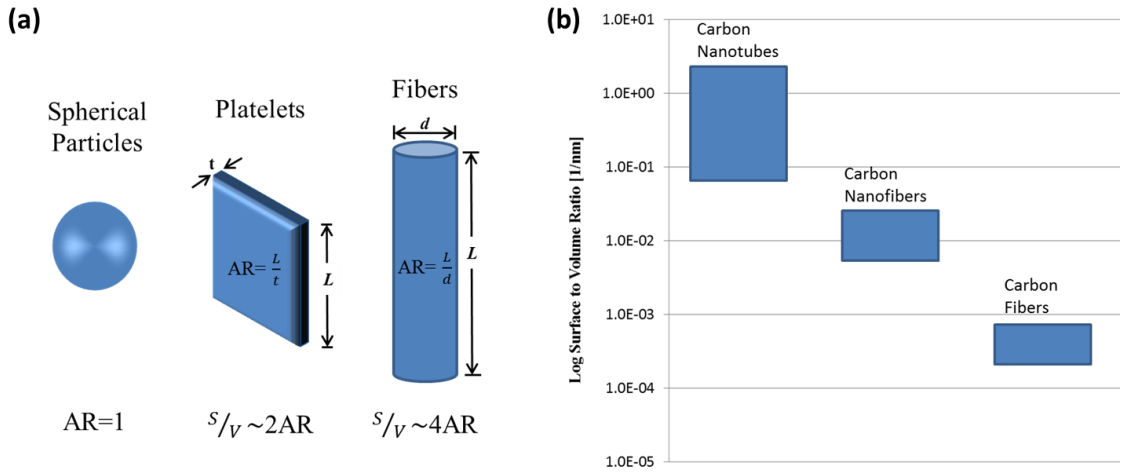

Figure 1. (a) Schematic showing a comparison of aspect ratio (AR) and surface-to-volume ratio (S/V) between different nanoparticles. (b) surface-to-volume ratio for carbon nanotube CNT (diameter=1-50nm), carbon nanofiber CNF (diameter=100-500 nm) and carbon fiber CF (diameter=5-10μm).

Of the nanoparticles available, large aspect ratio particles, such as CNTs and CNFs, show the most potential, not only due to their high aspect ratio, but also due to their unique intrinsic properties such as high strength and modulus [11, 12], along with electrical and thermal conductivity [14-18]. Due to these properties, these nanoparticles become a favorable candidate for developing a multifunctional composite material with enhanced capabilities. As the particle size approaches smaller length scales, the interface between particle and matrix becomes of significant interest, as mentioned before, the reason being the increase in surface-to-volume ratio [2, 19]. Taking advantage of this large surface area, one promising application is the use of these nanoscale particles as energy dissipaters. A large interfacial contact area is introduced if these nanoparticles are internally embedded into the structure, with minimal increase in weight. Such an approach would lead to significant introduction of interfaces (contact between the

nanoparticle and matrix) which would act as sites for energy dissipation. This internal mechanism would be in addition to any existing inherent structural damping capability of the composite.

The above approach to enhance damping in nanocomposites is referred to herein as "passive damping" which includes the study of inherent capability of composite to damp vibrations in the absence of external stimuli, such as electrical signals, by exploiting damping mechanisms introduced to the polymer by the presence of the nanoscale reinforcements. This approach is attractive to many applications due not only to the minimal increase in weight and lack of external components, but also the additional improvement in mechanical properties, such as elastic modulus and yield strength, electrical and thermal conductivity.

Energy dissipation within the composite structure, or passive damping, via high aspect ratio fillers focuses on one major mechanism known as stick-slip. A stick-slip mechanism results from the interfacial interaction between the filler and matrix. As a dynamic tensile stress is applied to the composite both the nanoparticle and matrix move in phase (at low frequencies). Load transfer from the matrix to the nanoparticle is through shear stress at the interface. If the shear stress at the interface is below some critical value, the nanoparticle and matrix remain bonded (stick). As the shear stress increases to a critical value (critical shear stress), there is debonding of the particle and matrix (slip) [20, 21]. During this slip process, energy is dissipated through heat caused by the frictional sliding at the interface. The effect of slippage on damping has been modeled by Glaz et al. by a micromechanics approach. They show that if only frictional

factors at the interface are considered, the tan δ increases with dynamic strain [1]. Tan δ, or the ratio of loss modulus to storage modulus, is one of the metrics used for damping in materials. However, this model ignores the presence of any stress concentration at the fiber ends [1]. A local increase in stress at the surrounding matrix might contribute to damping via viscoelastic effects and thus should be considered.

Recent studies have alluded to the potential of nanoscale fillers to augment damping in materials. For example, Suhr and Karatkar studied the CNT slip mechanism in a randomly oriented CNT/polycarbonate system. They observed a significant increase (4 to 5 times) in loss modulus with the addition of 1.5wt% single-wall CNTs [21]. *However, random alignment of CNTs introduces complicated stress fields within the matrix, leading to energy dissipation mechanisms, such as matrix tearing, in addition to CNT sliding. Therefore, quantitatively, it is not clear how much of the improvement in loss modulus is due to interfacial sliding in the nanocomposite.*

Ogasawara *et al.* showed a hysteretic behavior in multi-walled CNT/PEEK composites under both tensile and compressive loading, while the neat PEEK polymer shows no hysteretic effect at strains below 1.5%. They attribute this behavior to slippage of the CNT-PEEK interface resulting from weak interaction [22]. Studies by Gong *et al.* pointed to an initial increase in loss modulus of polycarbonate/MWCNTs composites with increasing strain [10]. At sufficiently large strains, once a maximum value in loss modulus was reached, the loss modulus decreased with strain. They attributed the

decrease in loss modulus with increasing strain to a decrease in free volume and fractional free volume, resulting from the order arrangement in the chain segments.

Analytical models have also been developed to explain damping in composite materials. Cox developed a shear lag model in which a single fiber surrounded by matrix in the form of concentric cylinders are considered [23]. This model considers perfect bonding between the fiber and matrix. According to this model, the enhanced damping of a discontinuous fiber reinforced matrix, compared to the neat matrix, is mainly due to a viscoelastic energy dissipation mechanism associated with stress concentration at the fiber ends, induced by elastic mismatch between the filler and matrix. Ang *et al.* extended the shear lag model to CNTs with a non-bonded interface [24]. This model points to the importance of interfacial factors such as mechanical interlocking, van der Waals interactions, thermal residual stress, and Poisson's contraction on the stress transfer and energy dissipation at the CNT/polymer interface. Esteva *et al.* concluded through micromechanics modeling that interface weakening significantly influences nanocomposite properties only for high SWCNT volume fractions (>0.6%) [25]. Glaz *et al.*, developed a micromechanics model to study the effect of interfacial slippage on damping and energy dissipation in nanocomposites [1]. According to their model, frictional forces at the interface increase the loss modulus with dynamic strain. If the shear stress at the interface is below a critical value, the nanoparticle and matrix remain bonded. As the shear stress increases to a critical value (critical shear stress), the particle will debond from the matrix (slip) [20, 21]. During the slip process, energy is dissipated through heat caused by the frictional sliding at the interface.

I.A.2. Active Damping in Nanocomposites

In addition to enhancing the damping capability of nanocomposites by adding energy dissipation mechanisms to the matrix, addition of electrically conductive nanoparticles, such as CNTs, allows for *actively* enhancing the damping capability of nanocomposites via electric signals by utilization the conductive network of CNTs within the nanocomposite. This method damping augmentation is referred to herein as *active damping*. The basic premise of active damping in nanocomposites is to take advantage of the electrically conductive path formed by the fillers. Joule heating of these fillers can result in local heating of the matrix, to near the glass transition temperature where polymer damping is most effective, thus allowing for the viscoelastic properties of the matrix to additionally contribute to damping.

Active damping consists of modulating the damping properties of a structure via external stimuli, mainly but not limited to, electrical signals. Since the viscoelastic properties of the matrix, which are highly temperature-sensitive especially near glass transition temperature, can also add to the energy dissipation of a structure and thus enhance damping, one approach to take advantage of the viscoelastic effects is by temperature control of the polymer via an external stimulus. Some polymers show a significant increase in tan δ with temperature, such as polystyrene (PS), with more than 2 orders of magnitude increase in tan δ at the glass transition temperature. According to [1], rotor blades, specifically soft-in-plane blades, suffer from air and ground resonance aeromechanical instabilities. Inherent blade damping is in the order of 0.5% while an order of magnitude additional increase in damping is required to obtain stability.

Polymers are capable of increasing damping by orders of magnitude, however, this is achieved at a decrease in stiffness. For example, an order of magnitude increase in polystyrene comes at a decrease in storage modulus of 42%. While the decrease of modulus may adversely affect the structural performance in some applications, it has been shown that a reduction in stiffness of structural components in civil structures has led to a decrease in absolute accelerations and related forces [26]. In addition, vibration suppression has been pursued by using variable-stiffness members [27]. Therefore, the decrease in storage modulus can have a positive effect on the composite performance. Active heating of the polymer to exploit the thermomechanical coupling inherent to polymers has been shown to have potential in damping applications. Smith et al. developed a tuned-mass damper that could be continuously varied, and thus self-tuned, by taking advantage of the temperature-sensitive viscoelastic properties of the polymer [28]. The polymer relaxation mechanism has also been shown to be effective in improving the impact response of carbon fiber polymer matrix composites [29]. Similar techniques have also been used to actively control the damping capabilities of carbon microfiber reinforced composites leading to reduced deflection and stresses in the composite [30]. Even though these results show that this mechanism is effective in improving the damping capabilities of microfiber composites, a more effective activation of this mechanism is expected with the addition of nanoscale reinforcements. This is because the high surface to volume ratio of the fillers will facilitate the transfer of heat from the particle to the matrix.

In order to exploit the polymer behavior to temperature, applying an external stimulus to the nanocomposite should result in an enhancement in damping. While there is no report in open literature on the utilization of nanoscale reinforcements as potential heat sources to trigger matrix damping, one important interfacial property that must be considered is interfacial thermal resistance.

Heat conduction in carbon materials is dominated by phonons resulting from strong sp^2 covalent bonds [31], making carbon materials very efficient in the transfer of heat. Weak coupling of phonons, due to the difference in phonon vibration frequencies between the two phases of a nanocomposite (e.g. CNT and the polymer matrix), suppresses the transmission of vibrational modes and heat energy at the interface [32]. This interfacial resistance acts as a boundary layer resistance to heat flow, leading to a discontinuity of temperature at the interface for any finite heat flux across the interface [33]. This issue was addressed via Molecular Dynamics simulations by Shenogin et al., who demonstrated that the heat flow between a CNT and an octane liquid is limited by low frequency phonon vibration modes due to weak coupling at the interface [34]. The thermal transport process in carbon nanofiber (CNF)/epoxy composites was addressed through combined micromechanics and finite element modeling in our work [35]. It was found that very high interface resistance leads to heat entrapment near the interface close to the heat source, as shown in Figure 2, which can promote interface thermal degradation.

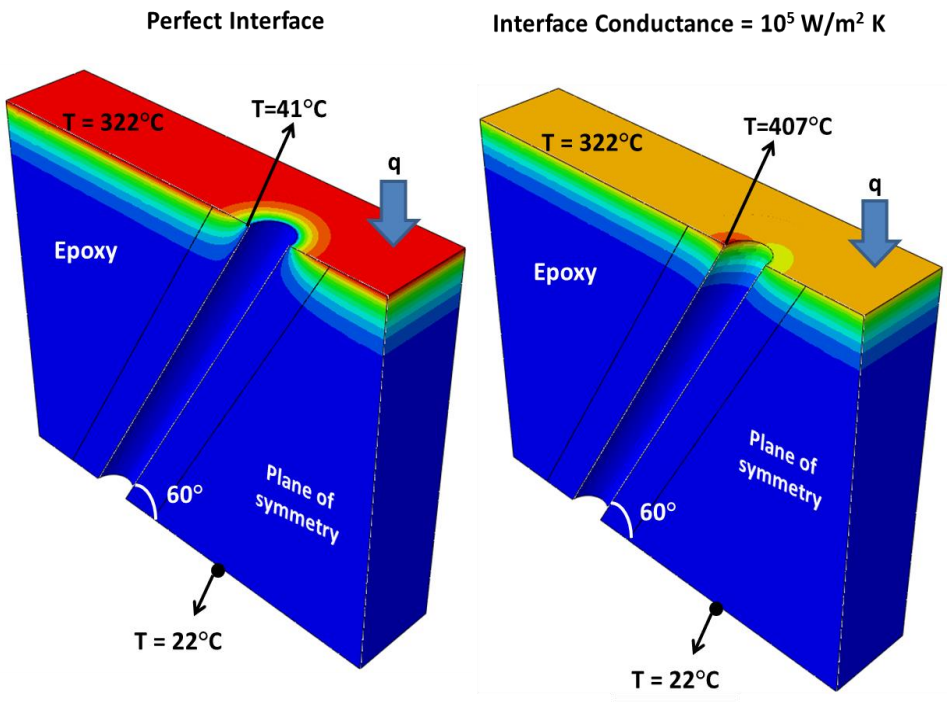

Figure 2. Carbon nanofiber/epoxy composite showing heat entrapment near the CNF-matrix interface with low interface conductance as compared to the perfect interface case.

The magnitude of heat entrapment, quantified via the peak transient temperature at the interface, in the case of high thermal resistance interfaces becomes an order of magnitude more intense compared to the case of low thermal resistance interfaces. Moreover, high interface thermal resistance in the case of discontinuous fibers leads to a nearly complete thermal isolation of the fibers from the matrix, which will marginalize the contribution of the CNF thermal conductivity to the heat transfer in the composite.

I.B. Objectives and Outline of Present Work

The present work aims at gaining an understanding of the damping mechanisms, both passive and active, present in CNT/polymer composites. This work centers around obtaining knowledge on the mechanisms present and on the root causes responsible for enhanced damping in CNT nanocomposites and not on the fatigue life of the damping mechanisms or the composites themselves. The objectives will focus on investigating the effect of interfacial factors on passive damping in addition to studying the modulation of damping capabilities of the matrix via local heating. The focus of this work is experimental characterization of the damping behavior and damping augmentation. However, continuum modeling methods are used to support the obtained results and to further shed light on the damping behavior of these composites. Specific objectives of this study are presented below:

1. Develop new insights into the role of interactions between CNTs and a polymer matrix in enhancing the energy dissipation of nanocomposites, with a focus on CNT arrangement and present damping mechanisms.
2. Test hypothesis that damping of a polymer based nanocomposite can be actively, controllably and reversibly augmented via electrical signals.

Chapter II presents the study on the contribution of interfacial slippage to composite damping in highly aligned CNT composites. High degree of alignment achieved via innovations in nanocomposite processing was induced to suppress the contribution of

damping mechanisms other than interfacial slip for a systematic study. Chapter III further investigates the effect of orientation on damping and the energy dissipation mechanisms in nanocomposites with randomly oriented CNTs. In addition, the effect of CNT distribution is addressed. The next chapter, Chapter IV, presents a study on the energy dissipation in nanocomposites by thermal activation. The focus of this chapter is on semi-crystalline polymers to minimize the loss in storage modulus. Chapter V and Chapter VI follow with the experimental characterization and modeling of the polymer relaxation mechanism in semi-crystalline polymer composites, respectively. In addition, Chapter VI presents continuum models, including micromechanics modeling on the effect of interfacial thermal resistance on the effective thermal conductivity of the composite. Finally, Chapter VII summarizes the conclusions of this study, and recommends future directions of this work on damping in nanoparticle reinforced composites.

CHAPTER II

VIBRATIONAL DAMPING DUE TO INTERFACIAL SLIDING IN CARBON NANOTUBE COMPOSITES

Even though nanoscale reinforcements have the potential to improve effective composite properties, this ability is highly dependent on the mechanics of the reinforcement-polymer interface. In general, enhancing the strength and stiffness of a polymer by adding nanoscale fillers, e.g., CNTs, requires efficient load transfer between the filler and matrix, with limited or no sliding. On the other hand, relative sliding of the filler and matrix along their interface can lead to mechanical energy dissipation due to frictional sliding. This mode of energy dissipation is augmented by the large surface-to-volume ratio of the nanoscale reinforcements. This mechanism of energy dissipation is in addition to the inherent structural damping capability of the matrix. In general, the sources for energy dissipation in aligned composite materials, shown in Figure 3, can be divided into the following [36]: (1) far field viscoelastic damping in the matrix, (2) damping due to stress concentration at the matrix region surrounding the filler, (3) damping due to interfacial slip, (4) inherent damping in the filler. However, in most cases, CNTs behave elastically [37] at low strains, and thus the contribution of the latter mechanism is negligible. Moreover, by aligning the CNTs in the loading direction, it is

Reprinted with permission from “Energy Dissipation due to Interfacial Slip in Nanocomposites Reinforced with Aligned Carbon Nanotubes." by Gardea, F., Glaz B., Riddick J, Lagoudas D, Naraghi M. ACS Appl Mater Interfaces. 2015;7(18):9725–35.

possible to considerably suppress damping mechanisms such as matrix shearing, and perform a targeted study on identifying the role of interfacial slip on overall damping in the nanocomposite.

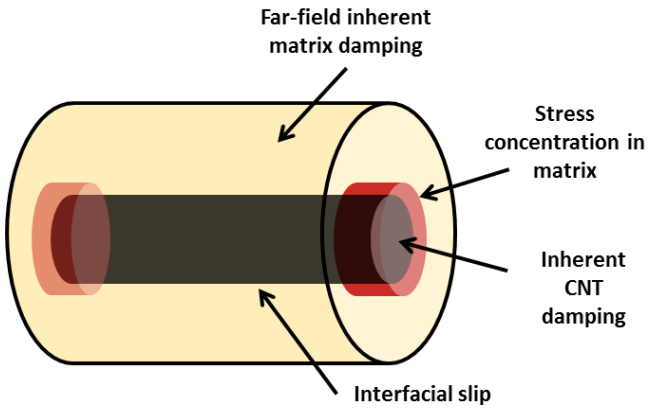

Figure 3. Schematic showing the sources of dissipation in an aligned CNT composite.

The steps of debonding and damping are assumed to follow that shown in Figure 4. In the initial configuration, step 1, CNT and matrix interact with each other via a combination of covalent bonds, mechanical interlocking, and van der Waals interactions. The interface of the CNT and matrix remains intact upon the application of static or dynamic load, as shown in step 2, until a critical shear stress for debonding is reached, at which the initial bonds and interactions are broken (step 3). Broken covalent bonds are non-reversible while mechanical interlocking and van der Waals (vdW) are reversible. This leads to the "stick" mechanism. Upon dynamic loading, the mechanical interlocking and vdW interactions that were reformed are once again broken and slip occurs at the interface (during step 4 to step 5, dissipation of energy occurs). These interactions are again reformed upon reverse loading. The critical strain to initiate slippage is again

reached at step 6, followed by slippage at the interface and further dissipation of energy (step 6 to step 7). Upon reaching step 7, the mechanical and vdW interactions are reformed. The cycle is then repeated.

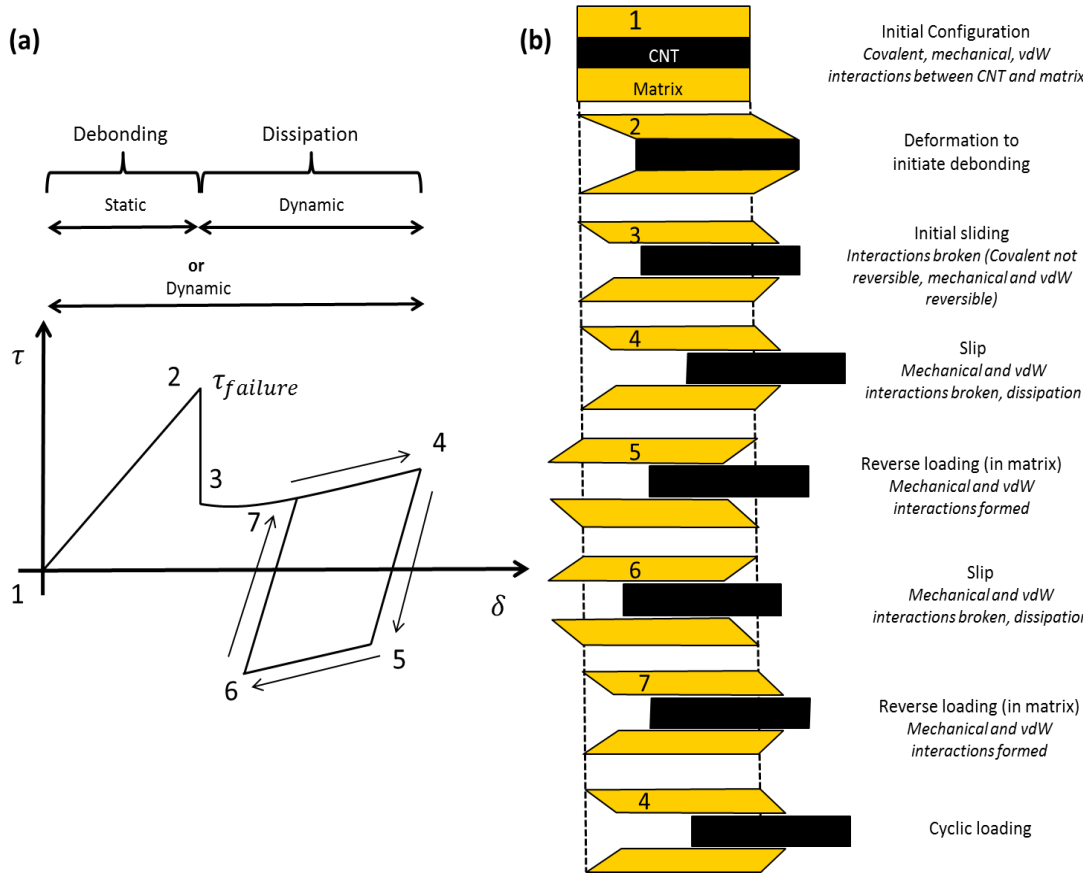

Figure 4. a) Schematic showing steps of debonding and damping as a function of relative displacement δ. b) schematic representation of CNT slippage during loading. Numbers correspond to critical steps during the loading cycle as mentioned in the text. Dissipation of energy occurs at steps 4 and 6.

This chapter will focus on the experimental investigation of the potential of CNT fillers in enhancing the damping properties of polymer matrix composites. The CNTs in our nanocomposites are mainly oriented along the loading direction via hot-drawing

(above the glass transition temperature of the matrix), in order to suppress energy dissipation modes, such as matrix tearing, such that the effect of interfacial sliding to overall damping can be quantified. A study on damping via dynamic mechanical analysis was performed, and the ratio of the loss to storage modulus are used to compare the damping performance of neat polymer and CNT reinforced polymer. Through exploring the dependence of damping on frequency of loading and dynamic strain history, we have shed light on the nature of the CNT-matrix interactions. Modeling was used to further give insight on the nature of the damping enhancement.

II.A. Experimental

II.A.1. Processing

Multi-walled carbon nanotubes with an outer diameter of 30-50 nm and length of 10-20 μm were purchased from Cheap Tubes Inc. and were used as is with no surface functionalization. Polystyrene (PS), with a density of 1.04 g/cm^3, was purchased from Sigma-Aldrich Co. and used as the matrix material. The fabrication of composites consisted of mixing a 1wt% concentration of pristine CNTs in PS via a twin-screw micro-extruder. To this end, the polymer was first heated to 150 °C (above Tg of ~100 °C) inside the extruder. The dry CNTs were then directly poured into the extruder. Mixing was carried out at 100 rpm and 150 °C for 30 min. The CNT/polystyrene mixture was then extruded through a 5 mm x 0.5 mm dye at 25 rpm. As the polymer mixture was being extruded, mechanical stretching (hot-drawing) was performed. The aim of mechanical stretching was to induce CNT alignment within the matrix. A stretch

ratio of 8 was achieved, estimated as the ratio of the cross section area of the unstretched to stretched samples, assuming volume conservation. Neat polymer samples were fabricated for comparison (stretch ratio was kept the same between the neat and reinforced samples).

II.A.2. Characterization

Dynamic mechanical analysis (DMA) was performed on CNT reinforced polystyrene nanocomposites and neat polystyrene samples at various dynamic strain amplitudes using a TA Instruments RSAIII DMA. All dynamic testing was performed in the direction of CNT alignment. The tests consisted of a dynamic strain sweep, in which the amplitude was varied from 0.01-1%. The samples had dimensions of approximately 0.56 mm thickness, 9.5 mm length and 2.5 mm width, therefore, no sample buckling was observed during the compressive half-cycles, within the dynamic strain range studied. The frequency was set to 1.0 Hz. From an application perspective, frequencies for this study were ≤ 1 Hz, which is in the order of magnitude required for rotor aeromechanical stability [1]. Due to the low frequency loading, the study remains quasi-static with in-phase relative motion of the filler and matrix when responding to the applied strain. During this test the offset strain was set to zero. Accumulation of damage was also studied by measuring the repeatability of damping at varying dynamic strains. In order to identify the frequency dependence on the interfacial sliding and damping, tests were performed at 0.1 and 1 Hz. Through these experiments, the nature of shear interactions

between the matrix and the filler was identified. High resolution scanning electron microscope (SEM) images of the cross-sections of the composite, with planes of cut being parallel and perpendicular to the stretching direction, were used to study the effectiveness of hot-drawing in inducing alignment of CNTs. SEM images were obtained using a JEOL JSM-7500F FE-SEM. In addition, polarized Raman spectroscopy was performed to study the alignment of CNTs using a Horiba Jobin-Yvon LabRam Raman Confocal Microscope with a 785 nm laser. The polarized incident laser was rotated in the direction parallel and perpendicular to the stretching direction using a half-wave plate. The ratio of the D-band peak, corresponding to disorder in the CNT crystalline symmetry, between the parallel and perpendicular directions was used as a measure of CNT alignment.

II.B. Modeling

In order to interpret the experimentally measured damping in CNT reinforced nanocomposites, the model developed by Glaz *et al.* which considers interfacial slip as the sole source of damping in addition to the inherent damping of the matrix, was used [1]. The interfacial shear stress in the model by Glaz *et al.* is taken from the continuum model by Cox [23] developed originally for discontinuous fiber reinforcements prior to fiber-matrix slippage. In the post-slip regime, the frictional energy dissipation is assumed to be proportional to the interfacial shear force, $f(\varepsilon_{xx})$, as shown in Eq.(1)

where $r_{NI}$is the radius of the nano-inclusion, τ_c is the critical interfacial shear stress, and l' is the interface length over which interfacial slip occurs.

$$f(\varepsilon_{xx}) = 2\pi r_{NI}\tau_c \frac{l'(\varepsilon_{xx})}{2} \tag{1}$$

The critical shear stress to initiate slip is calculated by setting x=0 and $\tau(x) = \tau_c$ in Eq.(2) [23] where d_{NI} is the diameter of the inclusion, E_{NI} is the longitudinal modulus of the inclusion, ε_{xx} is the applied strain. The value of β is obtained from Eq.(3), where G_m is the matrix shear modulus, A_{NI} is the area of the inclusion, v_f is the volume fraction, and l is the inclusion length. The model assumes once the slip is initiated, the shear stress remains constant along the slipped zone, equal to the critical shear stress, since the matrix can transfer no more load to the CNT over this zone [1].

$$\tau(x) = \frac{d_{NI}E_{NI}\varepsilon_{xx}\beta}{4}\left[\frac{sinh\left(\beta\left({}^{l}/_{2} - x\right)\right)}{cosh\left({}^{\beta l}/_{2}\right)}\right] \tag{2}$$

$$\beta^2 = \frac{2\pi G_m}{A_{NI}E_{NI}ln\left({}^{1}/_{\sqrt{v_f}}\right)} \tag{3}$$

Furthermore, the critical applied strain at which interfacial slip initiates, ε', is calculated Eq. (4).

$$\varepsilon' = \frac{4\tau_c}{d_{NI}E_{NI}\beta \tanh(\beta l/2)} \tag{4}$$

Also, the length over which slip occurs is obtained from Eq. (5),

$$l' = l - \frac{2}{\beta} sinh^{-1}\left(\frac{4\tau_c cosh\left(\beta l/2\right)}{d_{NI}E_{NI}\varepsilon_{xx}\beta}\right) \tag{5}$$

Once interfacial slip initiates, the stiffness contribution from the nano-inclusion, K_{NI}, decreases and can be estimated by an appropriate decay function or through the experiments. The effective composite stiffness, $\overline{K}$, post slip is shown in Eq. (6). K_M is the matrix stiffness, $K_{NI,0}$ is the initial inclusion stiffness, $\varepsilon_1 = \max(\varepsilon', \varepsilon_0)$, $\varepsilon_{min} = \min(\varepsilon', \varepsilon_0)$ and $\varepsilon_{max} = \varepsilon_0 + \varepsilon_\omega$ where ε_0 is the offset strain and ε_ω is the dynamic strain.

$$\overline{K} = \frac{(K_M + K_{NI,0})(\varepsilon' - \varepsilon_{min}) + \int_{\varepsilon_1}^{\varepsilon_{max}} (K_M + K_{NI}(\varepsilon_{xx}))d\varepsilon_{xx}}{\varepsilon_{max} - \varepsilon_{min}} \tag{6}$$

From the effective stiffness, the corresponding storage modulus, $E_{storage}$, can be calculated (Eq.(7)) while the maximum strain energy, $2\pi U_0$, and the dissipated energy, δU, can be calculated from Eq. (8) and (9), respectively.

$$E_{storage} = \frac{\overline{K}\, l/2}{A_{RVE}} \tag{7}$$

$$2\pi U_0 = \frac{\pi}{4}\bar{K}(\varepsilon_\omega l)^2 \tag{8}$$

$$\delta U = 2\int_{\varepsilon_1}^{\varepsilon_{max}} f(\varepsilon_{xx})\frac{l'(\varepsilon_{xx})}{2}d\varepsilon_{xx} \tag{9}$$

Therefore, the loss factor, $\eta = \tan\delta$, is obtained from Eq.(10) and the loss modulus, E_{loss}, calculated from Eq. (11).

$$\eta = \frac{\delta U}{2\pi U_0} \tag{10}$$

$$E_{loss} = \eta E_{storage} \tag{11}$$

II.C. Results and Discussion

II.C.1. Alignment of CNTs in the Matrix via Hot-drawing

The samples tested were fabricated using the method described in Section II.A.1. Alignment of CNTs was qualitatively studied by fracturing the sample in the directions perpendicular and along the stretching direction, and observing CNT directions via SEM. The two directions are schematically shown in Figure 5a. SEM images of the fracture surface parallel to the stretching direction (Figure 5b) contains many cases of CNTs laid parallel to that direction, qualitatively verifying the preferred alignment of CNTs in the stretching direction during sample processing. The arrangement of CNTs on the surface parallel to the stretching direction is in contrast to the surface which is

perpendicular to the stretching direction (Figure 5c), on which mostly broken CNT and holes (evidence of pull out) are observed.

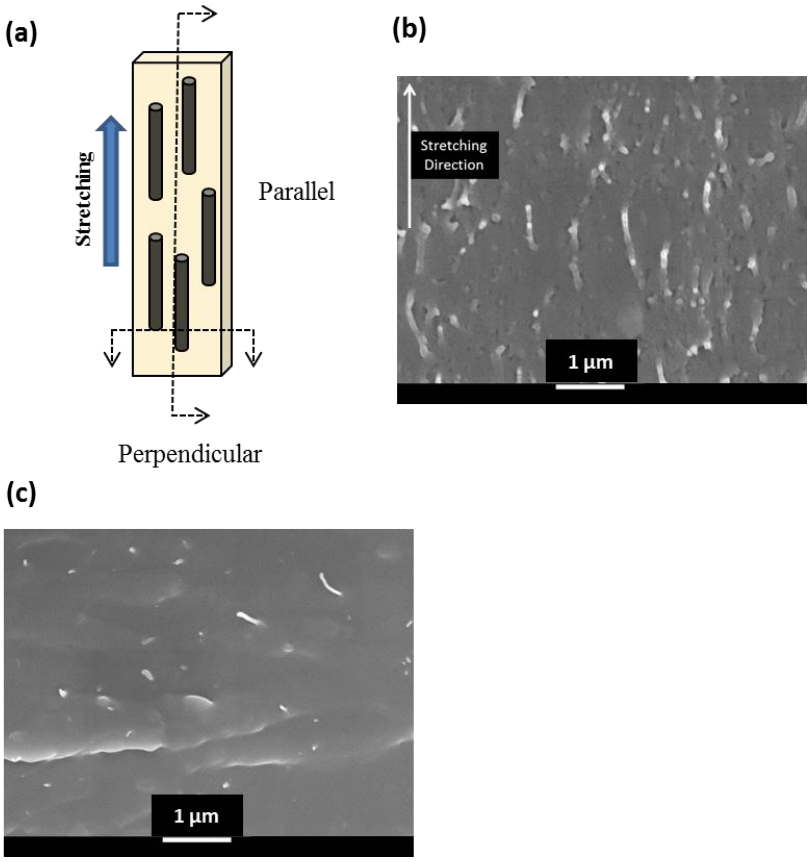

Figure 5. a) Schematic of fractured surfaces perpendicular and parallel to stretching direction. b) SEM image of fractured surface parallel to stretching direction showing alignment of CNTs in the direction of stretching. c) SEM image of fractured surface perpendicular to the stretching direction showing the cross-section of fractured CNTs.

Further evidence in support of the alignment of CNTs in the direction of hot-drawing was obtained via Raman spectroscopy. The basics of detecting CNT alignment via Raman spectroscopy relies on prior studies demonstrating that the intensity of the G-band and D-band in multi-walled carbon nanotubes depend on the laser polarization direction [38]. Specifically, the disorder peak (D-band) shows a correlation with the

angle between the polarization of the incident laser and the CNT axis, with maximum scattering intensity along the CNT axis direction [39]. The G-band was not used as the metric for alignment due to the polystyrene matrix containing a peak in the same wavelength as the G-band (1520-1600 cm^{-1}). To detect CNT alignment, hot-drawn samples were subjected to polarized Raman spectroscopy with the polarization of the incident laser being parallel (0º) and perpendicular (90º) to the stretching direction. The ratio of the intensities of the D-band peak between the two polarization directions was used as a measure of the CNT alignment. This ratio was also measured on nanocomposites with randomly oriented CNTs (no hot-drawing) as the benchmark. The results are shown in Figure 6. The ratio of the parallel to perpendicular D-band (1310 cm^{-1}) intensity peak for the aligned CNT specimen was 1.36 while the random CNT specimen showed a considerably lower ratio of 1.15. This result shows that the CNT orientation coincides with the stretching direction, verifying the CNTs are aligned in the stretching direction.

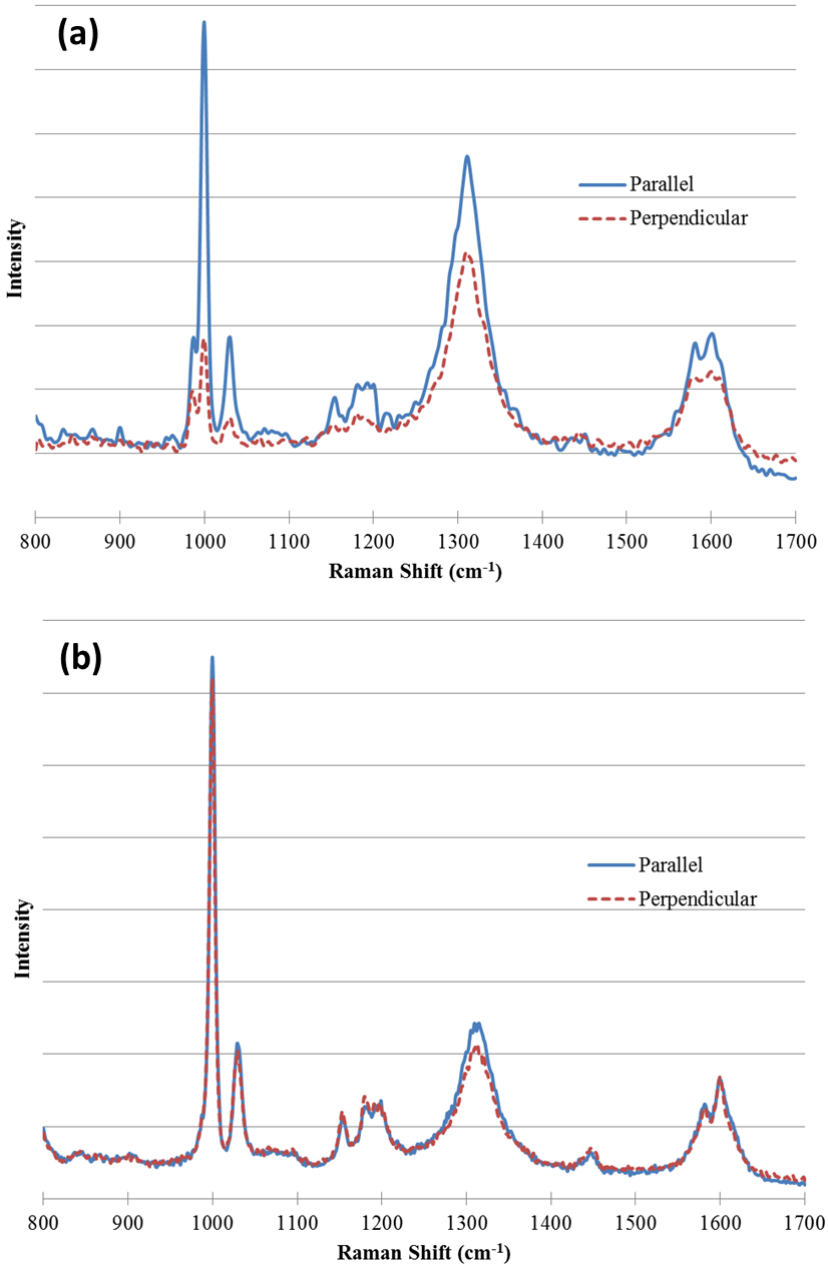

Figure 6. Polarized Raman spectra at 0º (parallel) and 90º (perpendicular) to the stretching direction for a) aligned CNT/polystyrene composite and b) randomly oriented CNT/polystyrene composite.

II.C.2. Energy Dissipation Through Interfacial Slippage

The dependence of the storage modulus on dynamic strain of CNT reinforced polystyrene nanocomposites and neat polystyrene are shown in Figure 7. As shown in the figure, at dynamic strains (< 0.1%) the storage modulus of the 1 wt.% composite is slightly higher than the neat PS. This is consistent with a rule of mixtures (RoM) prediction, obtained for the case of highly aligned and high aspect ratio CNTs.

The storage modulus of the CNT was calculated using a rule of mixtures approach with input from the experimental results, Figure 7, at the lowest tested strain. It was assumed that the load was carried only by the outmost shell. The composite modulus, E_c=1781 MPa, and the neat polymer modulus, E_m=1630 MPa, were taken from an average value of the modulus at the lowest strains tested (below the critical dynamic strain). The volume fraction, v_f, was calculated using Eq.(12) for a weight fraction, w_f, of 0.01 and a CNT and polymer density of 2.1 and 1.04 g/cm^3, respectively.

$$v_f = \frac{w_f \rho_m}{w_f \rho_m + (1 - w_f)\rho_{CNT}} \tag{12}$$

In reality the CNTs are hollow and the outer shell carries the majority of the load. The modulus of the CNT, $E_{shellCNT}$, was calculated using Eq. (13), assuming highly aligned, cylindrical inclusions.

$$E_c = (1 - v_f)E_m + v_f E_{shellCNT}\frac{4t}{d} \tag{13}$$

The thickness of the outer shell, t, was assumed to be 0.34 nm and the diameter of the CNTs, d, to be in the range of 30-50 nm. This leads to a CNT modulus range of 702 GPa< $E_{shellCNT}$ < 1.17 TPa. This range of values of CNT shell stiffness is comparable to measured/predicted modulus of CNT shells [40].

The storage modulus of the CNT composite samples remains nearly independent of dynamic strain amplitude until a critical value of 0.028% is reached, after which, the storage modulus decreases with dynamic strain amplitude. The loss in storage modulus and deviation from RoM calculation is likely due to a loss in interfacial load transfer. In other words, the decrease in storage modulus with dynamic strain suggests that slippage initiates at this critical strain. SEM images of the fracture surfaces of CNT-PS composites, with many instances of CNT pull out and holes within the matrix from which CNTs have likely pulled out (Figure 8), provides further evidence in support of interfacial slippage, facilitated by sufficiently weak interfaces.

This result points to the significance of CNT-polymer interface engineering in enhancing the mechanics of polymer composites, as with no surface functionalization (the case studied here), interfacial slip can initiate at very low strains (as low as 0.028%), suppressing or eliminating the reinforcing effect of CNTs. Therefore, assessment of the contribution of CNTs to composite stiffness should also be carried out at sufficiently low strains (below the critical sliding) and by considering the state of interfacial damage. For instance, in the case of pristine CNTs in PS which was studied here, where the interfacial slip occurs at 0.028%, the storage modulus at strains as low as 0.1% drops to the value

of neat matrix, while at sufficiently lower strains, it follows the RoM predictions, as discussed earlier. This factor, interfacial slip promoted by the elastic mismatch between CNTs and polymer and weak interfaces, next to other microstructural defects, such as CNT agglomeration (not observed in this study) commonly referred to in the literature, should be considered in the assessment of mechanics and design of CNT composites.

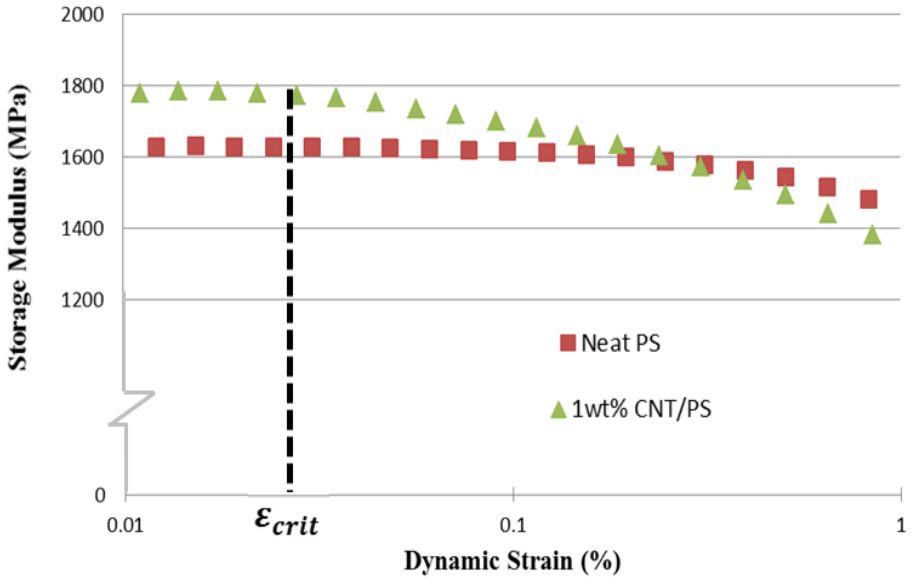

Figure 7. Experimental results of storage modulus as a function of dynamic strain for neat polystyrene (PS) and 1wt% aligned CNT/PS composite. Offset strain= 0.0%, frequency=1Hz.

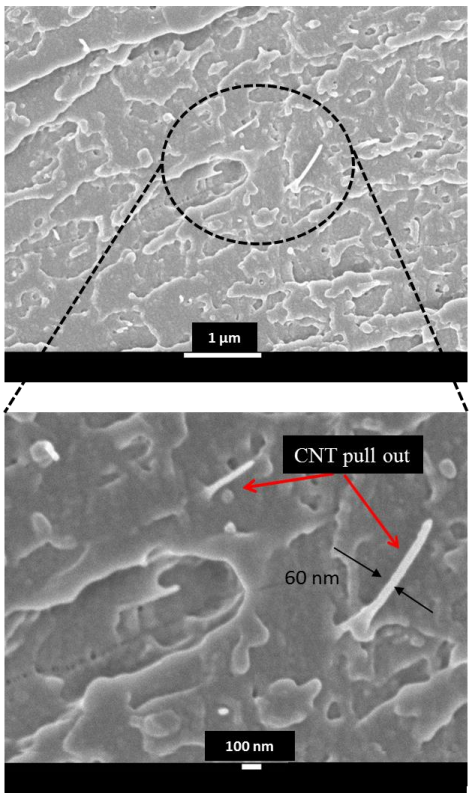

Figure 8. SEM images of fracture surface showing CNT pull out.

Further evidence in support of the initiation of interfacial sliding at the critical strain of 0.028% is obtained by considering the variations of the damping capabilities of CNT-PS composites. As shown in Figure 9a, the tan δ of CNT-PS composite varies in a non-linear fashion with dynamic strain amplitude in contrast to the nearly linear variations of the neat polymer. More specifically, at low strains, below the critical strain value, the measured tan δ is the same for both systems and nearly independent of the dynamic strain (Figure 7 and Figure 9). However, when the critical dynamic strain is reached, the damping and energy dissipation in CNT-PS composite is markedly enhanced and increases with the dynamic strain. Assuming that the CNTs themselves remain elastic at

these low values of average stress (below 100 MPa, compared to the strength of CNTs of several to tens of GPa) [37], the source of energy dissipation in excess of inherent energy dissipation in matrix could have stemmed from [36] (i) dissipation at the interface through slip or (ii) dissipation by the matrix due to stress concentrations at the CNT ends [41-43], as schematically shown in Figure 3. The latter mechanism is considered to be one of the main damping mechanisms in microfiber reinforced composites [44, 45]. Since the initiation strain of the additional energy dissipation mechanism coincides with dynamic strain at which material degradation starts (loss in storage modulus as shown in Figure 7), the former mechanism is considered to be the dominant factor contributing to the additional energy dissipation in CNT-PS composites. It is to be noted that by aligning the CNTs in the loading direction, other energy dissipation mechanisms, such as matrix plasticity and tearing, are suppressed.

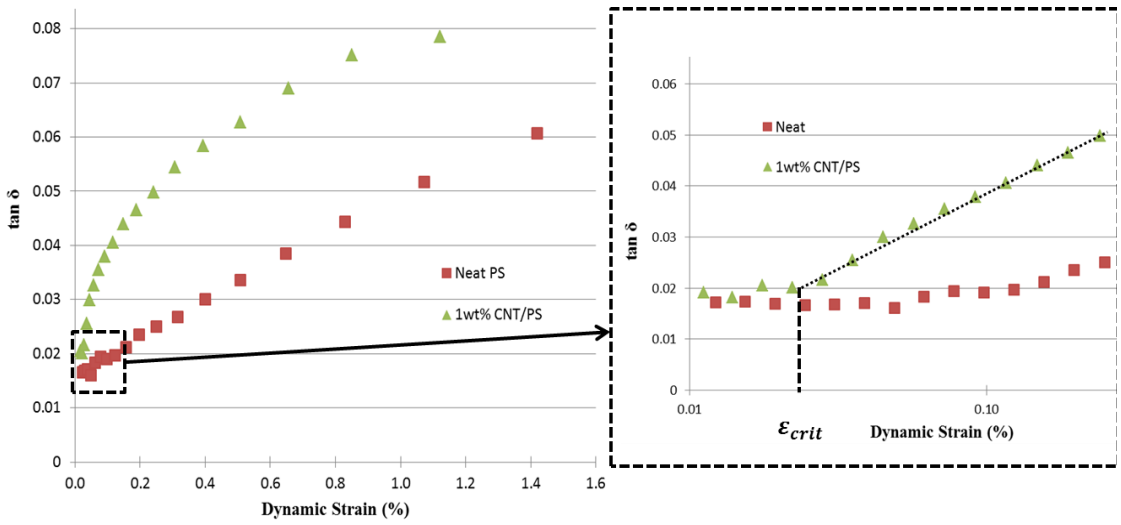

Figure 9. Experimental results of tan δ as a function of dynamic strain for neat polystyrene (PS) and 1wt% aligned CNT/PS composite. Offset strain= 0.0%, frequency=1Hz.

II.C.3. Micromechanics Modeling of Interfacial Dissipation Through CNT Slippage

To better illustrate the role of interfacial slip, a micromechanics model by Glaz *et al.*[1], which only accounts for energy dissipation of aligned matrix inclusions from slippage, was implemented. As shown experimentally in the previous section, the additional energy dissipation is dominantly caused by friction between CNT and matrix during slippage. The experimental results shown in Figure 10 correspond to only the contribution to damping resulting from the presence of the CNT; i.e. the polymer tan δ was subtracted from the composite tan δ. The model parameters used are shown in Table 1. The density of both the CNTs and the matrix were obtained from the manufacturer specifications. In addition, the diameter of the CNT was taken as the average value of the diameter range given by the manufacturer. The elastic modulus of the matrix was taken from the DMA results of the neat polymer at the lowest tested strain. Using the onset strain, 0.028%, at which the CNT composite experimental tan δ deviates from that of the neat polymer, the interfacial shear strength was calculated using Eq. (4). The values obtained for the interfacial shear strength, τ_c, range from 0.443-0.523 MPa for the cases studied. These results are comparable to that reported in literature for CNT composites [46]. The calculated value of τ_c varies for each case due to the varied length of the CNT or the modulus of the CNT, according to Eq. (4), however the critical strain to initiate slip is obtained from the experiment and kept constant.

The result in Figure 10a shows that the additional damping is highly depended on the aspect ratio of the filler. The best approximation to the experimental result consists of fillers with an aspect ratio between 10 and 50, CNT length of 400 nm and 2 μm,

respectively, shorter than the length reported by the manufacturer (10-20 μm). One explanation for this result would be that the CNTs were possibly cut during the fabrication process, resulting in much shorter CNTs. This is verified by the SEM images, Figure 8, showing CNT pull-out. Assuming that only half of the length of the CNT on average is pulled out of the matrix, the images show an aspect ratio of about 15, consistent with the modeling results. The comparison of the model to the experimental results suggests that there exists additional energy dissipation mechanisms, such as accentuated energy dissipation in the matrix at the two ends of each CNT due stress concentration [44, 45]. The fact that this additional energy dissipation – the difference between the model prediction and experiment- is the largest at the lowest dynamic strain (onset of sliding), and decreases with dynamic strain amplitude (as the slippage zone spreads along the CNT) further supports this hypothesis.

Table 1. Input data for micromechanics model

Matrix elastic modulus	1.6 GPa
Critical strain (slip initiation)	0.028%
CNT concentration	1wt%
Matrix density	1.04 g/cm^3
CNT density	2.1 g/cm^3
CNT diameter	40 nm
Frequency	1 Hz

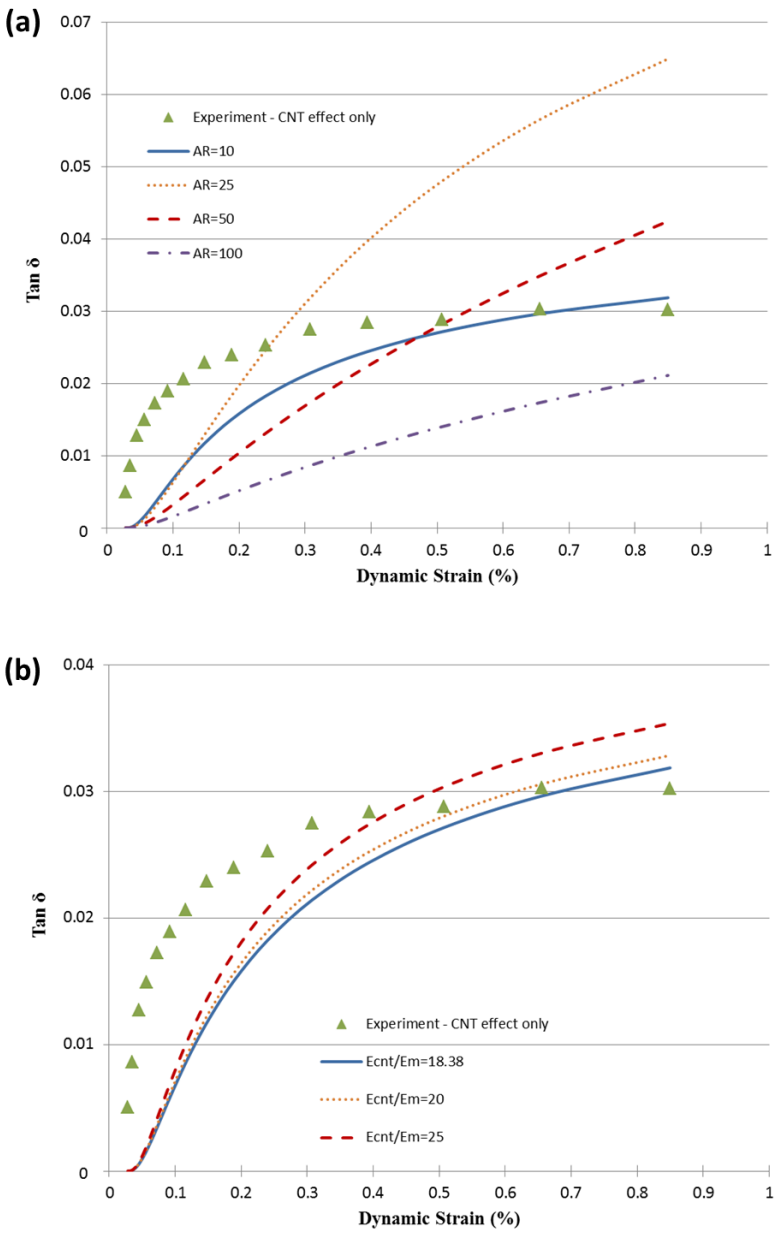

Figure 10. Results of tan δ as a function of dynamic strain for 1wt% aligned CNT/PS. Experimental results (with the matrix contribution subtracted) are compared to the micromechanics model from Glaz *et al* [1]. a) Parametric study on the effect of aspect ratio, AR (diameter of CNT was kept constant while the length of the CNT was varied). Ecnt/Em=18.38 (the effective CNT modulus of 29.9 GPa is taken from the experimental data and the rule of mixtures. τ_c= 0.443, 0.521, 0.523, 0.523 MPa for AR of 10, 25, 50, and 100, respectively). b) Parametric study of modulus ratio between CNT (Ecnt) and matrix (Em) (AR=10 and τ_c= 0.443, 0.454, 0.482 MPa for modulus ratios of 18.38, 20, and 25, respectively).

Using an energy approach [44], the energy dissipated due to interfacial shear stresses can be accounted for. In this approach the dissipation of energy takes place solely in the matrix due to shear deformation resulting from the presence of the CNT. By accounting for the energy dissipation contribution due to the shear stress concentration in the polymer surrounding the CNT it becomes possible to add this contribution, assuming the energy contributions are additive, to the energy dissipated due to solely interfacial slippage, obtained previously. The resulting behavior (dissipation due to both interfacial slippage and stress concentrations in the matrix) is shown in Figure 11. The modeling result shows an improved fit to the experimental result. In addition, the discrepancy between experimental results and modeling at the initial strains when accounting for solely interfacial slip, Figure 10, is reduced with the addition of the matrix contribution.

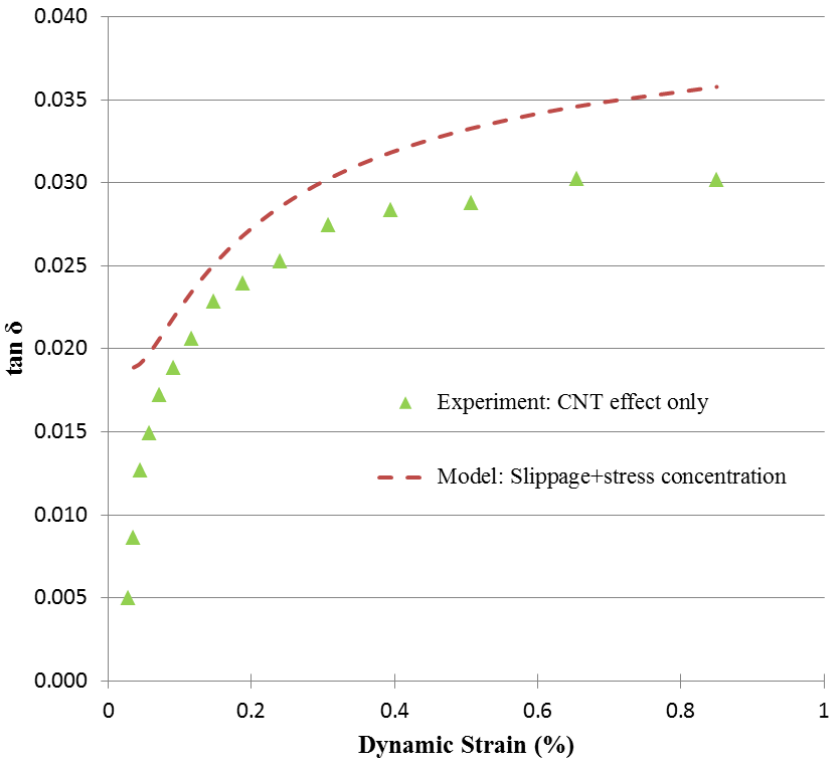

Figure 11. Modeling result of tan δ as a function of dynamic strain for a 1wt% aligned CNT/PS composite accounting for both energy dissipation due to shear stress concentration in the polymer and interfacial slip.

II.C.4. Further Insight into the Nature of Shear Interfacial Forces

The interfacial shear strength is due to a combination of mechanical interlocking (compressive) and adhesion (attractive) interactions. The former reflects the tendency of the matrix and filler to prevent interpenetration during sliding, thus, it depends on surface topography and the mechanics of each phase. Mechanical interlocking arises from the surface roughness present on the CNT. The polymer conforms to this surface topography during the fabrication process. Upon relative displacement between the polymer and CNT, the roughness will give rise to a frictional component for dissipation.

On the other hand, adhesion is a function of chemistry of the two surfaces, and may stem from a combination of vdW interactions and/or covalent bonds. Therefore, three main mechanisms are responsible for load transfer from a matrix to a filler: mechanical interlocking, chemical bonding, and van der Waals interactions [47], as schematically shown in Figure 12.

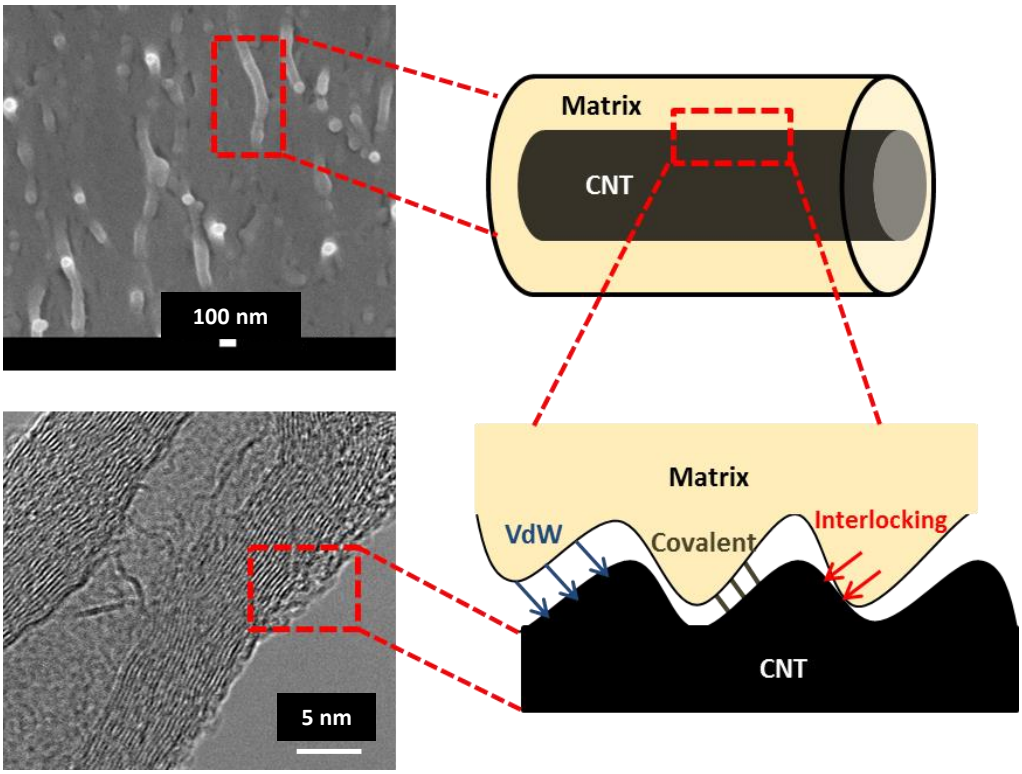

Figure 12. Schematic of interfacial interactions between a CNT and polymer in a CNT/polymer composite inspired by the SEM image of the composite and the TEM image showing the surface topography of the CNT.

Experiments were designed to shed light on the relative significance of these three types of interactions on the interfacial energy dissipation and damping in CNT-PS

composites. First, we considered the ability of the vdW interactions and mechanical interlocking to reform upon initial rupture, for instance during interfacial sliding, which distinguishes them from covalent bonds. As shown in Figure 13, the dissipation in the CNT-PS composite samples as a function of the dynamic strain amplitude is nearly independent of the prior history of dynamic loading in the material. For instance in the first cycle of loading, the material demonstrates additional energy dissipation mechanisms, relative to neat PS, at a critical strain of 0.028%, suggesting an initiation of interfacial slippage. However, at the beginning of the second cycle, when the dynamic strain is reduced to below the critical strain, the energy dissipation reduces to the levels of the neat PS, indicating the reformation of the initial interfacial interactions. Therefore, the observed strain energy dissipation is mostly caused by the reformable interfacial interactions, vdW interactions and/or mechanical interlocking, and covalent bonds do not significantly contribute to the damping. This result is consistent with studies performed on the interactions between CNTs and polystyrene, which show that van der Waals and mechanical interlocking are the dominating interfacial interactions [48, 49], and covalent bonding is not significant, for instance as a result of chain scissoring and repolymerization at high temperatures during extrusion. The result shown in Figure 13 consists of three total cycles, which leads to no visible damage accumulation in the composite. Further cycling of the dynamic strain could possibly lead to damage in the composite, however, damage due to further cyclic loading is not investigated here.

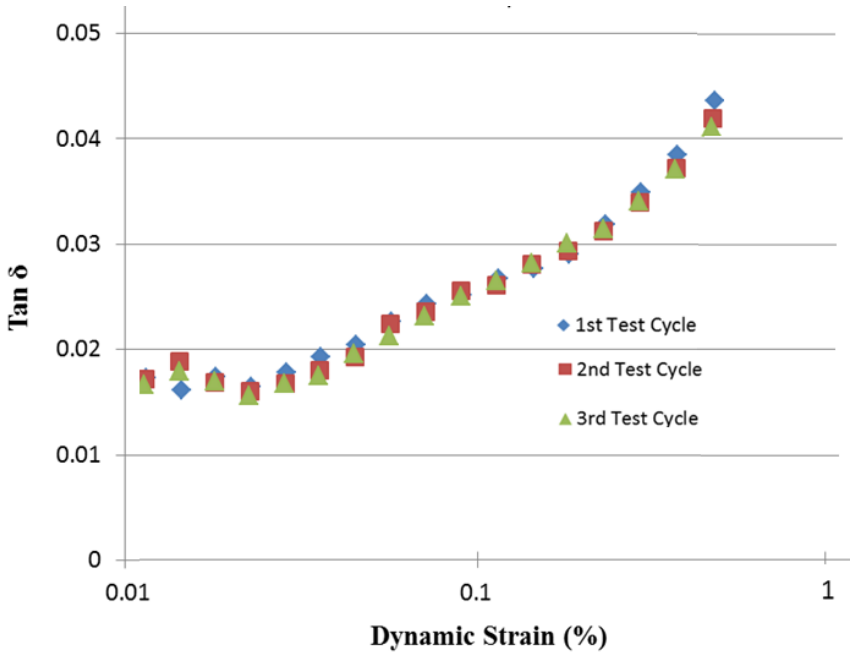

Figure 13. Experimental results of tan δ as a function of dynamic strain for a 1wt% aligned CNT/PS sample. Multiple test cycles were performed on the same sample.

Further insight into the relative contribution of mechanical interlocking and vdW interactions on interfacial slip was obtained via exploring the frequency dependence of interfacial shear strength, as shown in Figure 14. We considered two frequencies: 0.1 Hz and 1.0 Hz. The results show that the critical dynamic strain amplitude for slip initiation increases as the frequency is decreased, suggesting that polymer relaxation at the interface has reduced the interfacial shear stress, requiring higher axial strains to overcome the interfacial shear strength at the lower frequency.

Since the polystyrene chains and pristine CNTs are both unpolar, the vdW forces are expected to be mainly caused by interactions between instantaneously induced dipoles (dispersion forces). Moreover, it is argued here that adhesive vdW interactions do not

contribute significantly to interfacial shear interactions, since they depend on fluctuations in charge distribution [50], which occurs at much higher frequencies than those studied here. Moreover, some of the relaxation modes of polymer chains are active in the explored range of frequency [51]. These relaxation modes facilitate the reconfiguration of polymer chains around the CNT reinforcements and conformal to CNT surface roughness, suppressing the stresses accumulated in the polymer due to mechanical interlocking during sliding. A clear indication of the active relaxation modes within the polymer at the studied frequencies is the reduction in composite storage modulus by ~3% at 0.1 Hz compared to the 1.0 Hz storage modulus. Therefore, these results indicate that the mechanical interlocking is the dominant strain energy dissipation mechanism for the nanocomposite system studied here. This is in contrast to previous studies, e.g. [21], in which vdW forces have been postulated but not quantitatively substantiated as the dominant interfacial slip mechanism. In addition, the slope of the tan δ vs dynamic strain data for 1 and 0.1 Hz, shown in Figure 14a increases with the applied loading frequency. This result shows that, not only does the onset of slippage occur earlier for higher frequency, but also debonding propagates faster at higher rates. That is, for a given strain, the length over which slip occurs is larger for the higher frequency case, as verified by observation of Eqs. (9) and (10). This justifies the claim that lower frequency leads to suppression of stress accumulation at the interface, postponing interfacial failure.

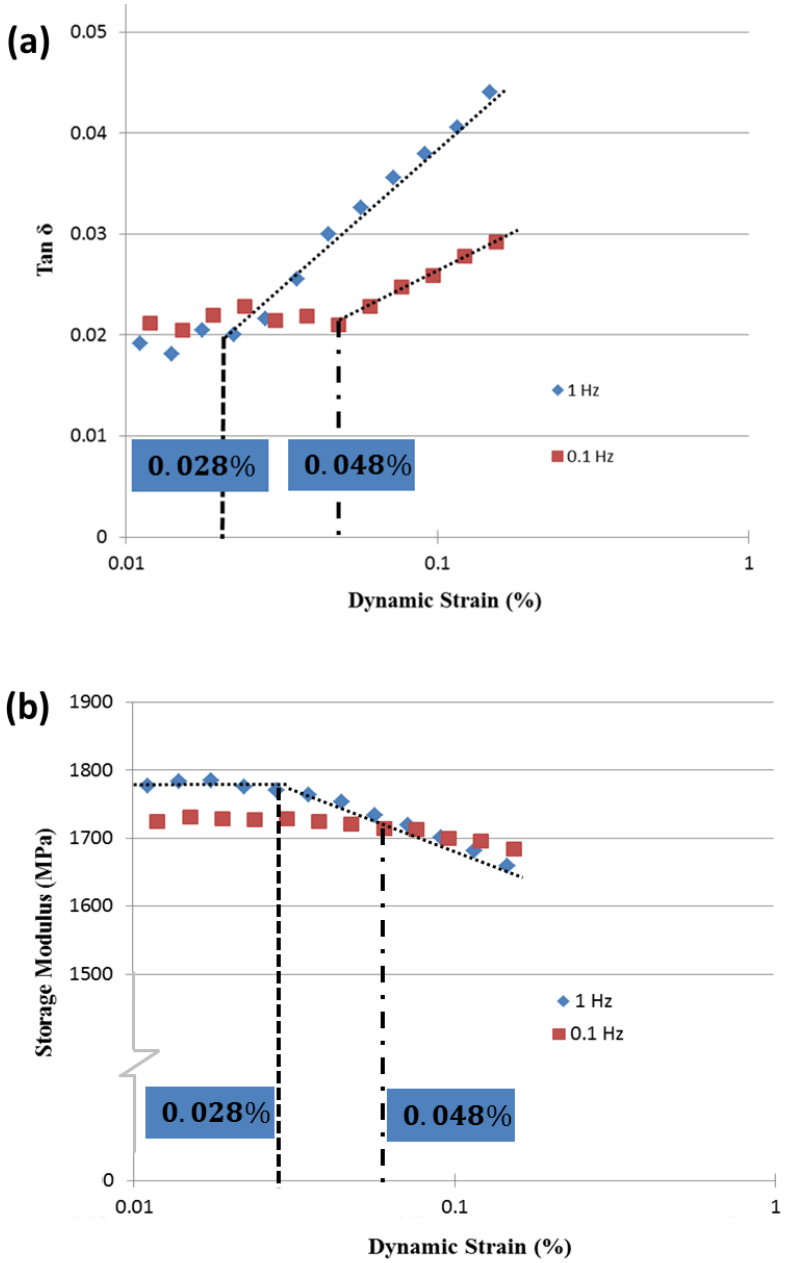

Figure 14. Experimental results of (a) tan δ and (b) storage modulus as a function of dynamic strain for 1wt% aligned CNT/PS composite at frequencies of 0.1 and 1 Hz. Offset strain= 0.0%.

II.D. Conclusion

Among the targeted passive damping mechanisms in nanocomposites is a ‘slip-stick’ mechanism in which the interactions between the filler and polymer results in energy dissipation along the interface. The CNT composites studied here consisted of CNTs dominantly oriented parallel to the loading direction, the purpose being to minimize the contribution of damping mechanisms other than the inherent damping of the matrix and interfacial slip. After the initial interface failure, the frictional sliding at the interface increased the energy dissipation by as much as 100% compared to the inherent damping capability of the matrix, depending on the magnitude of the dynamic strain amplitude. An analytical model was used to provide additional insight into the experimental observations by showing that the nonlinear variation of damping with dynamic strain can be attributed to slip-stick behavior. The results point to the major contribution of mechanical interlocking, after the initiation of interfacial slip, to energy dissipation in the composite.

CHAPTER III

EFFECT OF CARBON NANOTUBE ORIENTATION AND DISTRIBUTION ON COMPOSITE VIBRATIONAL DAMPING

As pointed out in Chapter II, a variety of mechanisms including the interactions between filler and matrix and the inherent damping of the matrix amplified by the stress concentration due to elastic mismatch between filler and matrix contribute to damping capability of nanocomposites. The relative significance of these mechanisms depends on the stress distribution within the nanocomposite, which can be controlled by the manipulation of CNT orientation and distribution. In the previous chapter, the CNTs were oriented parallel to the loading direction in order to minimize the contribution of damping mechanisms other than the inherent matrix damping and interfacial sliding of the CNT relative to the matrix. However, a randomly oriented CNT composite can introduce additional damping mechanisms, both involving the CNT and the matrix. One of these mechanisms is the friction between CNTs in an entangled network of CNTs. The significantly lower percolation threshold of randomly oriented CNTs compared to aligned ones increases the likelihood of CNT-CNT interaction in the former. Therefore, for a given volume fraction, the contribution of CNT-CNT friction to energy dissipation scales inversely with the randomness of the orientation of CNTs. In addition, the orientation of CNTs with the loading direction can significantly influence the local stress fields and thus energy dissipation within the matrix. The viscoelastic nature of the matrix

will contribute to the enhancement in damping at the stress concentrations sites throughout the complex stress field in the composite.

For a given average volume fraction and alignment, distribution of the CNTs can also add to the dissipation of energy in the composite. CNT-CNT interaction is minimized if the dispersion of CNTs is uniform. The presence of agglomeration of CNTs will lead to an enhancement in the CNT-CNT interactions, and thus enhance the energy dissipation through relative sliding of CNTs within the composite. In addition, agglomerates serve as stress concentration sites which can enhance the viscoelastic contribution of the matrix to damping.

In this chapter, the effect of CNT orientation and distribution on energy dissipation (damping) within a nanocomposite will be studied, with a focus on random distribution and agglomeration. Experimental characterization results will be presented which point to the enhancement in damping due to misorientation and non-uniform CNT distribution. Through SEM imaging, fractography and Raman spectroscopy, the origin of the damping enhancement is elaborated in terms of the microstructure of the material and stress fields.

III.A. Experimental

III.A.1. Processing

The fabrication procedure follows that presented in Chapter II and is summarized below. Multi-walled carbon nanotubes were used as is with no surface functionalization and polystyrene (PS) was used as the matrix material. The fabrication of composites

consisted of mixing a certain concentration of pristine CNTs in PS via a twin-screw micro-extruder. The polymer was first heated to 150 °C (above Tg of ~100 °C) inside the extruder. The dry CNTs were then directly poured into the extruder. Mixing was carried out at 100 rpm and 150°C for 30 min. The CNT/polystyrene mixture was then extruded through a 5 mm x 0.5 mm dye at 25 rpm. To develop nanocomposite with aligned CNTs, as the polymer mixture was being extruded, hot-drawing was performed to induce alignment of the CNTs. The fabrication of the randomly distributed CNT composite samples followed the same procedure except that no hot drawing was performed on the samples after extrusion.

Samples with a concentration of 1, 2, and 4wt% CNT were fabricated. Developing nanocomposites with various CNT concentrations allowed us to further study the contribution of CNT-matrix interfacial sliding on damping. Moreover, increasing CNT concentration typically increases the likelihood of CNT agglomeration, allowing for the investigation of the role of CNT-CNT interactions on damping. In this regard, comparison will be made on the damping capability of aligned CNTs (with minimal CNT-CNT interaction) and agglomerated CNTs, with both composites fabricated using the same procedure.

III.A.2. Characterization

Dynamic mechanical analysis (DMA) was performed on CNT reinforced polystyrene nanocomposite samples at various dynamic strain amplitudes using a TA Instruments

RSAIII DMA. All dynamic testing was performed in the direction of extrusion (and hot-drawing for the nanocomposites with aligned CNTs). The tests consisted of a dynamic strain sweep, in which the amplitude was varied from 0.01-1% at a frequency of 1.0 Hz and an offset strain of zero. The amplitude of the dynamic strain was kept sufficiently low to avoid buckling. High resolution scanning electron microscope (SEM) images of the cross-sections of the composite were used to study the local CNT distribution and orientation. SEM images were obtained using a JEOL JSM-7500F FE-SEM.

In order to analyze the distribution and uniformity of the dispersion of CNTs at the micrometer scale, Raman spectroscopy was performed. A spatial image of the CNT distribution within the matrix is possible to obtain by characterizing the CNT Raman active atomic vibrations in the composite [52, 53]. A spatial image can be obtained by scanning a laser beam over the area of interest on the composite and obtaining a Raman spectrum at each step, as shown in Figure 15. A qualitative assessment of the CNT distribution is obtained.

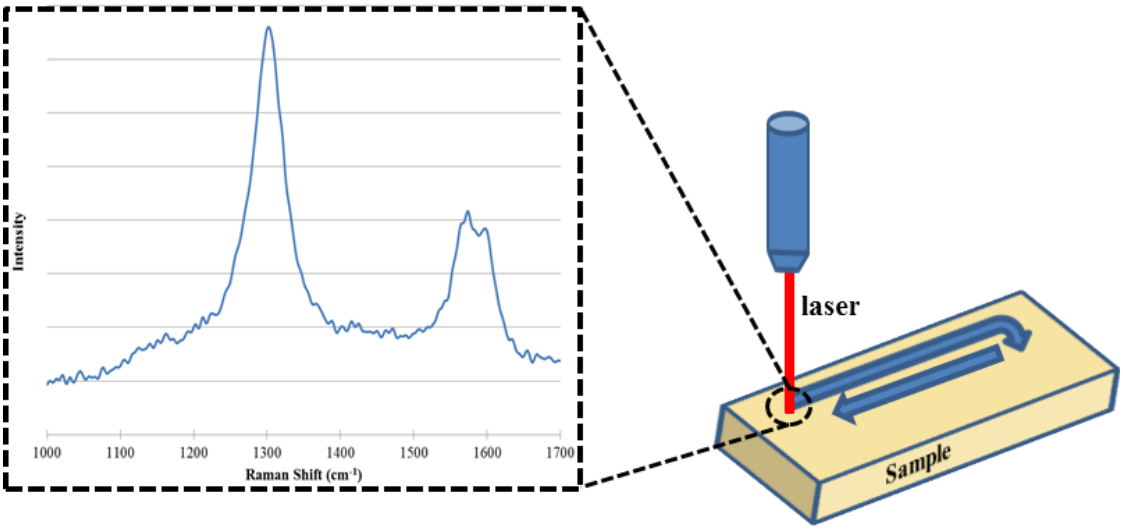

Figure 15. Schematic of Raman imaging scanning technique. The laser spot scans the sample and a Raman spectrumis obtained at every step.

The Raman peaks of interest in this study are the D and G-band, shown in Figure 16. The D-band is a measure of the disorder in the CNT with a spectrum range from 1290-1360 cm^{-1}. The presence of a D-band in a crystalline structure arises from the breaking of symmetry [39, 54]. The tangential C-C stretching vibrations in a CNT lie in the range of 1520-1600 cm^{-1} (G-band). This peak represents the graphitic nature of the CNTs [39, 54].

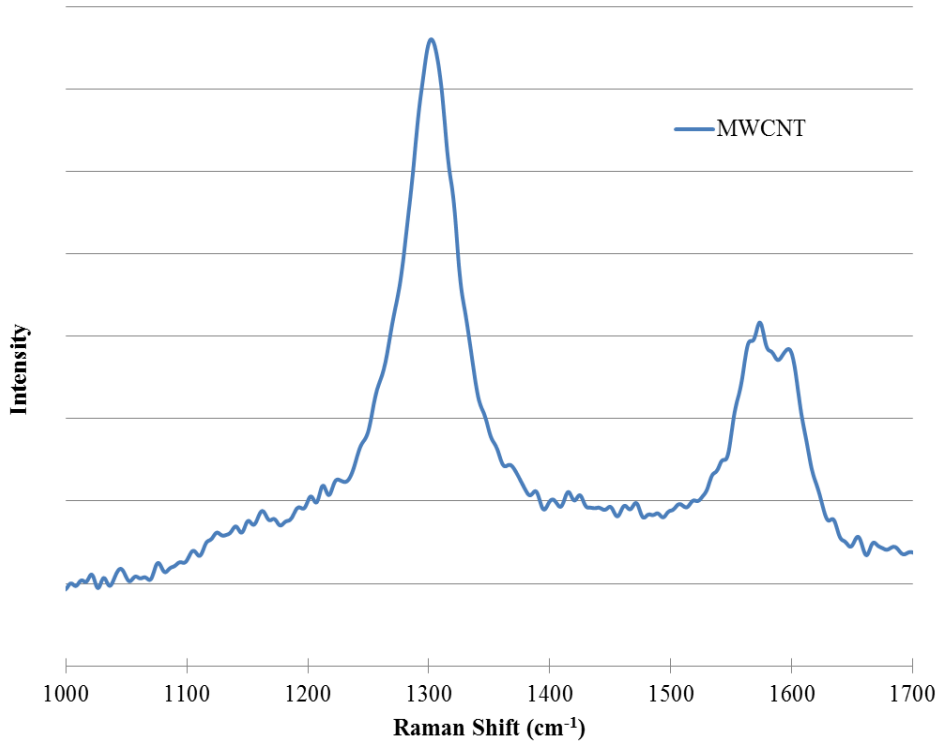

Figure 16. Raman spectrum for the multi-walled CNTs used in this study.

Raman spectroscopy was performed on each test specimen using a 785 nm laser focused with a 50X microscope objective. The laser beam was scanned over a 100 x 100 μm^2 area on the sample surface and spectra acquired at steps of 2 x 2 μm^2. The high intensity of the D-band in the CNTs used in this study allows for a more practical use of this band to derive the Raman image. In addition, the PS matrix has a peak in the 1520-1600 cm^{-1} range, which coincides with the G-band of CNTs, thus only the D-band will be used as an indication of the presence of CNTs in the matrix.

III.B. Results and Discussion

III.B.1. The Distribution of Aligned CNTs in Hot-drawn Nanocomposites

The distribution of CNTs in nanocomposites with aligned CNTs was first qualitatively studied by fracturing the sample in the direction perpendicular to the hot-drawing (similar to Figure 5) and observing the composite fracture surface via SEM. The comparison of the CNT distribution for the 1, 2, and 4wt% CNT composite samples is shown in Figure 17.

As shown previously in Figure 5 and discussed in Chapter II, the 1wt% CNT/PS composite contains CNTs which are preferentially oriented along the hot-drawing direction, which is evident from the presence of broken CNTs and holes (evidence of pull out) in the fracture surface perpendicular to the hot-drawing direction (also shown in Figure 17a). The fracture surface of the high weight fraction composites, Figure 17b and c, show patterns of CNT alignment similar to the 1wt% CNT/PS sample, verifying that the preferred orientation is also in the direction of hot-drawing. However, the 2wt% CNT/PS sample does show some evidence of agglomeration, Figure 18b, with average agglomerate diameter in the order of 1-2 μm. Moreover, the 4wt% CNT/PS composite fracture surface, shown in Figure 17c and Figure 18c, shows severe agglomeration, with agglomerate diameter in the order of 5-10 μm.

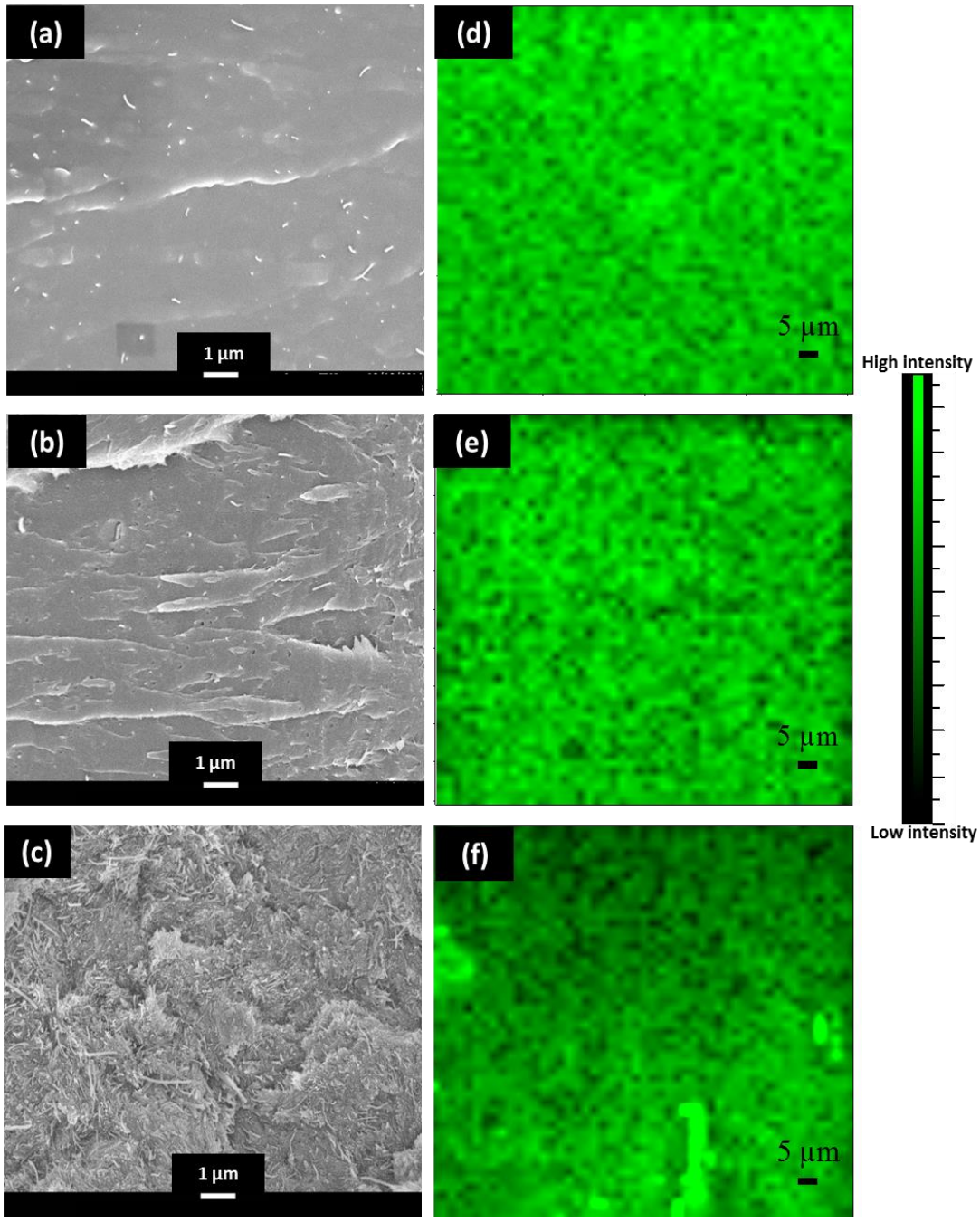

Figure 17. SEM images of fractured surface perpendicular to the stretching direction for (a) 1wt% CNT/PS composite(b) 2wt% CNT/PS composite and (c) 4wt% CNT/PS composite. Raman image of (d) 1wt% CNT/PS composite (e) 2wt% CNT/PS composite and (f) 4wt% CNT/PS composite.

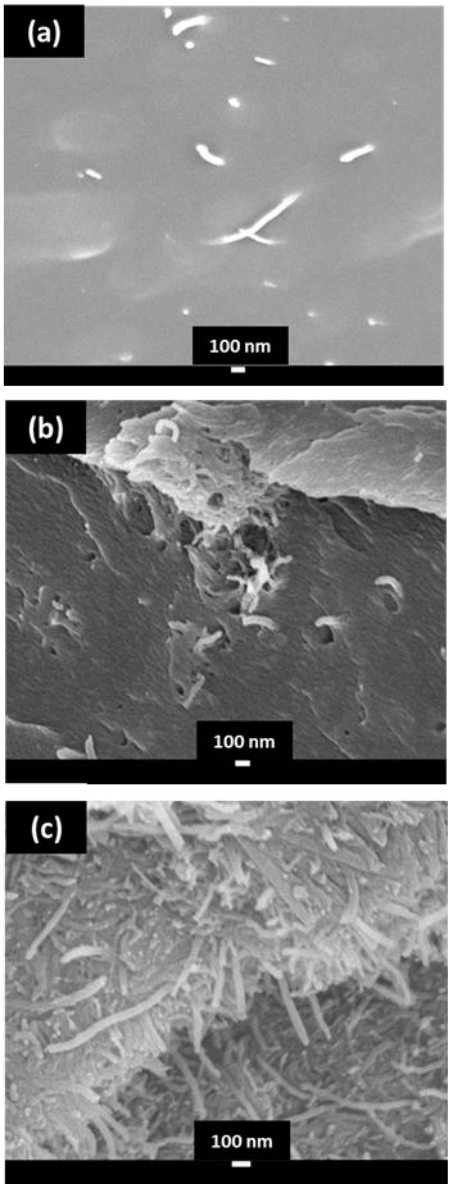

Figure 18. SEM image of fractured surface for a (a) 1wt% CNT/PS (b) 2wt% CNT/PS and (c) 4wt% CNT/PS composite showing evidence of agglomeration as CNT concentration increases.

Evidence of agglomeration is studied quantitatively by Raman imaging, as shown in Figure 17. The 1wt% CNT and 2wt% CNT show similar D-band intensity distribution throughout the scanned area, Figure 17d and e. As pointed out earlier in this chapter, D-

band is a characteristic of CNTs. This suggests that the dispersion of CNTs is very similar. However, the agglomeration observed in the SEM images for the 2wt% CNT composite is not captured in the Raman imaging due to the agglomerate size (~1-2 μm) being below the laser spot size (2 μm). The agglomeration of CNTs is captured in the 4wt% CNT sample image, Figure 17f, which shows spots of much higher intensity than the rest of the scanned area. These spots of high intensity correspond to CNT agglomerates with a diameter of about 5 μm, consistent with SEM observations.

III.B.2. Effect of CNT Agglomeration on Energy Dissipation in Aligned CNT Composites

The dependence of the storage modulus on dynamic strain of the aligned CNT reinforced polystyrene nanocomposites with varying weight fraction is shown in Figure 19. As the weight fraction of CNTs increases from 1wt% to 2wt%, the storage modulus increases by 10.9% from 1777 to 1971 MPa, indicating the reinforcing effect of CNTs. As the weight fraction further increases to 4wt%, the storage modulus of the composite shows a decreases. This decrease can be attributed to the significant CNT agglomeration observed in the SEM images. Within CNT agglomerates, CNT-CNT interactions is weak compared to the rest of composite since there is a deficit of polymer chains to transfer load between CNTs. Therefore, stress in the matrix is not effectively transferred to the CNTs and thus the reinforcing effect is lost.

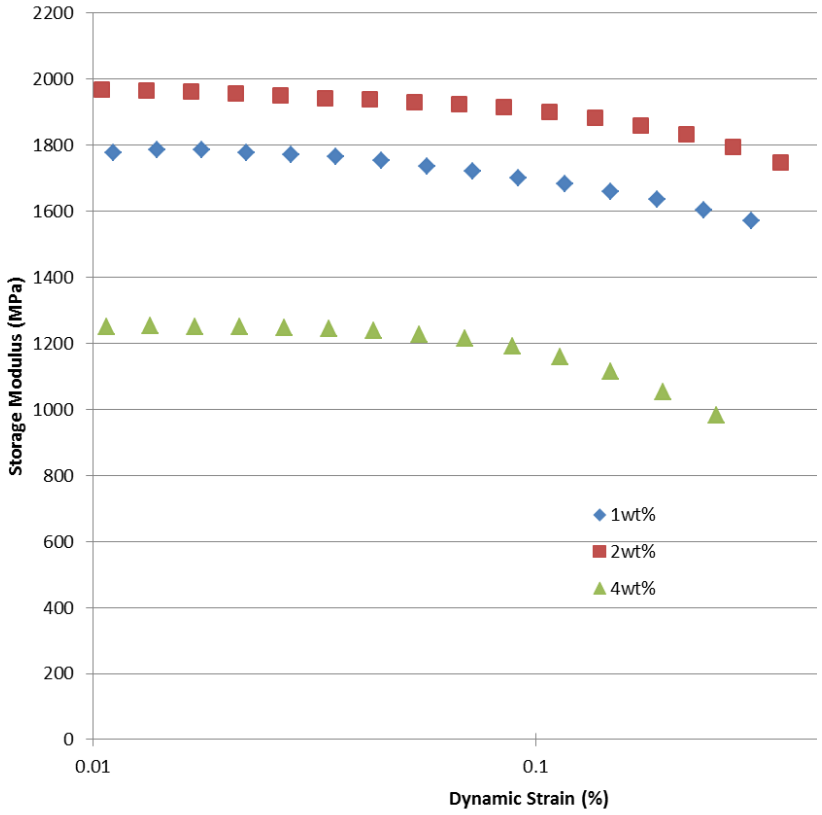

Figure 19. Storage modulus of a CNT/PS composite as a function of dynamic strain for various CNT weight fractions.

The damping in CNT/PS composites shows a strong dependence on weight fraction, as Figure 20. As the weight fraction increases from 1% to 4%, the initial damping measured at low strains increases monotonically from a tan δ of 0.0192 to 0.0667. The enhancement of damping with CNT concentration becomes more pronounced at higher dynamic strain. For instance, at a dynamic strain of ~ 0.2%, the tan δ of the 1 wt.% composite is about 0.0466, compared to the corresponding values of 0.0844 and 0.2109 for the 2 wt.% and 4 wt.% composite at the same strain, respectively. The increase in damping capability of composites with CNT content correlates well with the degree of CNT agglomeration suggesting that CNT-CNT interaction and friction

within agglomerates are a source for energy dissipation in the material. Another possible source of energy dissipation which partly explains the enhanced damping capability of composites with added CNTs is local and nonuniform stress fields that emerges in the composite as a result of the addition of CNTs. While such stress fields were not measured directly in this study, indirect evidence of their development are present in SEM fractographs of the samples, Figure 14, where the fracture surface of the composite increases monotonically with CNT content. The increased roughness of the fracture surface can be considered to be the effect of microcrack formation and stress concentration within the matrix, caused by elastic mismatch between the matrix and CNTs and CNT agglomeration. Stress concentration increases the viscoelastic energy dissipation in the matrix.

The aforementioned energy dissipations in CNT composites, namely the CNT-CNT friction within agglomerates and development of stress concentration sites due to the presence of CNTs, together with CNT-matrix sliding, which was discussed in the previous chapter, lead to the enhancement of damping with CNT content. While identifying the relative contribution of any of these mechanisms to the overall damping is not trivial, the enhancement of initial damping (at low dynamic strain) can only be attributed to CNT-CNT friction and stress concentration within the matrix, since at such low dynamic strains, where damping is nearly independent of dynamic amplitude, CNT-matrix sliding has not yet taken place.

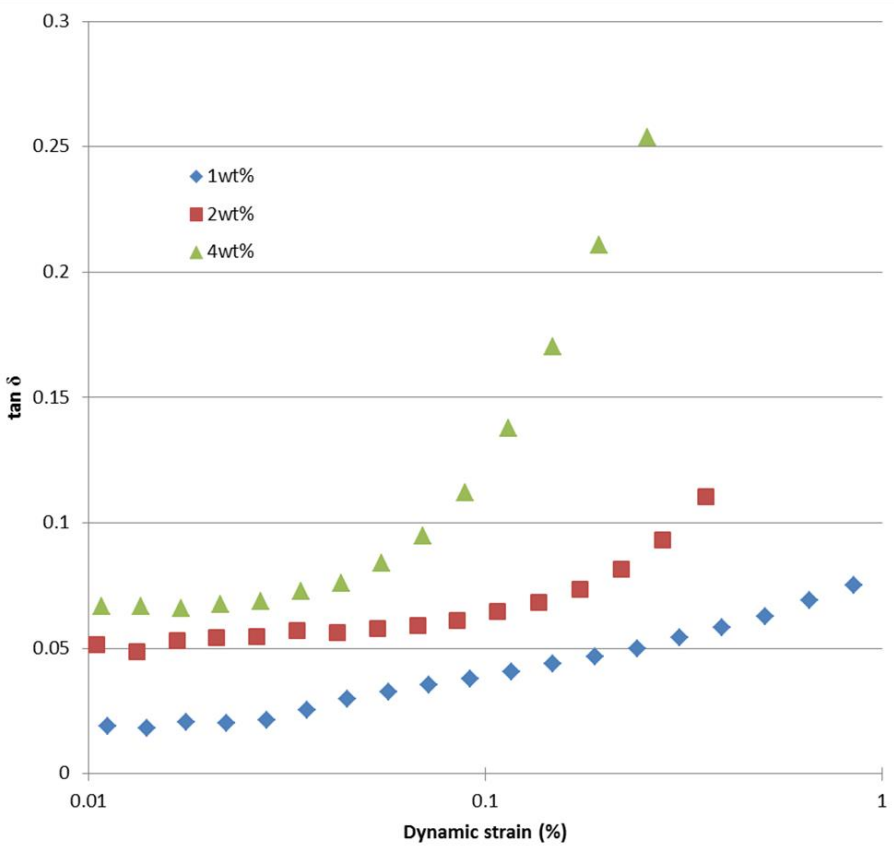

Figure 20. tan δ of a CNT/PS composite as a function of dynamic strain for various CNT weight fractions.

III.B.3. Developing CNT Composites with Randomly Oriented CNTs

The fracture surface of the randomly oriented CNT sample is shown in Figure 21. As shown in the figure, by avoiding the hot-drawing step composites with randomly oriented CNTs can be developed. In addition, the distribution of the CNTs is not entirely uniform throughout the sample. The samples contain areas of agglomeration, Figure 21b, with agglomerate diameter of ~2-5 μm. Similar information can be inferred from Raman imaging of the sample, Figure 22. As shown in the figure, the D-peak intensity

distribution, a characteristic of CNTs has a rather uniform distribution, especially when compared to highly agglomerated cases such as the 4 wt.% aligned CNTs (Figure 17). In addition, some high intensity spots, with diameter of about 5 μm, are also captured in the Raman imaging. These high intensity spots correspond to the location of agglomerates in the samples, in line with SEM observations. A comparison between the CNT agglomeration in the hot-drawn (Figure 17) and samples processed with no hot-drawing (Figure 21), points to the contribution of hot-drawing in disentangling the CNT agglomerates and leading to the development of more uniformly dispersed CNTs within the matrix.

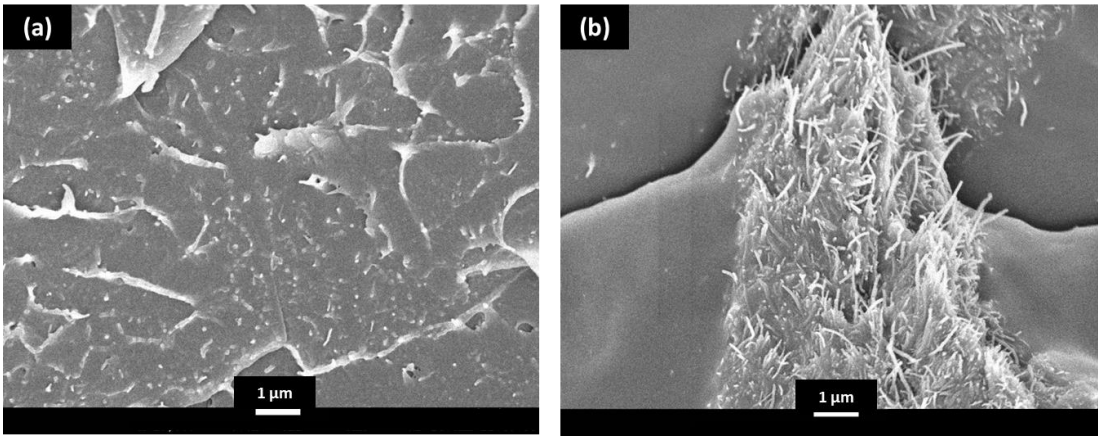

Figure 21. SEM images of the fracture surface of a 1wt% CNT/PS composite with randomly oriented CNTs showing a) misorientation and b) agglomeration.

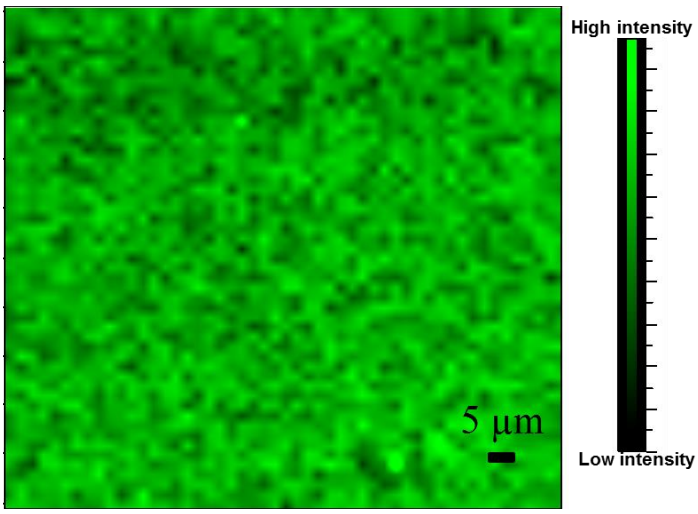

Figure 22. Raman image of a 1wt% CNT/PS composite with randomly oriented CNTs.

III.B.4. Effect of CNT Random Orientation on Energy Dissipation

The comparison in damping capability, quantified as tan δ, between randomly oriented and aligned CNT composites is shown in Figure 23. Even at low strains, the tan δ of randomly oriented CNTs is observed to increase with dynamic strain. This is in contrast to the aligned CNT composites, in which within a dynamic strain of 0-0.028%, tan δ remained nearly unchanged (Figure 23). In addition, throughout the range of dynamic strains studied, the damping of the randomly oriented CNT samples increased more rapidly with dynamic strain compared to the aligned samples. When compared to aligned CNT composites with the same CNT concentration, the CNT-CNT friction within CNT agglomerates (slight agglomeration observed in the material, Figure 21) is likely to be responsible for the sharp increase in damping in randomly oriented CNTs. In addition, the misorientation of the CNTs with respect to the loading direction can lead to

additional energy dissipation mechanisms, such as matrix tearing, within the composite. Observation of the fracture surface, Figure 21a, shows signs of matrix tearing as compared to the aligned fracture surface, Figure 17a, which shows a smooth fracture surface.

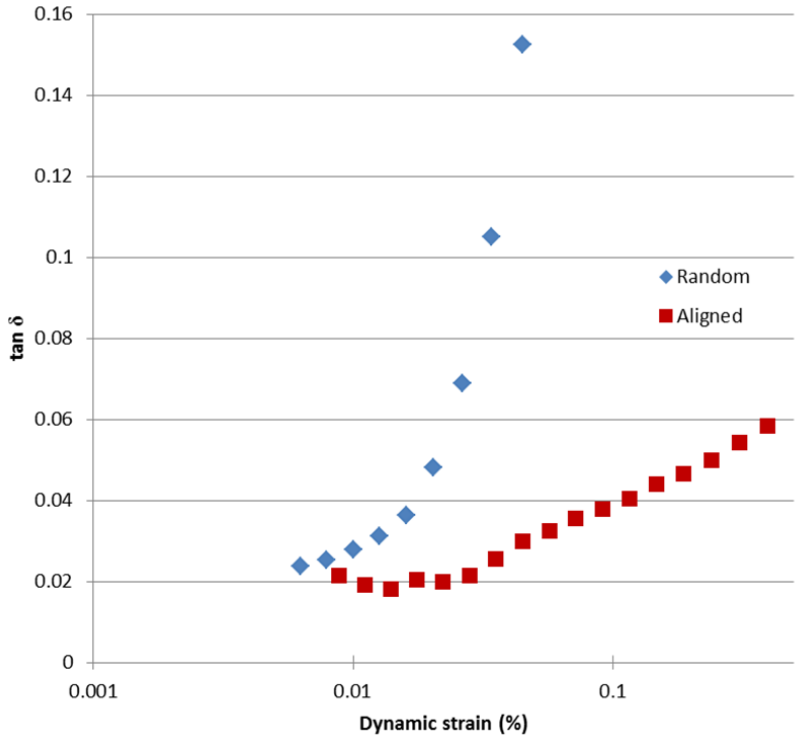

Figure 23. tan δ of a 1wt% CNT/PS composite as a function of dynamic strain for both composite samples with aligned and randomly oriented CNTs.

III.C. Conclusion

The effect of CNT orientation and distribution on energy dissipation within the nanocomposite was studied, with a focus on random distribution and agglomeration. Experimental characterization results were presented which point to the enhancement in damping due to misorientation and non-uniform CNT distribution. As CNT

concentration increases, the tendency of the CNTs to agglomerate also increases. This leads to the formation of an additional damping mechanism within the composite, relative slippage between CNTs. The effect of frictional dissipation within the CNT agglomerates is evident in the significant increase in damping at a concentration of 4wt.%, which showed significant evidence of agglomeration in SEM images.

In addition, randomly distributed CNT composites where characterized. The damping response shows significant improvement as compared to the uniaxially aligned CNT composites. The random distribution of the CNTs leads to not only increased CNT-CNT interaction, but also introduces complex stress fields within the composite, which can eventually lead to enhanced damping in the matrix due to the viscoelastic nature of the polymer.

CHAPTER IV

THERMALLY ACTIVATED ENERGY DISSIPATION IN NANOCOMPOSITES

Most polymers – thermoplastics and thermosets - show a significant increase in tan δ with temperature, such as polystyrene (PS), shown in Figure 24a. The significant rise in damping capability with temperature of polymers originates from thermally activated molecular relaxations [55]. By utilizing the remarkable temperature sensitivity of the viscoelastic properties of a polymer matrix, the capability of composites to dissipate mechanical energy can be significantly enhanced. Specifically, the dependence of the viscoelastic properties of a polymer with temperature can be exploited to dampen undesired mechanical vibrations. Typically, the highest energy dissipation in a polymer matrix, measured as the ratio of the loss modulus to storage modulus (known as tan δ), occurs near the glass transition temperature, Tg, which corresponds to a state where polymer chains have gained sufficient thermal energy to initiate bond rotation [55]. Even though, the tan δ of polymers increases by a few orders of magnitude near Tg compared to a glassy state, the increased damping capability is achieved at a decrease in stiffness, evident in a sharp decrease in storage modulus. For example in Figure 24a, an order of magnitude increase in polystyrene comes at a loss in storage modulus of 42%. However, the drop in storage modulus scales inversely with the degree of crystallinity in the polymer in semi-crystalline polymers. That is primarily due to the fact that the amorphous phase has a glass transition temperature below the melting temperature of the crystalline phase. Therefore, energy dissipation can be significantly enhanced through

polymer relaxation of the amorphous phase near its Tg, while the crystalline phase will retain a considerable portion of the initial stiffness. However, as the temperature reaches the glass transition of the amorphous phase, the crystalline phase may impede polymer relaxation in the amorphous phase, thus limiting the energy dissipation of the material.

To better illustrate the role of crystalline phase in loss of storage modulus near Tg the variations of the storage modulus vs. tan δ is made between PEEK (semi-crystalline thermoplastic) and polystyrene (amorphous thermoplastic). The storage modulus is normalized with respect to values at room temperature, as shown in Figure 24b. As shown in the figure, for a 10-fold increase in tan δ, the reduction in storage modulus is less drastic in semi-crystalline PEEK, as compared to amorphous PS. In addition, semi-crystalline PEEK maintains a minimum storage modulus of about 10% of the room temperature storage modulus, while the PS shows a much lower retained modulus. Moreover, as shown in the same figure a comparison of the variation of storage modulus with tan δ between PEEK and epoxy (thermoset with high degree of crosslinks) reveals that even chemical crosslinks between chains is not nearly as effective in maintaining the modulus near Tg as the crystalline phase.

In this chapter, we studied the microstructure-mechanical property relationships in semi-crystalline polymers. Our study was focused on Poly ether ether ketone (PEEK), mainly because high degrees of crystallinity of ~40% can be achieved in this material, limiting the decrease of storage modulus, especially at temperatures close to Tg where damping capability of the material is significantly enhanced. As a result of the preservation of mechanical properties at high temperatures, in addition to excellent

thermal stability and high-temperature resistance, the possible applications of this polymer expand throughout many industries, including electrical insulation, automotive bearings and piston skirts, industrial oil valves and seals, and flexible circuit boards [56]. Therefore, the study performed here has significant industrial relevance. This work will include the manipulation of the crystalline structure of polymers via annealing and microstructural characterization, followed by dynamic mechanical analysis. A study on the effect of annealing temperature and annealing time on the crystalline microstructure and degree of crystallinity was performed. In addition, the effect of the microstructure on the mechanical properties, specifically the storage and loss modulus, was pursued. Following the characterization of the neat polymer, CNT/PEEK composites were fabricated with feedback from the results obtained for the neat PEEK study. The fabrication parameters were chosen such that they provided the "most desired" PEEK microstructure, yielding increased damping with minimal decrease in stiffness. The CNT/PEEK study focused on analyzing the effect the presence of the CNT in the polymer matrix had on both the overall crystallinity and damping in the composite.

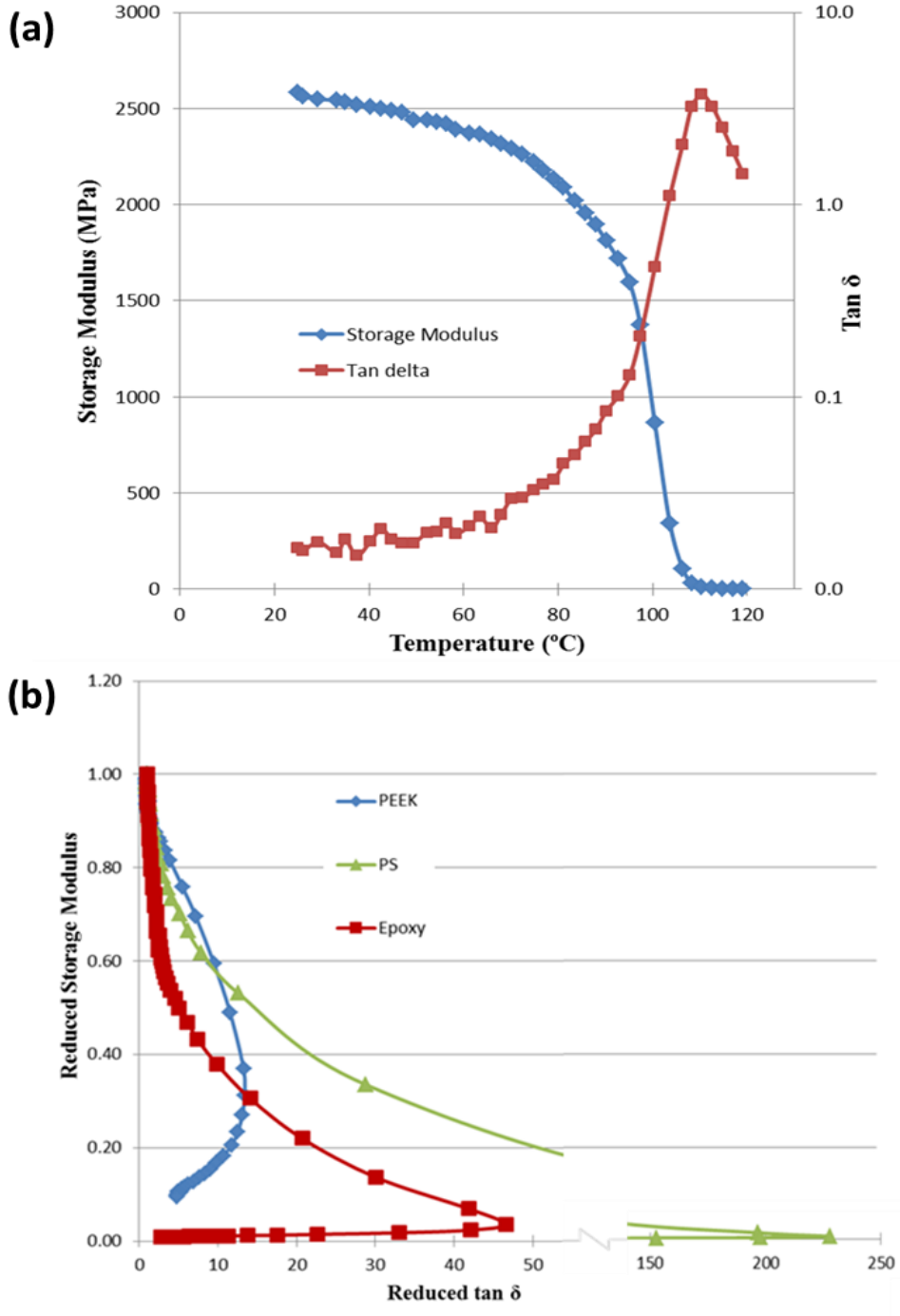

Figure 24. (a) Storage modulus and tan δ as a function of temperature for polystyrene (PS) (b) Comparison of normalized storage modulus vs normalized tan δ for polystyrene (PS), poly ether ether ketone (PEEK), and epoxy. Storage modulus is normalized by the storage modulus at room temperature and the tan δ is normalized by the room temperature tan δ.

IV.A. Experimental

IV.A.1. Processing

Poly ether ether ketone (PEEK) 450G was purchased in powder form from Victrex® and provided to us by Dr. Hung-Jue Sue at Texas A&M University. The PEEK powder was first dried in an oven at 150°C for 3 hrs in order to remove moisture. The powder was then cast into an aluminum mold and placed in a furnace at 400°C (above the crystalline phase melting temperature of 343°C) for 5 minutes. The cast polymer was immediately quenched in a water bath after removal from the furnace. The purpose of the quenching was to prevent the PEEK polymer from further crystallizing and to keep the crystallization at a minimum. The quenched polymer was then annealed at different temperatures, 175, 200, and 240°C for 1 min. A portion of the quenched samples were characterized without further processing, while the rest were annealed at 240°C for 1, 10 and 120 minutes to further increase the crystallinity.

In addition to neat PEEK samples, PEEK-CNT composites were also fabricated to investigate the effect of CNTs in morphology of PEEK and thermomechanical properties of the composite, mainly vibration damping. To this end, pristine HiPCO single-walled carbon nanotubes (SWCNTs) were used. The PEEK powder was mixed with 1wt% SWCNT powder to form a homogeneous mixture. The mixture was then cast and melted using the same procedure used with the neat PEEK samples. Nanocomposite samples were then annealed at 240 °C for 1 minute.

IV.A.2. Material Characterization

Differential scanning calorimetry (DSC) was conducted on all samples to obtain the transition temperatures and the degree of crystallinity. A temperature sweep from 25°C to 375°C at a heating rate of 10°C/min was performed. The degree of crystallinity was measured as the ratio of the difference in enthalpy of fusion at the melting temperature and the enthalpy of crystallization and the enthalpy of fusion of the totally crystalline polymer [57]. The enthalpy of fusion of the totally crystalline PEEK is taken as 130 J/g [58].

The energy dissipation capability of neat PEEK and PEEK-CNT composites, as the ratio of the loss to storage modulus (tan δ), was measured via Dynamic Mechanical Analysis (DMA) using a TA Instruments RSAIII DMA. A temperature sweep from 25°C to 200°C at a rate of 10 °C /min at a constant strain of 0.01% was performed in order to study the dependence of the viscoelastic response on temperature.

IV.B. Results and Discussion

IV.B.1. Crystallization of Poly Ether Ether Ketone

The effect of annealing time at 240°C on thermal properties of neat PEEK samples was studied via scanning differential calorimetry (DSC), Figure 25. With no annealing, there is a clear indication of a glass transition at 145.8°C. As annealing time is increased from 1 minute to 120 min, Tg increases monotonically from 159.3°C to 160.5°C. The dependence of Tg with annealing time, measured via DSC, is in agreement with the DMA measures of Tg as the temperature corresponding to the maximum tan δ, Figure

28. In addition, samples which were not annealed show an exothermic peak at 174°C, corresponding to the crystallization temperature. This peak disappears after 1 minute of annealing, indicating rapid crystallization of PEEK during such short periods of annealing.

The first endothermic peak is observed at ~252°C for annealing times above 1 minute. This peak shifts to higher temperatures and increases in magnitude as the annealing time is increased. The second endothermic peak, which has considerably stronger magnitude than the first one, occurs at a temperature of ~343°C. These two peaks correspond to the melting of two types of crystalline structures within PEEK and are referred to herein as minor and major endothermic peaks. The degree of crystallinity corresponding to each crystalline phase calculated from DSC curves is summarized in Table 2, in which the second crystalline phase increases from 1.56% to 2.48% for an annealing time of 10 and 120 min, respectively.

Table 2. Degree of crystallinity for PEEK annealed at different temperatures for varying durations.

Material	Annealing conditions	% crystallinity (first phase)	% crystallinity (second phase)	Tg (°C)	Max tan δ	E' at RT (MPa)
PEEK	No annealing	14.62	0	145.8	1.596	1890.9
	175°C for 1min	18.52	0	144.3	0.713	1907.7
	200°C for 1min	31.58	0	157.0	0.251	2168.4
	240°C for 1min	31.88	0	159.3	0.199	2277.8
	240°C for 10min	31.88	1.56	159.6	0.177	2278.5
	240°C for 120min	30.81	2.48	160.5	0.165	2538.0
1wt%CNT/ PEEK	240°C for 1min	25.5	0	152.6	0.311	2049.1

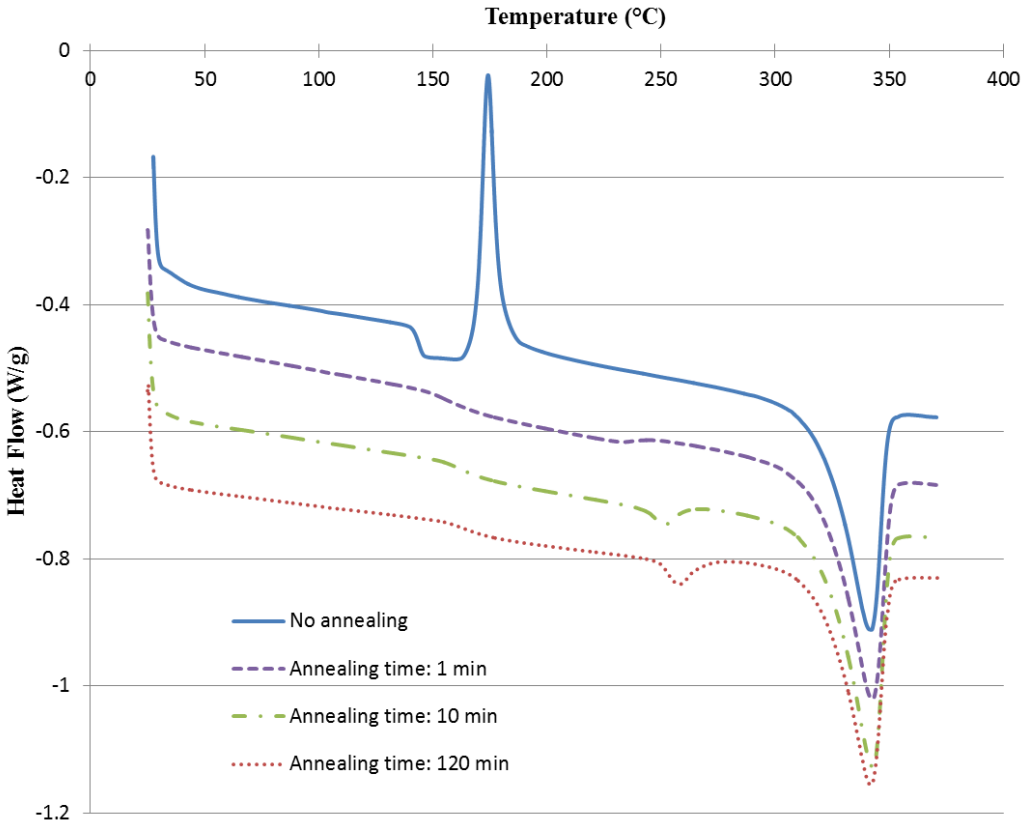

Figure 25. DSC results for neat PEEK samples with different annealing times at 240°C. (data was offset for clarity).

Considering the evolution of crystallinity and the formation of the minor crystalline peak (at 252°C), it is suggested that the minor crystalline phase (first peak) forms within the regions of amorphous material trapped within the lamellae, thus leading to two distinct crystal populations [58-60]. In other words, the major endothermic peak develops before the minor peak, as can be inferred by a comparison between the DSC curves of the not annealed and 1-min annealed samples, which is in line with prior studies in literature [58-60]. In order to avoid the complications related to interactions

between two crystalline phases in interpreting DMA experiments, samples with 1 minute annealing times were chosen for this study in which no traces of the minor peak can be found (Figure 25).

The DSC analysis for PEEK as a function of annealing temperature with a time duration of 1 minute is shown in Figure 26. As observed in the figure, the minor endothermic peak representing the secondary crystalline phase is not present when annealing with a duration of 1 minute, regardless of annealing temperature. The growth of the secondary crystalline phase is suppressed at small annealing times (1 minute). The degree of crystallization increased monotonically from 14.62% for the sample with no annealing to 31.88% for the sample annealed at 240°C. In addition, the Tg increased from 145.8°C to 159.3°C between the not annealed and samples annealed at 240°C, indicating that an increased restriction on the movement of amorphous polymer by the presence of the growing crystalline phase.

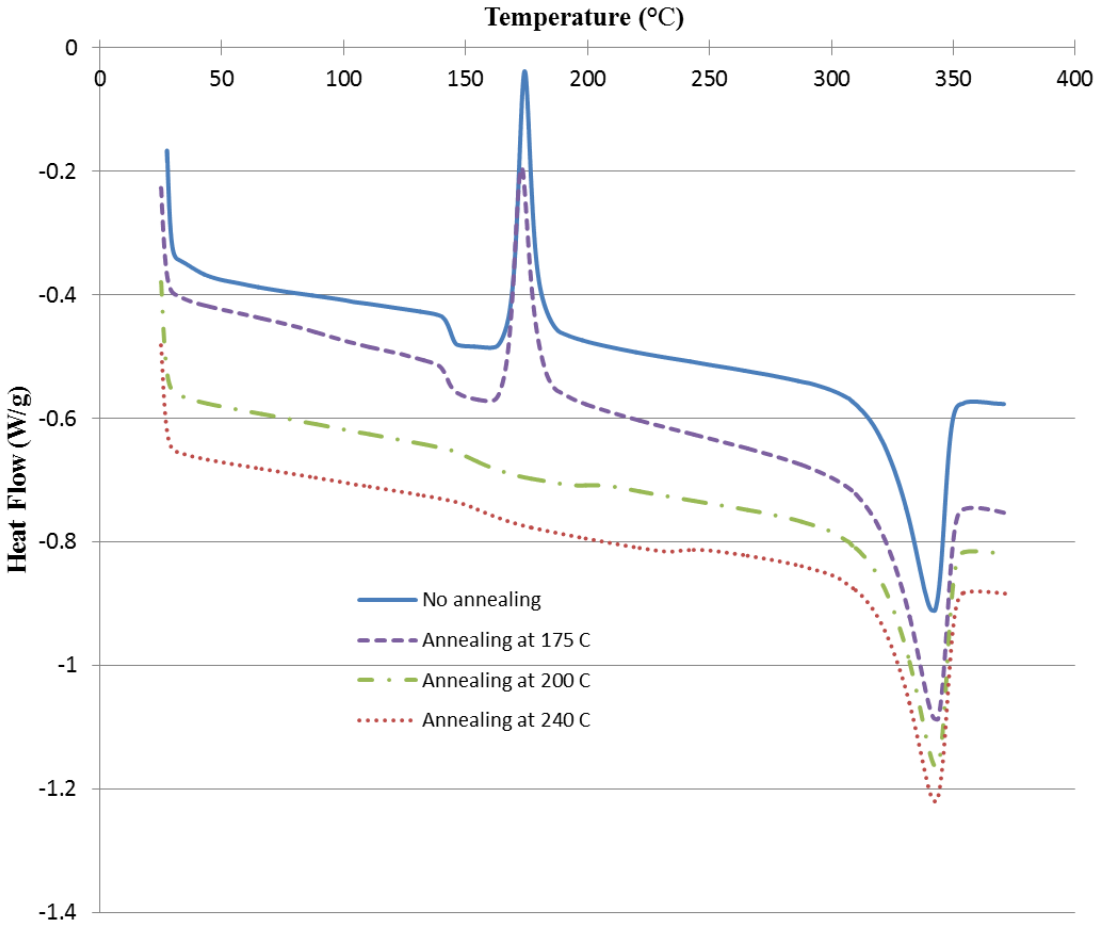

Figure 26. DSC results for neat PEEK samples with different annealing temperatures for a duration of 1 minute. (data was offset for clarity).

IV.B.2. Crystallization of PEEK in PEEK/CNT Composites

The effect of CNTs on the formation of the crystalline phase of PEEK in PEEK/CNT composites was studied via DSC, as shown in Figure 27. As observed in the figure, the addition of CNTs results in a significant loss in the intensity of the crystal melting peak. This suggests that the crystallization is considerably suppressed with the presence of CNTs. In fact, the degree of crystallization decreased from 31.9% in the neat

PEEK to 25.5% in the 1wt% CNT/PEEK composite. This loss of crystallinity with the addition of CNTs is likely due to the fact that CNTs restrict the growth of lamellae and thus the growth of the crystalline phase. The reduction in crystallinity also led to the decrease in the Tg from 160.5°C to 152.6°C. The Tg for the 25.5% crystalline composite falls between the values of Tg observed for the neat PEEK with crystallization of 18.52% and 31.58%, as expected.

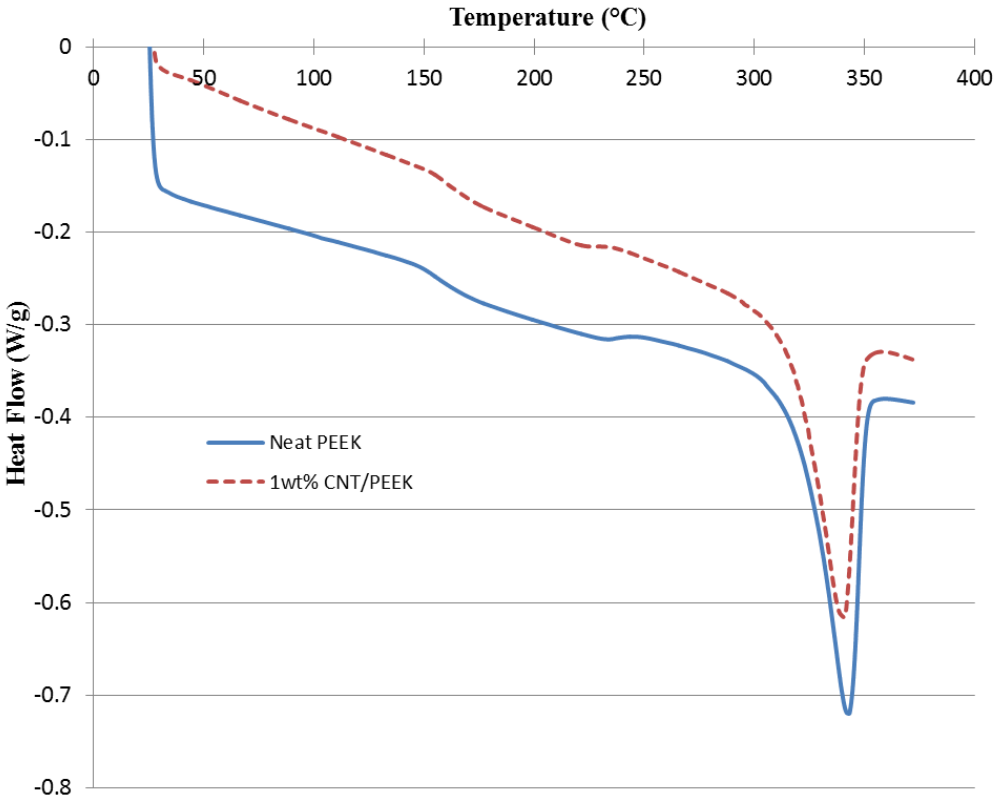

Figure 27. DSC results for neat PEEK and 1wt%CNT/PEEK samples with annealing temperature of 240°C for a duration of 1 minute. (data was offset for clarity).

IV.B.3. Dependence of Viscoelastic Response of PEEK on Temperature

The dynamic mechanical properties of the neat PEEK and CNT/PEEK composite samples were also studied as a function of temperature. As shown in Figure 28, at the annealing temperature of 240°C, the storage modulus measured at room temperature increases from 2277.8 MPa to 2538.0 MPa with increasing annealing time from 1 min to 120 min. This is likely due to the higher stiffness of the crystalline phase, which grows with annealing time, as shown in the DSC results of Figure 25.

Moreover, with no annealing, the polymer sample shows a significant drop in storage modulus at the Tg followed by an increase in modulus with temperature. This increase corresponds to the initiation of crystallization in the polymer. The tan δ shows a large peak for the sample with no annealing (magnitude of 1.596). However, the magnitude of the peak is significantly reduced with the increase in degree of crystallization (due to annealing) as a result of less available amorphous regions and the increasing movement constraints imposed on them by the growing crystalline phase, as summarized in Table 2. In the annealed samples, the tan δ does not significantly decrease with annealing time, but the Tg corresponding to maximum tan δ shifts to higher temperatures, again supporting the notion of restricted movement of the polymer chains by the presence of the crystalline phase.

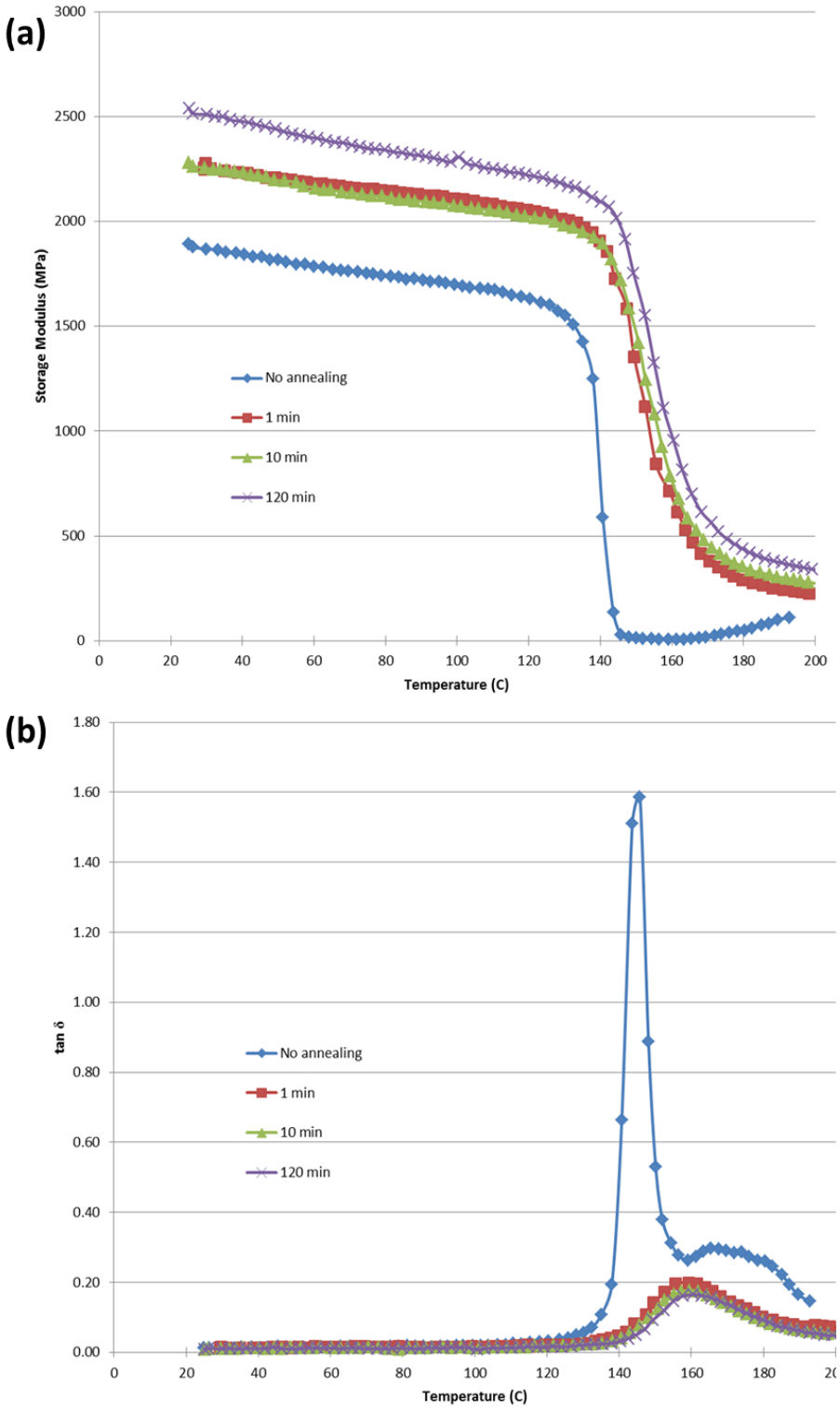

Figure 28. DMA results for neat PEEK samples for various annealing times at 240°C.

In addition, as shown in Figure 29, the storage modulus measured at room temperature increases monotonically with annealing temperature from 175°C to 240°C. The maximum tan δ does show a decrease with annealing temperature and also shows a shift in temperature, with the highest annealing temperature yielding the highest temperature at maximum tan δ (Tg corresponding to DMA experiments).

IV.B.4. Viscoelastic Response of PEEK/CNT Composites vs. Temperature

As mentioned previously, the degree of crystallinity of PEEK decreases with the introduction of CNTs into the PEEK matrix. This result is also evident in the decrease in storage modulus at room temperature from 2277.8 MPa to 2049.1 MPa, Figure 30. The value of storage modulus of the composite with a degree of crystallinity of 25% does fall between that of the neat PEEK at 18.52% and 31.58% crystallinity, suggesting the CNTs do not contribute to the overall composite storage modulus. This might be the case due to agglomeration of CNTs within the composite evident from SEM images, Figure 31, weak interactions between CNTs and PEEK, or random alignment of CNTs. On the other hand, the tan δ of the CNT composite, Figure 30b, shows a much broader curve as compared to the neat PEEK sample. The reason behind the broadening of this peak is hypothetically explained as follows.

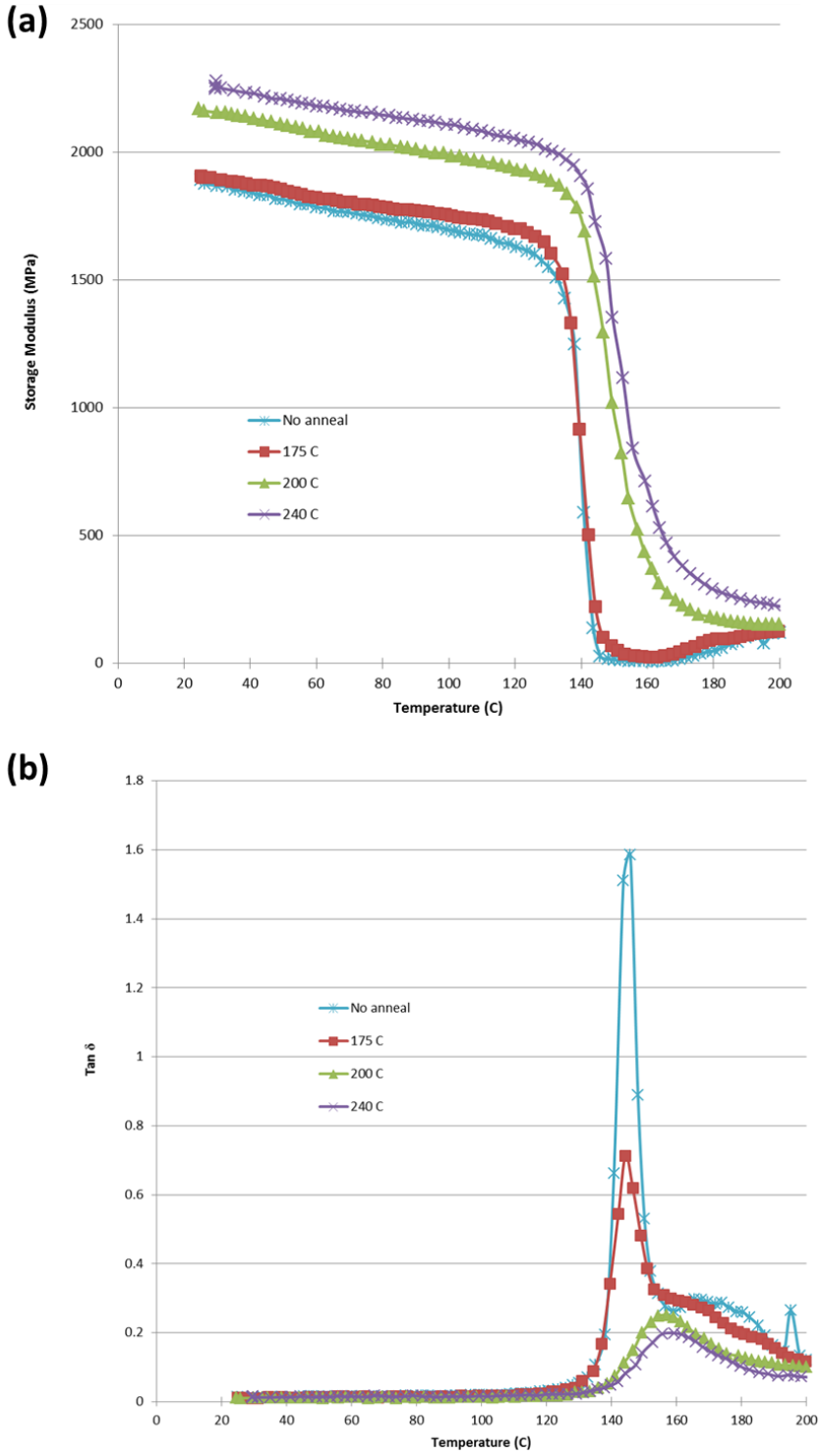

Figure 29. DMA results for neat PEEK samples as function of annealing temperature for a 1 minute duration.

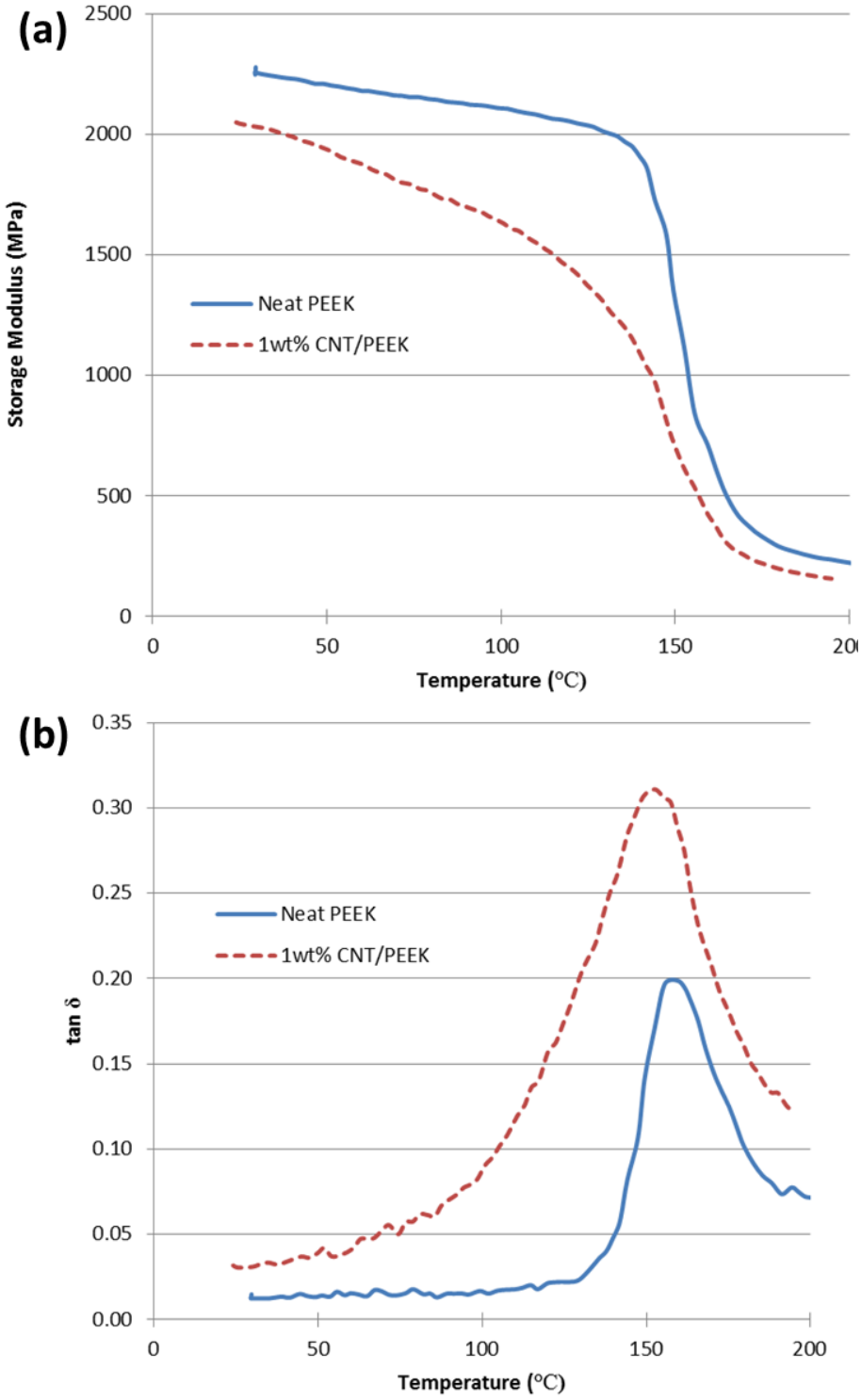

Figure 30. (a) storage modulus and (b) tan δ comparison between neat PEEK and a 1wt% CNT/PEEK composite.

According to [61], a nanotube/semi-crystalline polymer composite can consist of four regions: 1) a mobile amorphous phase 2) a crystalline phase 3) a rigid amorphous phase and 4) an immobilized amorphous phase near the surface of the CNT. The neat PEEK polymer studied here consists of a mobile amorphous phase (evident in the presence of a Tg), a crystalline phase (evident in the melting peak observed in DSC), and a rigid amorphous phase (evident in the formation of a secondary crystalline phase from the trapped amorphous regions within the lamellae). The introduction of the CNTs into the PEEK matrix can further contribute to a rigid amorphous phase, such that some polymer chains are trapped between agglomerates. The trapping of polymer chains between agglomerates will contribute to the restriction of movement, with a broad range of lost degrees of mobility of these chains, and thus result in a broader tan δ, as has been reported in literature [62-64]]. It has also been reported that the presence of CNTs can lead to two tan δ peaks, one for the mobile amorphous phase and the other for the restricted amorphous phase [64, 65]. In the case studied here, it is possible that there exists a restricted amorphous phase that can lead to a delayed motion of the polymer chains with a tan δ peak very close to that of the mobile amorphous peak. This would lead to the formation of two tan δ peaks combining to form a more broadened peak, which will result in the peak spreading over a larger temperature range, as seen in Figure 30b, and as has been reported before for composites with a high concentration of CNTs [64]. In addition, broad glass transition peaks have been attributed to restriction of movement of polymer chains [64, 66, 67] and to enhanced efficiency of load transfer from matrix to filler, which results in more energy loss and dissipation [68]. In this

study, it is possible that as the polymer around the agglomerates relaxes with temperature, the interaction between the polymer and CNTs (in terms of vdW) increases as the polymer chains conform to the CNTs. This might be the case since it has been shown that vdW interfacial interaction between a CNT and a polymer matrix is enhanced with temperature [69]. This promotes an increase in the load transfer between the filler and matrix and thus would enhance the relative movement of CNTs within the agglomerate, leading to frictional energy dissipation between CNTs. This dissipation will further enhance the energy dissipation of the composite and thus the loss modulus increases, contributing also to the broadening of the tan δ peak. In addition, the loss in crystallinity due to the presence of the CNTs will also lead to the broadening of the peak towards lower temperatures, since a lower crystallinity means a decrease in the glass transition temperature.

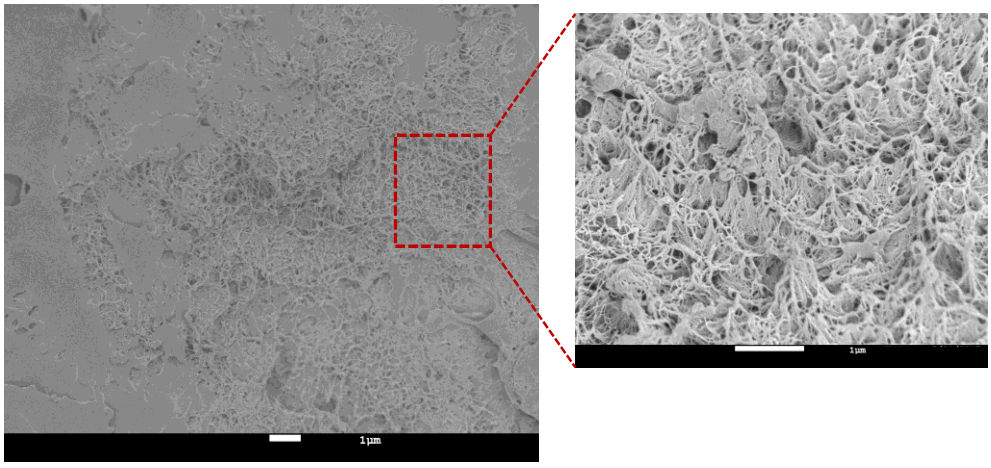

Figure 31. SEM image of 1wt% CNT/PEEK composite fracture surface showing CNT agglomeration.

IV.C. Conclusion

The temperature dependent viscoelastic properties of a PEEK thermoplastic polymer were studied. The degree of crystallinity was controlled by varying the annealing temperatures. In addition, the presence of a secondary crystalline phase was suppressed by controlling the duration of annealing. The neat PEEK polymer response shows an increase in loss modulus with temperature while still maintaining significant storage modulus. The addition of SWCNTs to the PEEK polymer shows a decrease in the crystallization. However, the presence of CNTs increases the energy dissipation significantly. Therefore, not only is the dissipation enhanced by the presence of CNTs, but the electrically conductive network of CNTs allows for resistive heating of these particles to trigger the polymer relaxation and thus further enhance the energy dissipation.

CHAPTER V

EXPERIMENTAL CHARACTERIZATION OF ACTIVE DAMPING IN NANOCOMPOSITES

Polymers typically show viscoelastic behavior at sufficiently low strains, which can be used to damp undesired vibrations. As discussed in the previous chapter, the energy dissipation capability of polymers, identified as the ratio of the loss to storage modulus, is highly sensitive to temperature. This temperature sensitivity of viscoelastic properties in polymers can be utilized to significantly increase the vibrational damping in structures, with the highest energy dissipation typically occurring near the glass transition temperature, as discussed previously. The source of this energy dissipation is chain relaxation, which scales with chain mobility and thermal energy stored in the material.

In addition, as discussed in the previous chapter, similar to neat polymers, CNT reinforced polymer composites demonstrate highly temperature sensitive energy dissipation capability, rooted in the thermally enhanced chain relaxation of the base polymer and interfacial energy dissipation due to relative slippage between CNTs and polymer. The latter mechanism was discussed in detail in Chapter II. In addition to introducing new energy dissipation mechanisms (interfacial friction), the electrically conductive network of CNTs within the nanocomposite can also be utilized to input heat to the nanocomposite, as a means to enhance chain mobility and energy dissipation. In other words, the CNT network allows for resistive heating of these particles, through

which heat is transferred to the matrix. Joule heating of these fillers can result in local heating of the matrix, to near the glass transition temperature where polymer damping is most effective, thus allowing for the viscoelastic properties of the matrix to additionally contribute to damping. As a result, the energy dissipation in CNT/polymer nanocomposites can be actively controlled and tuned via external electric stimulus.

This method of heating nanocomposites, Joule heating, which is applied for the first time to enhance energy dissipation, is similar to the methods used to trigger shape memory behavior in programmed shape memory polymers [70]. Since the generated heat is transferred to the matrix through the surface of CNTs, compared to conventional lab-scale methods such as insertion of the sample into the heat bath (e.g., oven), the high surface to volume ratio of the nanoscale reinforcements will accelerate the damping of the matrix by facilitating the heat transfer.

This chapter will focus on active damping of the CNT/PEEK nanocomposites. As described above, active damping is defined here as the modulation of energy dissipation capability, via an input of an electric signal. The temperature dependent viscoelastic mechanical properties of these nanocomposites were studied in the previous chapter. The goal here is to experimentally test the hypothesis that the damping in a polymer based composite can be actively and reversibly enhanced via an electrical signal, with the intended damping mechanism being the thermally activated relaxation of the matrix surrounding the nanoparticle. The validation of this hypothesis requires the achievement of sufficiently uniform temperature in the sample, both locally and globally, which will be evaluated in detail in this chapter and the following chapter.

V.A. Experimental

V.A.1. Processing

The fabrication procedure follows that presented in Chapter IV and is summarized below. Pristine HiPCO single-walled carbon nanotubes (SWCNTs) and PEEK were mixed in powder form to obtain a homogeneous mixture with a concentration of 1wt% CNT. The mixture was then cast and melted at 400°C for 5 minutes followed by quenching in a water bath. Nanocomposite samples were then annealed at 240 °C for 1 minute. Copper wire electrodes were attached to the sample ends using high purity silver paint, thus minimizing joule heating at the electrode-sample contact point.

V.A.2. Material Characterization

The active energy dissipation capability PEEK/CNT composites, quantified as the ratio of the loss to storage modulus, were measured via dynamic mechanical analysis (DMA) at a constant dynamic strain using a TA Instruments RSAIII DMA at various input power. The test set-up, shown in Figure 32, consists of the following. The sample was gripped to the DMA tensile grips with the wire electrodes extending out of the sample. The wire electrodes were attached to an Agilent 33220A waveform generator and a TREK 609E-6 high voltage amplifier using alligator clips. Joule heating of the composite sample consisted of applying a sinusoidal wave signal at 1 kHz at a specific voltage until a steady state temperature on the sample was reached. The magnitude of the average temperature on the sample was controlled via input voltage. The applied voltage, in the range of 0 to 143 V, corresponded to an input power varying form 0-

0.035 W/mm^3. The electrical resistance of the sample, with the electrodes attached, was measured via a 2-point method using a multimeter. The temperature of the sample was monitored during dynamic testing using a Testo 885 Thermal Imager. Once the steady state temperature was reached, DMA test was performed to obtain the storage and loss modulus of the composite at the applied voltage. The voltage was then increased and the damping properties measured after reaching a steady state temperature. The thermal equilibrium, steady state, is achieved when the input heat to the sample through Joule heating is balanced by the heat loss mainly through convection. The possibility of the thermal degradation of the sample was studied by comparing the viscoelastic properties of the sample before and after Joule heating, at zero input power.

V.B. Results and Discussion

V.B.1. Active Damping in a CNT/PEEK Composite via Joule Heating

The change in total input power with voltage for the 1wt% CNT/PEEK sample is shown in Figure 33. The input energy to the system was estimated as I^2R, where I is the input current and R is the resistance of the sample.

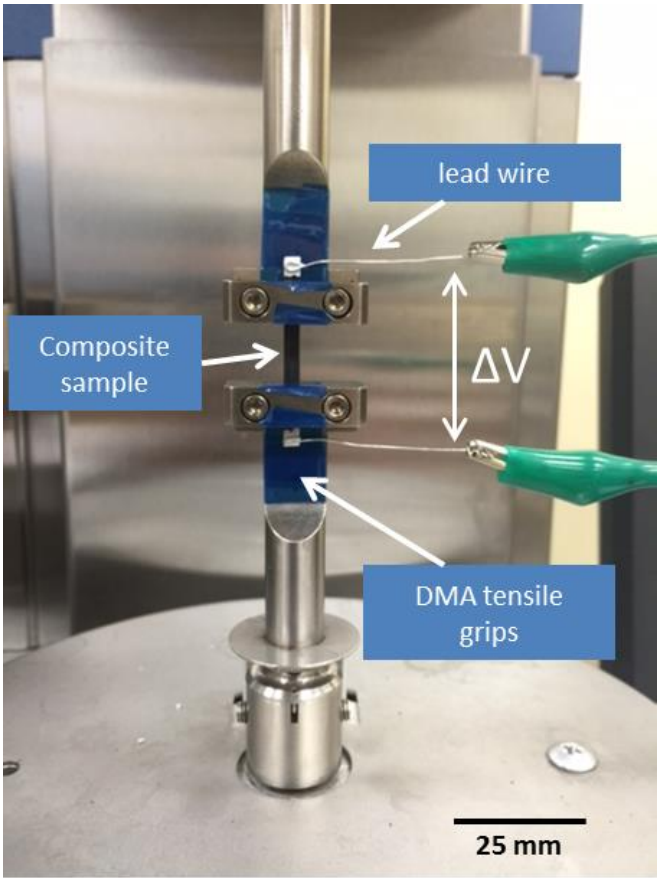

Figure 32. Test set-up showing composite sample gripped to the DMA tensile testing machine. Also copper wire leads for applying the potential difference and thus joule heating the composite are shown in the figure.

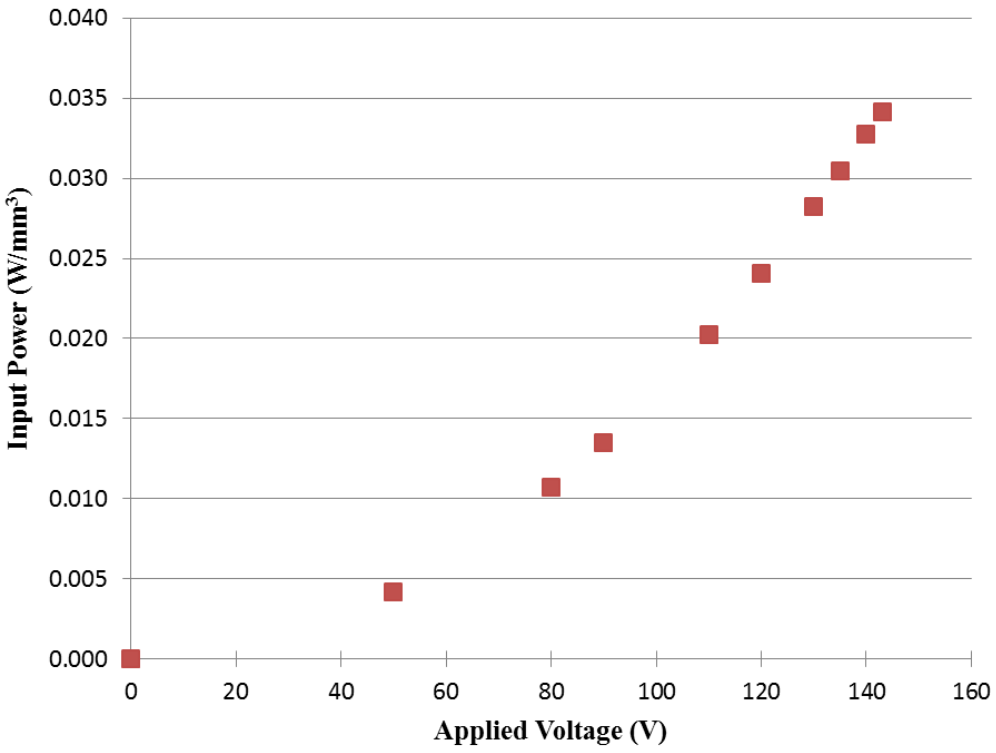

Figure 33. Applied voltage vs input power of a 1wt% CNT/PEEK sample.

The average temperature on the surface of the sample measure with the thermal imager as a function of the input voltage is shown in Figure 34. The average temperature of the sample measured from thermal graphs scales nearly linearly with applied power (Figure 34).

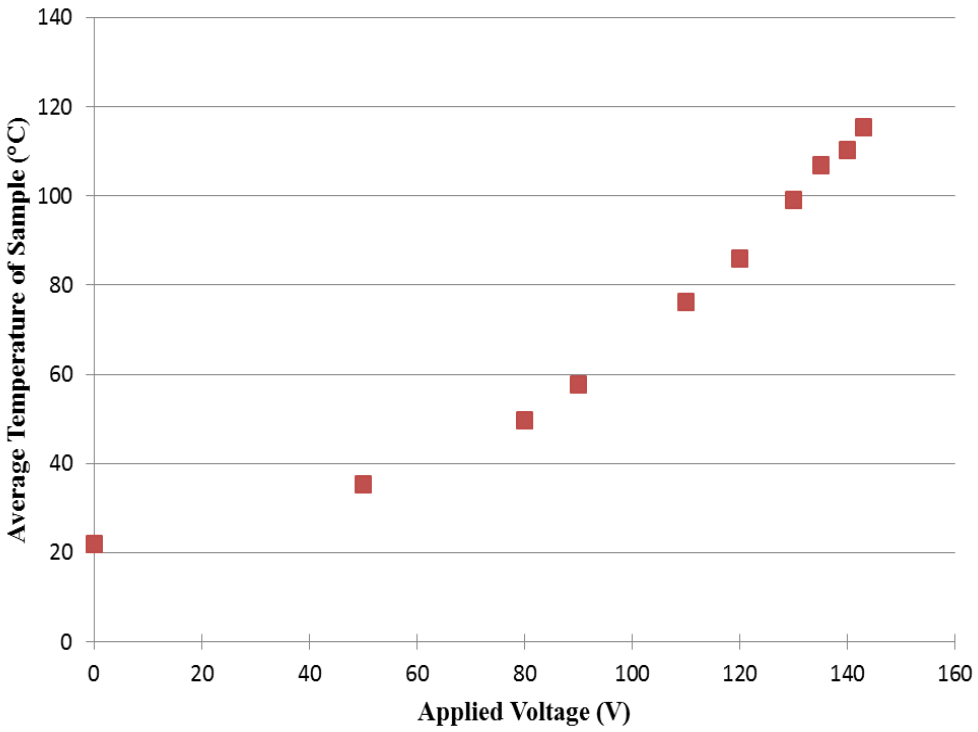

Figure 34. Applied voltage vs average temperature of a 1wt% CNT/PEEK sample.

The active damping performance of the CNT/PEEK composite as a function of applied power is shown in Figure 35. The viscoelastic measurements show that as input power is increased, the damping capability of the material increases, evident in the increase in tan δ, Figure 35b. This trend, enhancement in damping of nanocomposite is expected, since the increase in temperature accelerates chain relaxation and leads to further damping in the polymer (Figure 30).

The onset of enhancement in tan δ (~0.024 W/mm^3) correlates with a drop in storage modulus, potentially due to thermally activated chain relaxation, as is the case in the neat polymer (Figure 30). The sharp rise in damping and drop in storage modulus suggests

that a large volume of the material is approaching the Tg of the composite, in line with the thermal camera observations, Figure 35a.

For instance, as shown in Figure 36, at an applied power (0.0342 W/mm^3), a large part of the sample is within 5-10°C of the glass transition temperature of the composite. The tan δ increases by a factor of 4, with an average sample temperature of 115.4°C. This result points to polymer relaxation as the mechanism being activated for enhancing the damping behavior of the composite material. It is however to be pointed out that this 400% increase in damping is achieved at 42% loss in storage modulus, indicating the effectiveness of active damping in tuning the energy dissipation capability of the material.

Moreover, the loss of modulus in semi-crystalline polymers will be limited even at Tg compared to fully amorphous polymer (Figure 28). That is because the crystalline structure will still remain crystalline at Tg, since this temperature is below the crystal melt temperature. Therefore, the crystalline structure in the material will maintain some storage modulus while still allowing the amorphous regions to have some relative movement, which will contribute to the energy dissipation in the material. This factor becomes of importance in our study because the temperature of our samples was not completely uniform. As observed in Figure 35, there is a small hot spot with a temperature well above the glass transition temperature. The non-uniformity of the temperature in the composite likely comes from the presence of CNT agglomerates in the matrix, which lead to a non-uniform dispersion of CNTs. Therefore, some areas will have higher electrical resistance than others due to the lack of CNTs present. The areas

with CNT agglomerates present will likely lead to local overheating, and thus a hot spot in the composite. Even though this volume of the sample did not contribute to the dissipation, since it is at a temperature above the point of maximum dissipation, its stiffness did not drop to zero since a plateau in modulus is reached above Tg in semi-crystalline polymers. Therefore, in a structural setting, there is no risk of structural stiffness becoming negligible even if the material is overheated above the Tg. This is unlike amorphous polymers, such as polystyrene (Figure 24), which show significant decrease in modulus above the glass transition temperature. This factor becomes of importance in our study because the temperature of our samples was not completely uniform.

V.B.2. Reversibility of Thermally Enhanced Viscoelastic Properties

Non-uniform heating of the sample, due to a combination of heat dissipation through the surface and CNT agglomerates, may lead to local heating considerably above the Tg and might result in thermal degradation. This material degradation may reflect itself on viscoelastic properties of the material. The ability of the composite to recover its original state was tested by testing the dynamic properties (at room temperature) before and after the joule heating test. The results, Figure 37, show that both the storage modulus and tan δ are fully recovered after joule heating of the composite. This result indicates that the sample does not experience any noticeable permanent damage, thermal degradation, as a result of resistive heating of the nanoparticles and that the active damping mechanism in the composite is reversible.

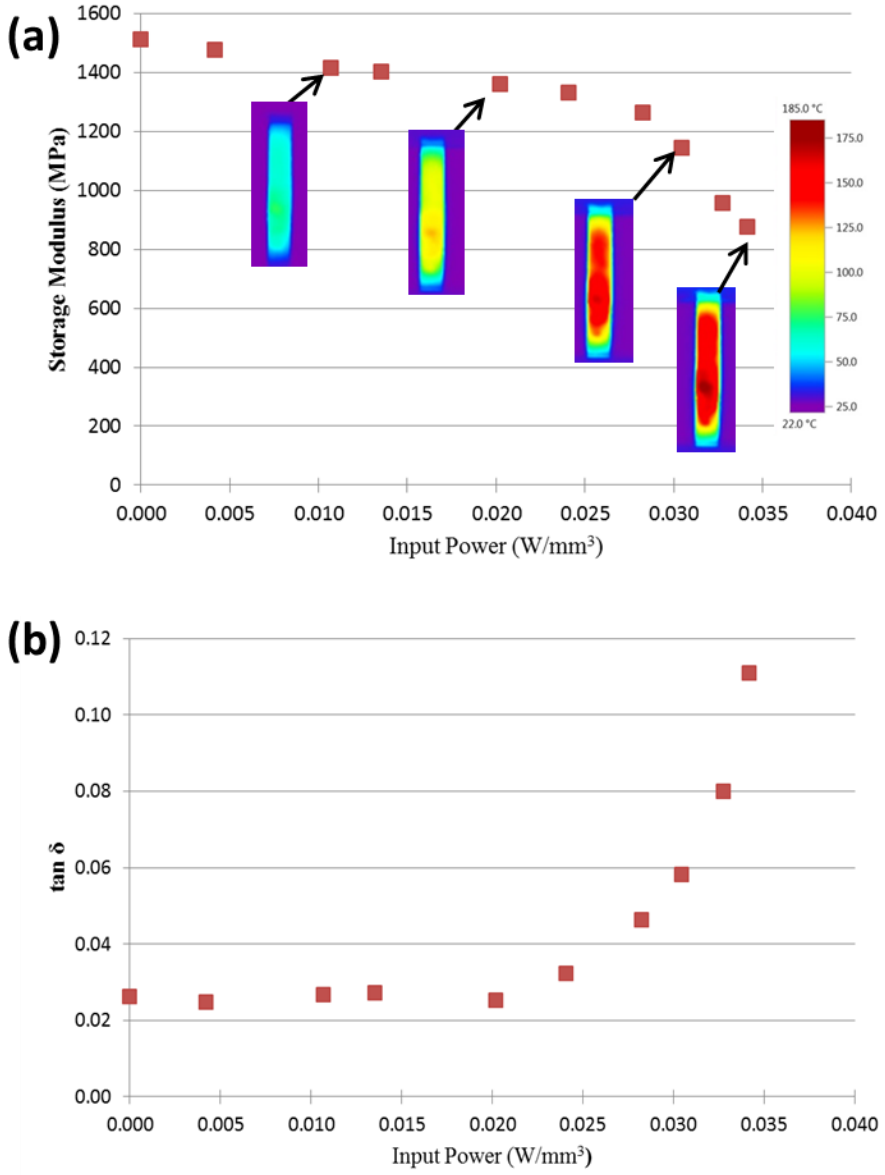

Figure 35. (a) storage modulus (b) tan δ of a 1wt% CNT/PEEK composite as a function of applied power. Images in plot (a) show the temperature distribution on the sample surface.

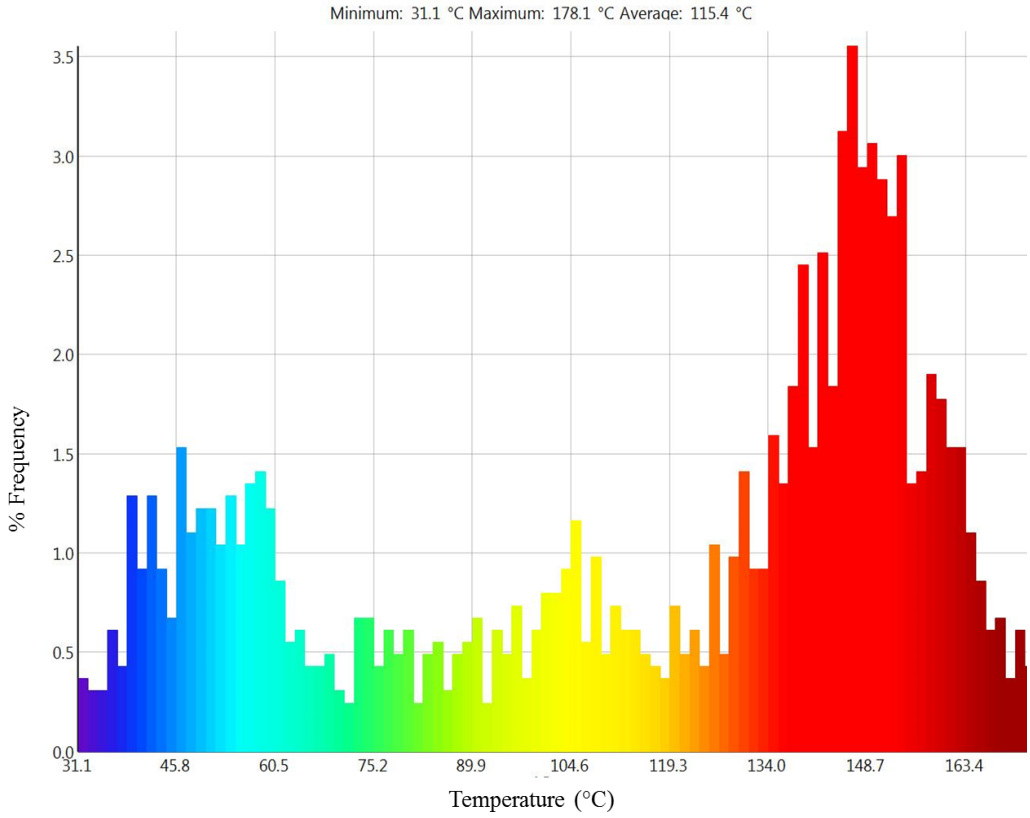

Figure 36. Histogram showing the temperature distribution in a 1wt% CNT/PEEK composite for an applied power of 0.0342 W/mm^3.

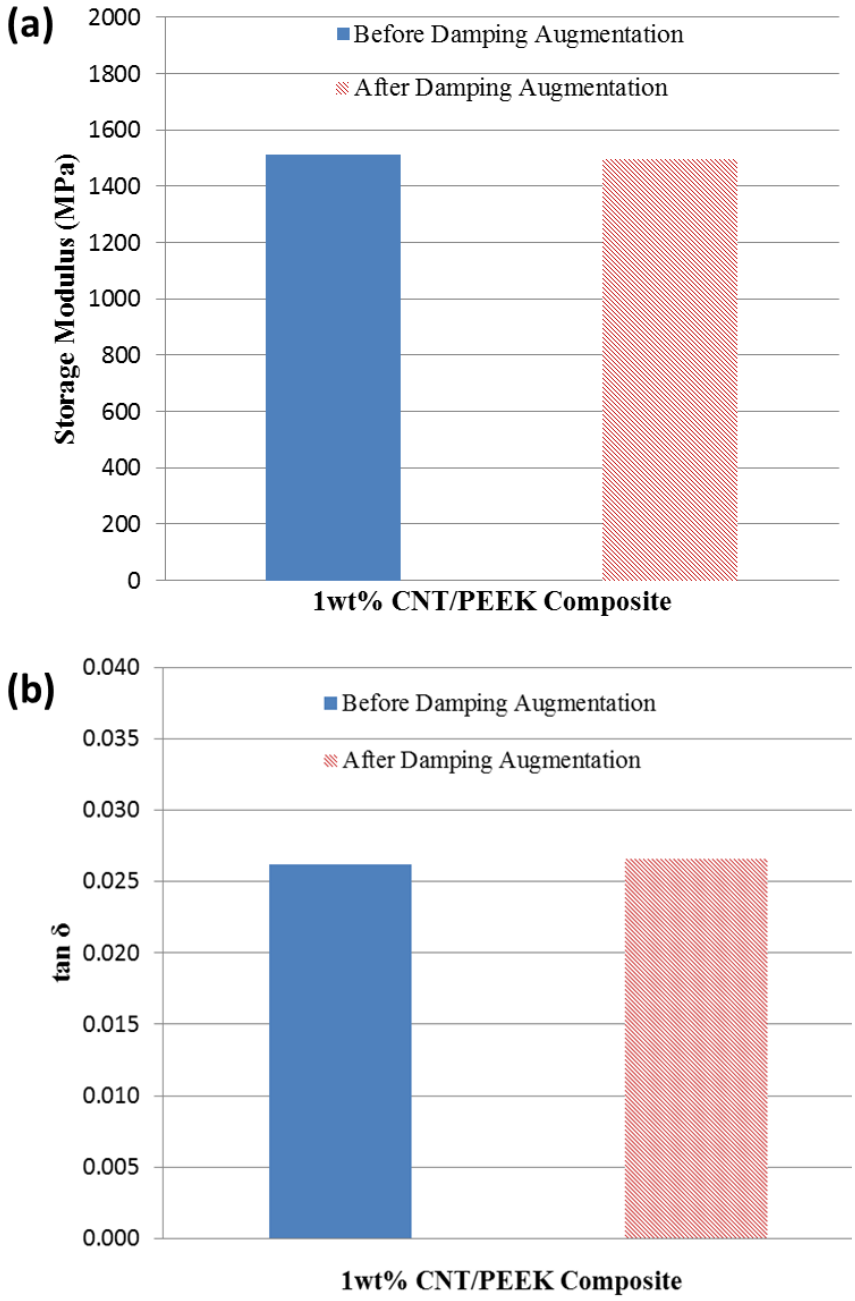

Figure 37. (a) storage modulus (b) tan δ of a 1wt% CNT/PEEK composite before and after active damping testing where joule heating was performed to near the Tg of the composite.

V.B.3. Comparison of Viscoelastic Damping Augmentation via Joule Heating and Heat Bath

An analysis of the temperature distribution on the sample at the highest applied power, Figure 36, shows that while most of the sample is near the Tg of the composite, a large volume of the sample is either below or above this temperature. The lower temperatures arise from the temperature gradient imposed by the tensile grips, while the higher temperatures might arise from a non-uniform distribution of CNTs. The control experiment performed (shown in the previous chapter and plotted again in Figure 38) with the temperature imposed by a furnace (heat bath) shows that for temperatures below ~60°C, no significant enhancement in tan δ is observed. The actively heated sample shows no significant improvement at average temperatures below 75°C, observed in Figure 38. The delay in enhancement of tan δ might arise from the global non-uniformity of temperature on the sample. Since the range of enhancement in tan δ of the composite lies within 50°C and the temperature distribution in the sample spans more the 130°C (for the highest applied power), as observed in Figure 36, the amount of polymer volume contributing to the damping enhancement is significantly reduced.

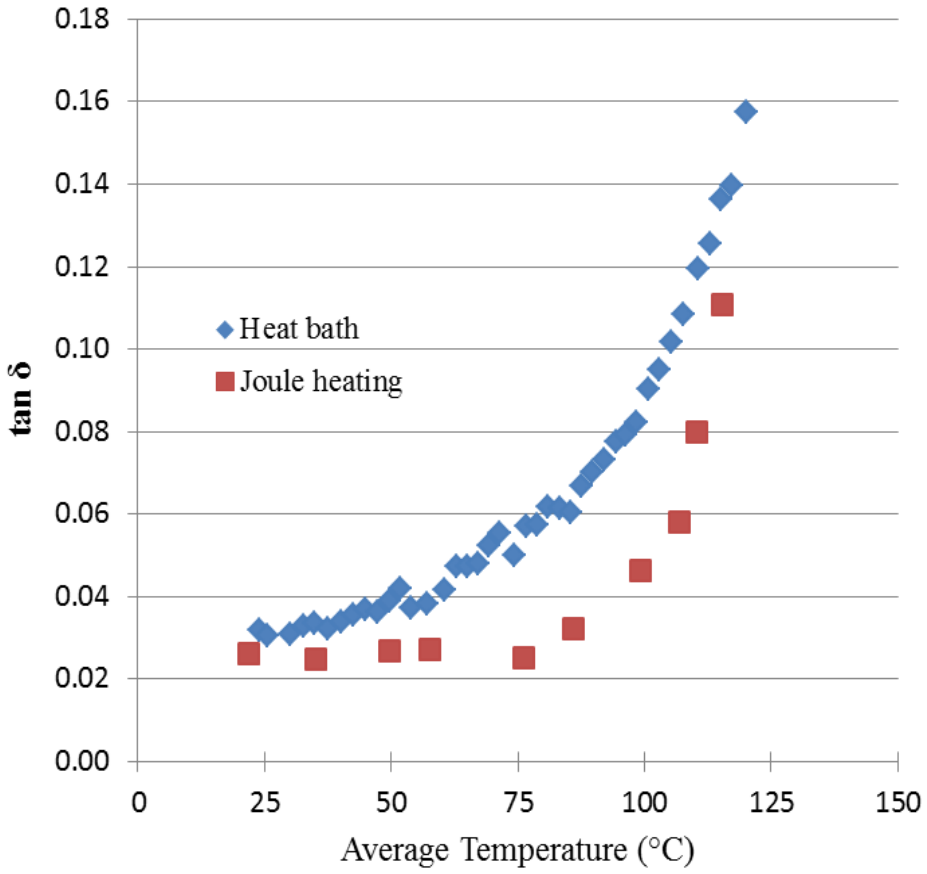

Figure 38. Comparison of tan δ as a function of temperature between a 1wt% CNT/PEEK heated using a heat bath and by joule heating of the nanofillers.

Another factor that might also contribute to the delay in damping enhancement is that locally (at the CNT scale) the composite might show a gradient in temperature as the CNT transfers heat to the surrounding matrix. Since the CNTs are the only heat source, the polymer surrounding the CNT must experience a temperature gradient in order to reach the equilibrium (average) temperature observed at the larger scale and captured by the thermal imager. Hence, this will be the focus of the following chapter.

V.C. Conclusion

The active damping potential of CNT fillers in a thermoplastic polymer matrix was investigated through experimental techniques. The thermomechanical response of the polymer was targeted and studied as a potential damping source within the nanocomposite. The nanoscale reinforcements were used as heat sources, via joule heating, to trigger this matrix relaxation. By taking advantage of the polymer relaxation resulting from an increase in temperature, the composite shows the potential for damping enhancement.

The damping mechanisms show an enhancement of up to 400%. This increase in damping comes at a cost of 42% decrease in storage modulus. However, the semi-crystalline nature of PEEK allows for damping enhancement while minimizing the undesired loss of storage modulus, as compared to amorphous polymers. In addition, the damping mechanism was found to be reversible since both the storage modulus and tan δ are fully recovered upon cooling of the composite.

The total enhancement is energy dissipation was limited by the fact that the temperature distribution in the sample was found to be non-uniform, as a result of the temperature imposed by the tensile grips and also likely due to the presence of CNT agglomeration. In addition, the possibility of non-uniformity of temperature at the local scale can lead to a further delay in the enhancement of damping.

CHAPTER VI

CONTINUUM MODELING OF NON-UNIFORM TEMPERATURE DISTRIBUTION IN ACTIVE DAMPING

The potential of CNTs as heat sources to trigger polymer relaxation shows potential for enhancement of the damping capability in CNT nanocomposites, as shown in the previous chapter. The temperature sensitivity of the polymer matrix viscoelastic properties allows for the tailoring of the damping ability by controlling the temperature in the composite. However, the overall damping is highly sensitive to the temperature distribution, as shown in the previous chapter. That is mainly due to the narrow temperature margin where maximum dissipation occurs, with decreases in tan δ at temperatures above and below the glass transition temperature. Thus, a study on the effect of non-uniform temperature distribution at the global scale on augmentation of damping in nanocomposites via electrical signals is required. In addition, locally and in the scale of individual CNTs surrounded by the matrix, joule heating of the nanocomposite might be non-uniform as it occurs mainly within the CNTs. Hence, a local temperature gradient may also develop in the nanocomposite, which may influence damping augmentation.

This chapter will focus on the modeling of thermally augmented damping of the CNT/PEEK nanocomposites at both a global and local scale. In the global scale, average

Part of this chapter is reprinted with permission from "Effect of thermal interface on heat flow in carbon nanofiber composites." by Gardea F., Naraghi M., Lagoudas D. ACS Appl Mater Interfaces. 2013;6(2):1061–72.

thermal and electrical properties of the nanocomposite, measured experimentally, will be used to capture the effect of heat loss on the surfaces of the sample due to air convection. In addition, the local temperature distribution, at the scale of the building block of the nanocomposite consisting of a single CNT surrounded by the matrix, will be analyzed in order to observe whether a non-uniform temperature distribution in the polymer surrounding the CNTs contributes to the delayed enhancement in damping observed in the previous chapter (Figure 38). A parametric study on the effect of filler diameter will also be presented to provide more insight on this aspect of active damping.

VI.A. Thermal Augmentation of Polymer Relaxation – Global Modeling

VI.A.1. Methodology

VI.A.1.1. Analytical Model

To study the effect of the non-uniform temperature distribution observed in the composite samples, the temperature dependent viscoelastic properties obtained experimentally (Chapter V) will be used as input into a theoretical model using both Voigt and Reuss structures [9]. The effective viscoelastic properties of Voigt and Reuss structures are discussed briefly as follows. In a layered two–phase composite with a Voigt structural arrangement, Figure 39a, each phase experiences the same strain and thus the composite modulus follows the rule of mixtures.

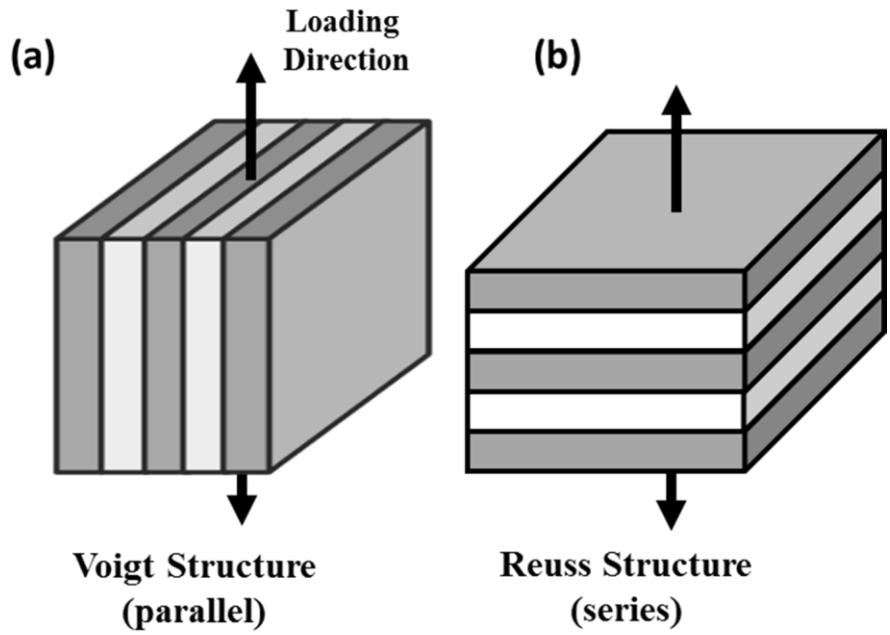

Figure 39. (a) Voigt parallel structure resulting in isostrain (b) Reuss series structure resulting in isostress.

Using the correspondence principle [71], the elastic relation is converted to a viscoelastic relation resulting in Eq. (14), where E_c^* is the composite complex modulus, E_1^* is the complex modulus of the first phase, E_2^* is the complex modulus of the second phase, and v_1 and $v_2$are the volume fraction of phase 1 and phase 2, respectively. The complex modulus is defined as $E^* = E' + iE''$, where E' is the storage modulus, E'' is the loss modulus, and $tan\,\delta = \frac{E''}{E'}$.

$$E_c^* = E_1^* v_1 + E_2^* v_2 \tag{14}$$

Thus, from the ratio of the real and imaginary parts, the $tan\,\delta_c$, the loss tangent of the composite, is given by Eq. (15).

$$tan\,\delta_c = \frac{v_1 tan\delta_1 + v_2\left(\frac{E_2^{'}}{E_1^{'}}\right)tan\delta_2}{v_1 + \left(\frac{E_2^{'}}{E_1^{'}}\right)v_2} \tag{15}$$

As for the Reuss structure, Figure 39b, the layered phases are placed in series and thus experience isostress. This structure follows the inverse rule of mixtures shown in Eq. (16). The $tan\,\delta_c$ can be expressed as Eq. (17).

$$\frac{1}{E_c^*} = \frac{v_1}{E_1^*} + \frac{v_2}{E_2^*} \tag{16}$$

$$tan\,\delta_c = \frac{(tan\delta_1 + tan\delta_2)\left(v_1 + v_2\frac{E_1'}{E_2'}\right) - (1 - tan\delta_1 tan\delta_2)(v_1 tan\delta_2 + v_2 tan\delta_1\frac{E_1'}{E_2'})}{(1 - tan\delta_1 tan\delta_2)\left(v_1 + v_2\frac{E_1'}{E_2'}\right) + (tan\delta_1 + tan\delta_2)\left(v_1 tan\delta_2 + v_2 tan\delta_1\frac{E_1'}{E_2'}\right)} \tag{17}$$

To estimate the effect of non-uniform temperature distribution on damping, the heated sample was approximated as several viscoelastic material sections with different viscoelastic properties in series and parallel as Voigt and Reuss structures. The variations in viscoelastic properties were caused by non-uniform temperature distribution. To this end, the temperature distribution in the composite sample was taken from thermal images shown in the previous chapter. The image was divided into seven sections, shown in Figure 40. Each phase corresponds to the polymer matrix experiencing a different temperature and thus having different viscoelastic properties. A

combination of Voigt and Reuss structures were used to solve for the effective $tan\,\delta$ of the composite. With the loading direction being parallel to the longest sample dimension, sections 1, 2, and 3 are in parallel with each other and in series with sections 4, 5, 6, and 7.

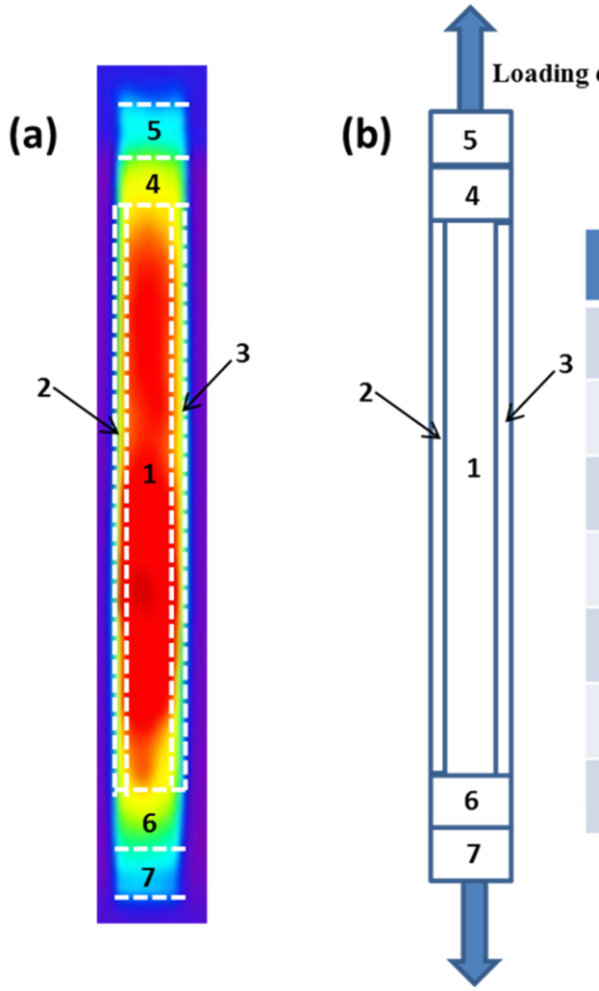

Section	$T_{average}$ (°C)	tan δ
1	149.6	0.3025
2	36.3	0.0315
3	37.0	0.0318
4	107.0	0.1054
5	52.8	0.0403
6	100.3	0.0878
7	50.9	0.0393

Figure 40. (a) composite sample thermal image showing sample area divided into seven different phases corresponding to the polymer being at a different temperature (b) Correponding phases with sections 1, 2, and 3 being in parallel to each other and in series with sections 4,5,6, and 7. The average temperature, $T_{average}$, and corresponding tan δ is shown for each section.

VI.A.1.2. Finite Element Model

In order to further shed light on the discrepancies between the comparison of the heat bath and joule heating experimental results, finite element analysis (FEA) was performed to more accurately account for the global non-uniform temperature distribution in the composite. The analysis involved the use of the commercial finite element software package, ABAQUS. A 2-D plane stress model was implemented with biquadratic plane stress quadrilateral elements (CPS8). The full-field temperature distribution in the sample, taken from image processing of the experimental thermal images, was input into the model as a predefined temperature field. The temperature of each point was maintained throughout the simulation. Both the storage and loss modulus as a function of temperature, obtained from experiments, were used for the material properties in the simulation. It was assumed that the Poisson's ratio remains constant with temperature. The effective composite modulus (either storage or loss) was taken from the load vs displacement curve. The tan δ was taken as the ratio of the effective loss modulus to effective storage modulus.

VI.A.2. Results and Discussion

The effective damping response comparison between modeling and experimental results for 1wt% CNT/PEEK composite is shown in Figure 41. The results show that both the analytical and FEA models follow the trend observed in the experimental results. Both models match the behavior at lower temperatures and then as temperature increases the modeling overpredicts the damping behavior. It should be pointed out that

the tan δ results for both of the models are plotted as a function of average temperature in the sample, while the heat bath results are plotted as a function of the uniform chamber temperature. This difference could possibly be the cause for the discrepancy between the modeling and heat bath experiments. At the higher temperatures (>100 °C) the finite element analysis deviates from the analytical model. This difference could arise from the more accurate temperature distribution in the FEA analysis, as compared to the averaging of the temperature in the sample sections in the analytical model. Since the temperature sensitivity is greater at the higher temperatures, the FEA analysis will yield a more accurate result since the temperature at each point is considered in the analysis. A comparison between the modeling and the joule heating experiments (both plotted as a function of average sample temperature) yields that accounting for the non-uniform temperature distribution at the macroscale does not capture the behavior observed in the joule heating experiments, suggesting that there is a possibility of a local temperature gradient near the nanotube scale, which is not captured by either the thermal camera or by macroscopic modeling of the damping behavior.

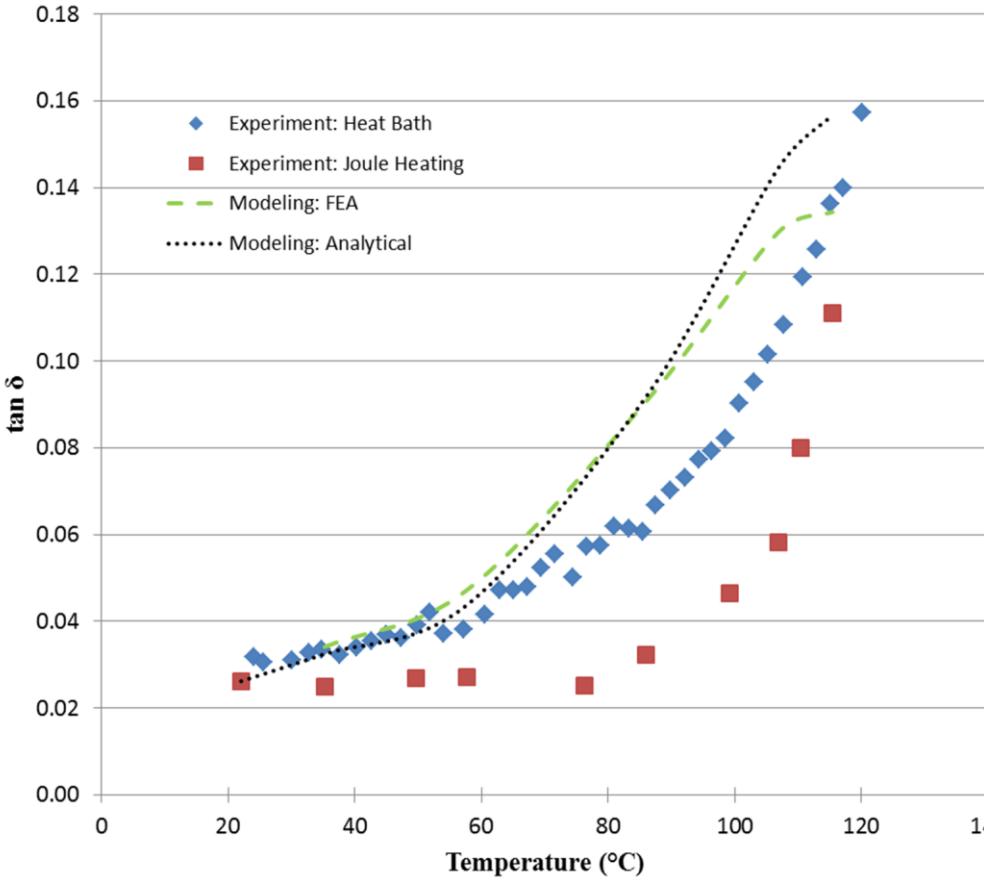

Figure 41. Comparison of tan δ vs Temperature between the modeling and experimental results. (For the joule heating, FEA and analytical results, the temperature corresponds to the average temperature of the sample. For the heat bath, the temperature corresponds to the temperature in the chamber.)

However, the non-uniform temperature at the macroscale does have an effect on the overall composite damping, since not the entire sample contributes the same amount to the effective damping of the composite. In addition, local effects could lead to an additional effect on composite damping, suggested by the difference in damping behavior between the macroscale modeling and the joule heating experiments. In order to observe whether local effects cause this discrepancy, a study was performed on the temperature distribution near the CNT. However, in order to accurately model the

temperature gradient near the CNT, the effect of interfacial resistance was first accounted for.

VI.B. Interfacial Thermal Resistance in Nanocomposites

The thermal conductivity of graphitic nanoparticles, which is in the range of 20-2000 W/m K [15-18], is significantly larger than the thermal conductivity of typical polymers, in the range of 0.1-0.4 W/m K [15]. However, various studies on thermal properties of graphitic particle-polymer composites show a large scatter, and in most cases only marginal improvements in the thermal conductivity of the nanocomposite upon the addition of nanoparticles to the matrix, Figure 42 [16-18, 72-77].

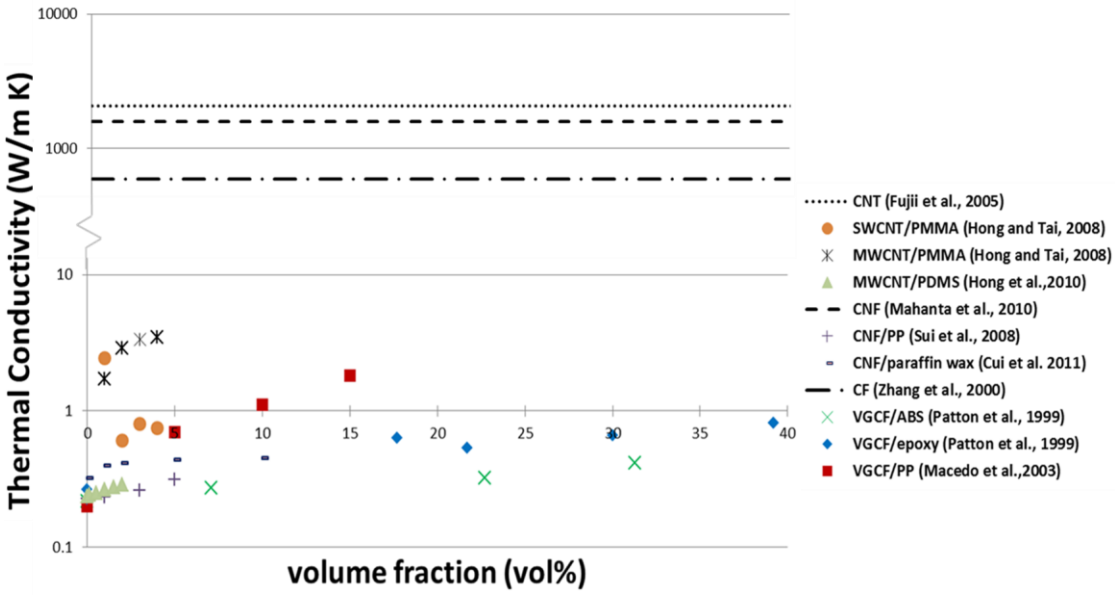

Figure 42. Reported experimental data for thermal conductivity of carbon nanotube (CNT), carbon nanofiber (CNF), carbon fiber (CF) composites.

More interestingly, some studies have suggested that the addition of particles with remarkable thermal conductivities, in some cases, may even reduce the thermal conductivity of the nanocomposite below the thermal conductivity of the matrix [14, 78]. For example, Yang et al. observed no detectable change in the thermal conductivity of vapor grown carbon nanofiber (VGCNF) liquid crystal polymer composites with VGCNFs content of as high as 15wt%, which was attributed to the non-uniform dispersion of nanofibers and the lack of a percolated network [79]. On the other hand, Patton et al. observed a 300% increase in thermal conductivity of vapor grown carbon fibers (VGCFs) polymer composites with 39vol% VGCF. However, the magnitude of the thermal conductivity remained relatively low (~0.8 W/m K) as compared to the intrinsic thermal conductivity of the filler. The low magnitude of composite thermal conductivity was attributed to the low efficiency in transfer of thermal energy between nanofibers and matrix along their interface [18].

As the particle size approaches smaller length scales, the interface between particle and matrix becomes of significant interest. That is mainly due to an increase in surface-to-volume ratio of the fillers with a reduction in their characteristic length scales [19]. At the nanoscale, heat transport becomes especially important when the particle size becomes comparable to the phonon mean free path, which can be in the range of 1-100 nm [80]. This can result in either diffusive heat transfer, having many scattering events, or ballistic transport of phonons [31]. The decrease in thermal conductivity has been attributed to the increasing dominance of the interfacial thermal resistance as particle size decreased [19], which results in significant scattering of phonons. This interfacial

resistance acts as a boundary layer resistance to heat flow, leading to a discontinuity of temperature at the interface for any finite heat flux across the interface [33]. This issue was been addressed many times in the literature [34, 81-86]. Therefore, accounting for interfacial resistance becomes of importance in CNT composites.

VI.B.1. Measuring Interface Thermal Resistance in Nanocomposites

Even though a full theoretical quantification of the interface thermal resistance requires the consideration of quantized density of states of phonons, continuum heat transfer equations (Fourier's law and conservation of energy) can reliably describe the heat flow in the presence of interface resistance in nanocomposites, by modeling the interface conductivity as the ratio of heat flux through an interface for a given temperature jump across an interface [87]. This ratio is a temperature dependent property of the interface.

We estimated the interface thermal conductivity in CNT/PEEK nanocomposites through integrated experimental and modeling approach. To this end, the thermal conductivity of the CNT nanocomposite samples was first determined experimentally at room temperature (25 °C) using a Hot Disk^{TM} Thermal Constants Analyzer. The testing equipment utilizes a resistor with a double spiral disk shape that serves as both a temperature sensor and heat source. The variation in electrical resistance caused by the transient change in temperature is related to the heat flow between the sensor and the specimen, from which the sample thermal conductivity is obtained [88]. The measured thermal conductivity of the nanocomposite was then used to calibrate a micromechanics

model which predict the thermal conductivity of the CNT/PEEK material system as a function of interphase conductivity. The micromechanics approach was obtained from Seidel and Lagoudas [89, 90] which is based on the composite cylinders method [91]. In the model, CNTs are assumed to be straight and randomly oriented. The modeling was carried out at multiple scales (nano and micro scales) as seen in Figure 43 in order to ultimately determine the effective nanocomposite conductivity. A composite cylinder assemblage was used as the representative volume element (RVE) for the CNT and interface at the nanoscale, as shown in Figure 43. This nanoscale RVE was used to obtain the effective conductivity of the CNT/interphase. Details on the derivation of the equations are presented in [89, 90].

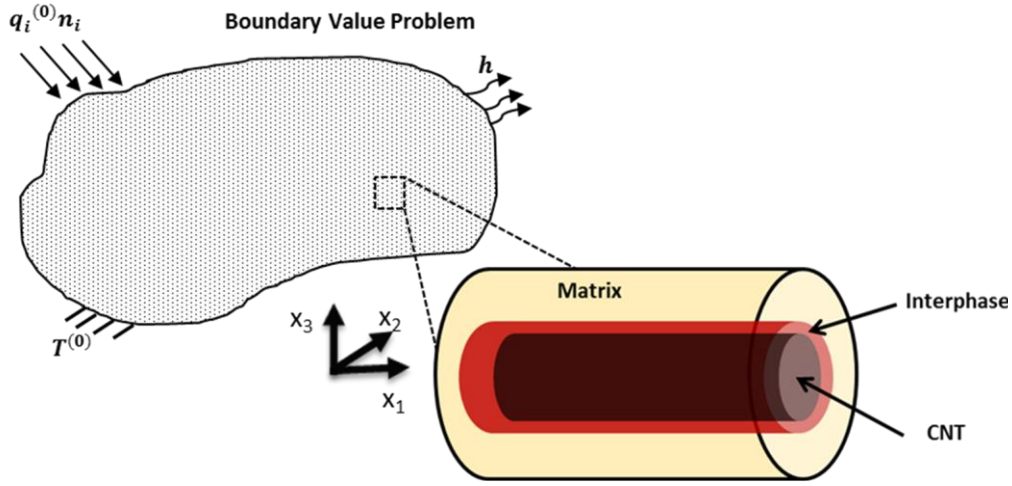

Figure 43. Multi-scale schematic of CNT composite showing a CNT embedded in a matrix as a representative volume element (RVE).

Here we have used a matrix thermal conductivity of 0.294 W/m K, obtained from experiments, and a CNT thermal conductivity of 2000 W/m K, in the range of the values reported for CNTs [92-94].

VI.B.2. Results and Discussion

The experimental results obtained show a minimal increase in thermal conductivity of about 7.1% over neat PEEK for 1.0 wt% CNT. When including the third phase (interphase) between the fiber and matrix in the micromechanics model, with a thickness, t_{int}, of 0.5% of the radius of the CNT, and a thermal conductivity of $k_{int} =$ $6x10^{-5}$ W/m K, the model predictions matches the experimental results most accurately. While physically the concept of interface thermal resistance refers to a temperature jump across an interface with zero thickness [95], the micromechanics formulation requires the attribution of a finite thickness to the interphase. Hence, in our analysis, the thickness of the interphase here is set to a small fraction (0.5%) of the radius of the CNT (2nm) to minimize circumferential changes in the temperature in the interphase. Therefore, the value of the thermal conductivity of the interphase corresponds to an interface conductance value, h_{int}, of $6x10^6$ W/m^2 K through the relation $h_{int} = {}^{k_{int}}/_{t_{int}}$.

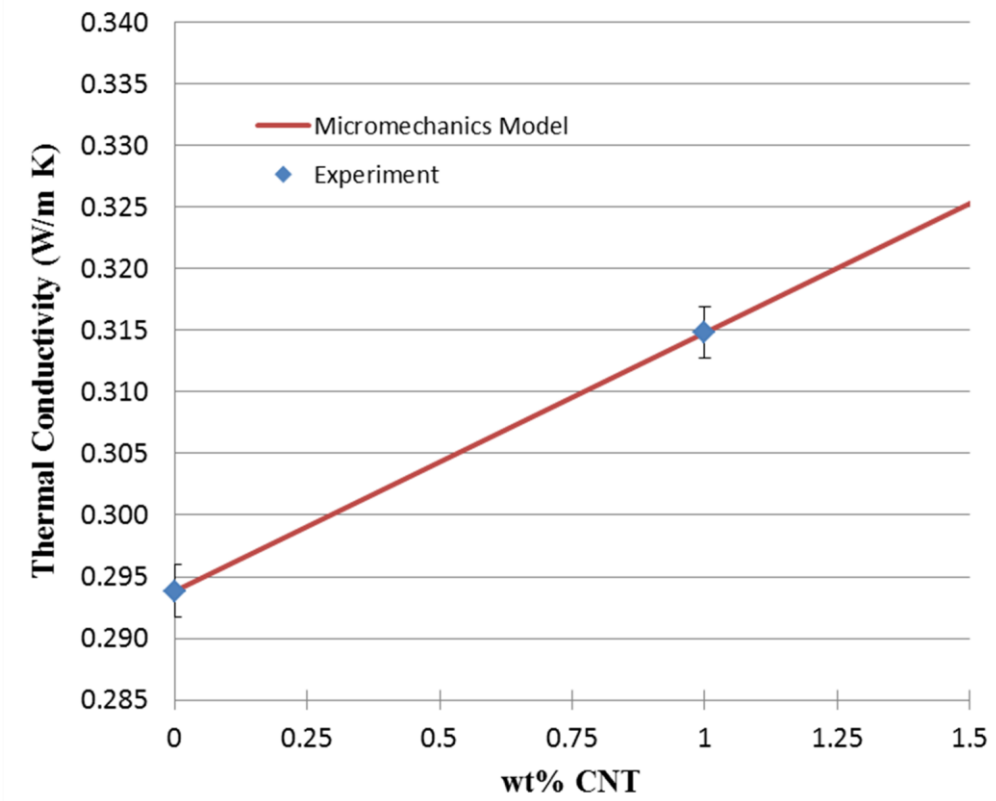

Figure 44. Thermal conductivity for a 1wt%CNT/PEEK composites and neat PEEK. Micromechanics model was fit to experimental data.

VI.C. Modeling of Local Heat Transfer in CNT Composites

Since the modeling prediction of damping showed differences with the experimental results (Figure 41), it is possible that the temperature distribution at the local scale near the CNT might affect the overall response of the polymer to composite damping. Therefore, the local temperature gradient was studied via an analytical heat transfer model.

VI.C.1. Methodology

In order to model local heat transfer in CNT composites, it is assumed that the medium is composed of two concentric solid materials, CNT and matrix, as shown in Figure 45. It is assumed that CNTs are straight rods with uniform diameters and identical dimensions, which are homogeneously dispersed in the matrix. It is assumed that the heat flux obeys Fourier's Law of heat conduction. Moreover, CNTs are volumetric heat sources which transfer heat to the matrix through CNT surfaces. Given the high aspect ratio of the CNTs (100s to 1000s), the heat transfer is mainly assumed to be radial. The steady state local heat transfer is calculated in this section.

While in the micromechanics model the interphase has a finite thickness to account for the interface thermal resistance within a micromechanics framework, in this section, the interface has zero thickness, with a finite temperature discontinuity for a given heat flux through the interface of the nanotube and the matrix. In the global scale, the heat generated per unit volume of the nanocomposite, q_v, is $J^2\rho$ where J is the current density and ρ is the resistivity. However, in reality the heat is mainly generated in the CNT, therefore, the total heat generated in the CNT is q_v times the volume of the CNT, which is transferred to the matrix through the CNT-matrix interface. Therefore, this input heat can be modeled as an input flux, q_s, with the dimension of heat per unit time per unit area, as

$$q_s = \frac{q_v r_{CNT}}{2v_f} \tag{18}$$

where r_{CNT} is the radius of the CNT and v_f is the CNT volume fraction.

Hence, it is assumed that there is a continuous heat flux, in the outward normal direction, at the CNT-matrix interface. In the steady state, the total heat passed through each radial cross section around the CNT will be the same, due to conservation of energy, hence, the heat flux at a radius r around the CNT will be:

$$q(r) = \frac{q_s r_{CNT}}{r} \tag{19}$$

Therefore, the temperature drop across the interface will be:

$$(T_{CNT} - T_I) = \frac{q_s}{h_{int}} \tag{20}$$

where h_{int} is the interfacial thermal conductance, T_{CNT} is the temperature of the CNT, T_I is the temperature at the boundary of the CNT and matrix.

Moreover, at a radius *r*, the temperature will change by *dT* with an increment of radius of *dr*, such that

$$dT = \frac{q(r)}{k_m} dr \tag{21}$$

where k_m is the thermal conductivity of the matrix.

As a result, the temperature of the CNT can be related to the temperature of the matrix, T_0, at the boundary, r_2, by integrating Eq. (21) and adding the temperature change across the interface, Eq. (20).

$$T_{CNT} - T_0 = \frac{q_s}{h_{int}} + \frac{q_s r_{CNT}}{k_m} ln\left(\frac{r_2}{r_{CNT}}\right) \tag{22}$$

This equation, Eq. (22), clearly shows the contribution of the interface (first term in the right-hand side of the equation) and the contribution of the matrix (second term) to the overall temperature change between the CNT and the outside boundary. In this study,

we are mostly interested in the temperature gradient in just the polymer matrix, and thus the second term on the right hand side of the equation is important.

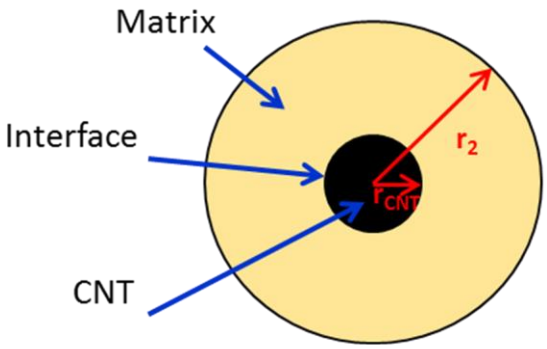

Figure 45. Schematic showing the composite made up of a CNT and matrix with an interface between them.

VI.C.2. Results and Discussion

The effect of CNT radius on the temperature difference in the matrix is shown in Figure 46 (only the second term of Eq. (22)). In this plot the value of the temperature difference in the matrix is independent of interfacial resistance, as suggested by the second term in Eq. (22). For small diameter fillers, the difference in temperature in the matrix is not significant. The temperature difference becomes important for larger diameter fillers, with carbon nanofibers (CNF) and carbon fibers (CF) significantly increasing the temperature difference, and thus introducing large temperature gradients in the polymer matrix. For the composite system studied here, the small diameter of the SWCNTs used does not significantly contribute to any temperature gradient in the polymer matrix and thus we can assume that with perfectly dispersed CNTs in the matrix, the temperature of the polymer matrix is nearly uniform throughout. As a result,

the discrepancies between model predictions and experimental results of damping is attributed to the agglomerations between CNTs, which leads to the development of temperature gradients in the matrix. To better illustrate the effect of agglomeration, we can consider an effective diameter of CNTs in the high agglomeration regions to be about the diameter of the CNT agglomerates. From SEM images, this diameter is as high as ~10 μm (Figure 31). The upper limit of the agglomerate size may lead to temperature gradients of ~10-50°C (Figure 46). This gradient of temperature is comparable to the full width at half maximum (FWHM) of the tan δ vs. temperature curve of the composite (Figure 30), suggesting that the mean temperature of the region may not reach Tg unless a good portion of the sample is heated to a temperature above Tg, leading to a loss in both storage modulus and tan δ.

While the magnitude of the temperature drop in the polymer, according to Eq. (21), is independent of interface resistance, it is to be noted that higher interface resistance reduces the average temperature within the matrix as it leads to higher temperature drop across the interface (Eq. (20)). Therefore, lower interface resistance is advised to augment damping with lower input energy.

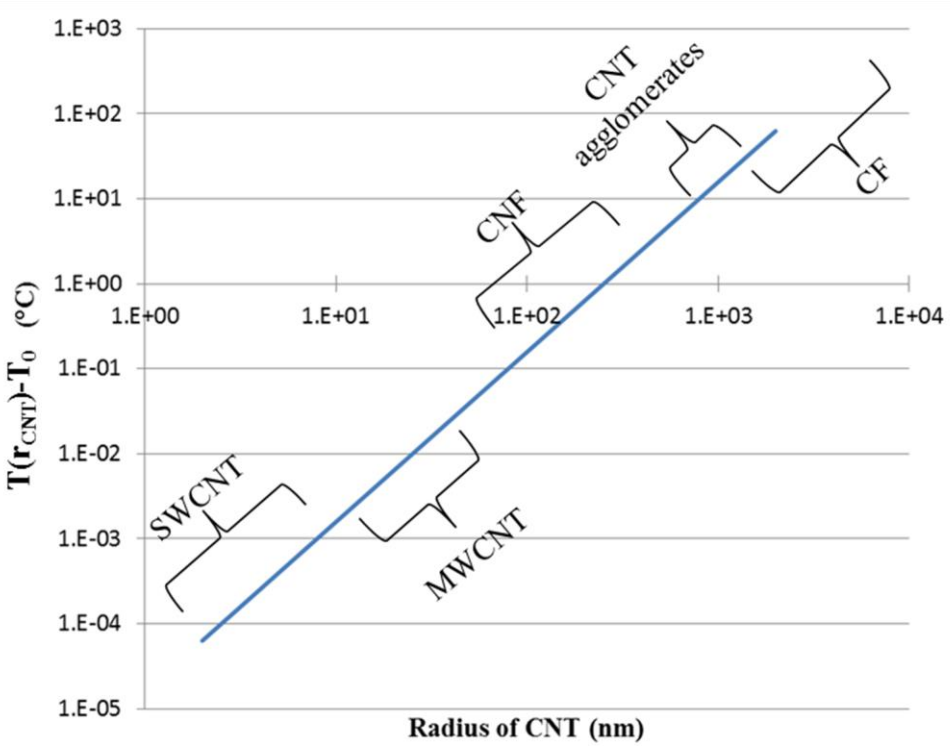

Figure 46. Effect of filler radius on the temperature difference between the CNT boundary and the outer element boundary of a 1wt%CNT/PEEK composite.

VI.D. Conclusion

The effect of non-uniform temperature distribution at both the macroscale and local scale was studied. While locally, the polymer seems to show uniform distribution of temperature due to the small diameter of the SWCNTs, globally the non-uniform temperature, present from both convection and temperature gradients induced by the testing grips, does show a significant effect on the overall composite damping capability. Locally, for the composite system studied here, the model shows no significant temperature gradient. However, it was found that with increasing filler diameter, the

temperature difference in the polymer matrix can be significant, with CNF resulting in up to 10°C difference in temperature and CF up to 100°C.

Even though the composite system studied here is made up of CNT with small diameters (> 10nm) the presence of agglomeration can lead to non-uniformity of temperature in the matrix, since the agglomerates in the composite are in the order of 10 μm. The effective diameter of the CNT agglomerates can lead to temperature gradients of ~10-50°C, suggesting that the mean temperature of the region surrounding CNT may not reach Tg unless a large partion of the sample is heated above Tg, which will result in a further local loss in both storage modulus and tan δ.

This result is significant due to the fact that the range of temperatures were tan δ is maximized for a PEEK polymer is narrow, and thus a wide range in temperature distribution in the polymer matrix will lead to different areas contributing less that other areas, in terms of damping. To achieve optimal enhancement in damping, the temperature distribution within the matrix should be much less than the FWHM of the tan δ vs. temperature curve, such that most of the material can be heated to a temperature close to Tg. For this, uniform distribution of small diameter CNTs is necessary.

CHAPTER VII

CONCLUSIONS AND FUTURE DIRECTIONS

VII.A. Conclusions

The unique interfacial characteristics between a CNT filler and a polymer matrix where studied for the enhancement of energy dissipation. Specifically, the studies were tailored to address the need for increased damping in composite structures. The present work investigated the damping potential of carbon nanotube (CNT) fillers in polymer matrix composites through integrated experiments and continuum modeling techniques.

Both “passive" and “active” damping were studied. The passive damping refers to the inherent capability of a composite to damp vibrations in the absence of external stimuli, such as electrical signals, by exploiting different damping mechanisms introduced by the presence of the nanoscale reinforcements. Among the targeted passive damping mechanisms in nanocomposites is a ‘slip-stick’ mechanism in which the interactions between the filler and polymer results in frictional energy dissipation along the interface. The CNTs were dominantly oriented parallel to the loading direction to minimize the contribution of damping mechanisms other than inherent damping of matrix and interfacial slip, in contrast to randomly oriented CNTs where other energy dissipation mechanisms, such as matrix tearing and plasticity, can also be active. An analytical model was used to provide additional insight into the experimental observations by showing that the nonlinear variation of damping with dynamic strain can be attributed to slip-stick behavior. The dependence of the interfacial load-transfer

reversibility on the dynamic strain history and characteristic time scale was experimentally investigated to demonstrate the relative significance of van der Waals (vdW) interactions, mechanical interlocking, and covalent bonding on shear interactions. Our results point to the major contribution of mechanical interlocking, after the initiation of interfacial slip, to energy dissipation in the composite. After the initial interface failure, the frictional sliding at the interface increased the energy dissipation by as much as 100% compared to the inherent damping capability of the matrix, depending on the magnitude of the dynamic strain amplitude. In addition, the effect of CNT orientation and distribution on energy dissipation within the nanocomposite was also studied, with a focus on random distribution and agglomeration. Experimental characterization results were presented which point to the enhancement in damping due to misorientation and non-uniform CNT distribution.

In this study, we also studied the controllability of energy dissipation capability in nanocomposites via electrical signals, referred to as active damping With respect to active damping, our studies was focused on semi-crystalline polymers in order to minimize the decrease in storage modulus at temperatures near the glass transition. We first studied the thermomechanical properties of a PEEK thermoplastic polymer. The degree of crystallinity was controlled by varying the annealing temperatures. In addition, the presence of a secondary crystalline phase was suppressed by controlling the duration of annealing. The neat PEEK polymer response shows an increase in loss modulus with temperature while still maintaining significant storage modulus. The addition of SWCNTs to the PEEK polymer shows a decrease in the crystallization due to the

restriction of movement of the polymer chains by the both CNTs and CNT agglomerates. However, the presence of CNTs increases the energy dissipation significantly. Therefore, not only is the dissipation enhanced by the presence of CNTs, but the electrically conductive network of CNTs allows for resistive heating of these particles to trigger the polymer relaxation, leading to an active damping mechanism.

The active damping potential of CNT fillers in a thermoplastic polymer matrix was investigated through experimental techniques. The thermomechanical response of the polymer was targeted and studied as a potential damping source within the nanocomposite. The nanoscale reinforcements were used as heat sources, via joule heating, to trigger this matrix relaxation. The semi-crystalline nature of PEEK allows for damping enhancement while minimizing the undesired decrease of storage modulus, as compared to amorphous polymers. In addition, the damping mechanism was found to be reversible since both the storage modulus and tan δ are fully recovered upon cooling of the composite.

The total enhancement is energy dissipation was limited by the fact that the temperature distribution in the sample was found to be non-uniform, as a result of the temperature imposed by the tensile grips and also likely due to the presence of CNT agglomeration. Therefore, the effect of non-uniform temperature distribution at both the macroscale and local scale was also studied through modeling techniques. While locally, the polymer seems to show uniform distribution of temperature, due to the small diameter of the SWCNTs, it does show a significant effect on the overall composite damping capability. It was found that with increasing filler diameter, the temperature

difference in the polymer matrix can be significant, with CNF resulting in up to 10°C difference in temperature and CF up to 100°C. Even though the composite system studied here is made up of CNT with small diameters (<10nm) the presence of agglomeration can lead to non-uniformity of temperature in the matrix, since the agglomerates in the composite are in the order of 10 μm. The effective diameter of the CNT agglomerates can lead to temperature gradients of ~10-50°C, suggesting that the mean temperature of the region surrounding CNT may not reach Tg unless a large portion of the sample is heated above Tg, which will result in a further local loss in both storage modulus and tan δ. This result is significant due to the fact that the range of temperatures were tan δ is maximized for a PEEK polymer is narrow, and thus a wide range in temperature distribution in the polymer matrix will lead to different areas contributing less that others to the damping in the composite.

The nanofillers in this study allow for the development of high-performance multifunctional composites that can address many issues that are still of significant research interest, with one being the mechanical energy dissipation in structural components during oscillatory loads. This effort clearly points to the significance of interface phenomena, both friction between filler and matrix and energy transfer from the fillers to the matrix, in controlling the damping mechanisms in nanocomposites and presents insights, both qualitative and quantitative, into the origins of these effects.

VII.B. Future Directions

Future efforts shall be focused on further investigating the damping potential of nanofiller/polymer matrix composites. The present work has shown that interfacial slippage is a dominant energy dissipation mechanism in highly aligned CNT composites. However, that study was aimed at simplifying the problem in order to gain an understanding of the interfacial slip mechanism and the dominating shear interactions with the matrix. To extend on that work, tailoring of the interface to obtain desired damping properties is of interest. In addition, presenting additional damping mechanisms to enhance damping is an area that should be pursued.

Effectively controlling the load transfer between the filler and matrix is important when it comes to controlling the stress state at which interfacial slippage occurs. Since the shear stress distribution at the interface between a filler and matrix depends on the mismatch in elastic modulus, in this aspect of the research, the magnitude of the shear stress distribution can be controlled by creating a gradient in elastic modulus at the interface, allowing for the engineering of the interface to control damping. Controlling the magnitude of this gradient allows for the control of the stress state at which interfacial slip occurs, since it will result in the manipulation of the magnitude of the stress distribution at the interface. Achieving a control in the critical stress state to initiate slippage will allow for the tailoring of this interface depending on the application loading conditions. In addition, the interfacial thermal resistance will be altered by a modulus gradient at the interface, and thus the active damping will be directly affected.

Another area of interest is the study on the effect of surface roughness on interfacial shear strength, and thus on damping via interfacial slippage. The study presented here found that mechanical interlocking was responsible for the shear interactions between the CNT and matrix due to the presence of defects on the CNT surface, which lead to surface roughness. Thus, studying the effect the degree of surface roughness has on the magnitude of damping would be of interest.

A combination of active and passive damping mechanisms is also of interest, especially since the interface is the dominating factor in both cases. A study on the interfacial interactions between the filler and matrix as a function temperature will yield valuable information.

In addition repeatability of the damping mechanisms should be further studied. The fatigue life of the specimen and the accumulation of damage should be observed as a result of cyclic loading. Obtaining knowledge on the number of cycles the specimen will endure before showing a difference in its damping response.

Studying the damping capabilities of graphitic-based nanoparticle composites will allow for the development of the next generation of materials for advanced applications.

REFERENCES

[1] Glaz B, Riddick J, Habtour E, Kang H. Interfacial Strain Energy Dissipation in Hybrid Nanocomposite Beams under Axial Strain Fields. AIAA Journal. 2015:DOI: 10.2514/1.J053390.

[2] Schadler L, Brinson L, Sawyer W. Polymer Nanocomposites: A Small Part of the Story. JOM. 2007;59(3):53-60.

[3] Chen VC. Analysis of Radar Micro-Doppler with Time-Frequency Transform. Statistical Signal and Array Processing. Proceedings of the Tenth IEEE Workshop: IEEE; 2000. p. 463-6.

[4] Aiken EW, Ormiston RA, Young LA. Future Directions in Rotorcraft Technology at Ames Research Center. 56th American Helicopter Society Annual Forum. Virginia Beach, VA, 2000. p. 1-22.

[5] Finegan IC, Gibson RF. Recent Research on Enhancement of Damping in Polymer Composites. Composite Structures. 1999;44(2):89-98.

[6] Gangopadhyay R, De A. Conducting Polymer Nanocomposites: A Brief Overview. Chemistry of Materials. 2000;12(3):608-22.

[7] Harris P. Carbon Nanotube Composites. International Materials Reviews. 2004;49(1):31-43.

[8] Schmitt C, Lebienvenu M. Electrostatic Painting of Conductive Composite Materials. Journal of Materials Processing Technology. 2003;134(3):303-9.

[9] Chen C, Lakes R. Analysis of High-Loss Viscoelastic Composites. Journal of Materials Science. 1993;28(16):4299-304.

[10] Gong Z, Gong J, Yan X, Gao S, Wang B. Investigation of the Effects of Temperature and Strain on the Damping Properties of Polycarbonate/Multiwalled Carbon Nanotube Composites. The Journal of Physical Chemistry C. 2011;115(38):18468-72.

[11] Tserpes KI, Papanikos P. Finite Element Modeling of Single-Walled Carbon Nanotubes. Composites Part B: Engineering. 2005;36(5):468-77.

[12] Lau K-T, Chipara M, Ling H-Y, Hui D. On the Effective Elastic Moduli of Carbon Nanotubes for Nanocomposite Structures. Composites Part B: Engineering. 2004;35(2):95-101.

[13] Naraghi M, Chawla S. Carbonized Micro-and Nanostructures: Can Downsizing Really Help? Materials. 2014;7(5):3820-33.

[14] Moisala A, Li Q, Kinloch I, Windle A. Thermal and Electrical Conductivity of Single-and Multi-Walled Carbon Nanotube-Epoxy Composites. Composites Science and Technology. 2006;66(10):1285-8.

[15] Han Z, Fina A. Thermal Conductivity of Carbon Nanotubes and Their Polymer Nanocomposites: A Review. Progress in Polymer Science. 2011;36(7):914-44.

[16] Mahanta NK, Abramson AR, Lake ML, Burton DJ, Chang JC, Mayer HK, et al. Thermal Conductivity of Carbon Nanofiber Mats. Carbon. 2010;48(15):4457-65.

[17] Fujii M, Zhang X, Xie H, Ago H, Takahashi K, Ikuta T, et al. Measuring the Thermal Conductivity of a Single Carbon Nanotube. Physical Review Letters. 2005;95(6):1-4.

[18] Patton R, Pittman Jr C, Wang L, Hill J. Vapor Grown Carbon Fiber Composites with Epoxy and Poly (Phenylene Sulfide) Matrices. Composites Part A: Applied Science and Manufacturing. 1999;30(9):1081-91.

[19] Every A, Tzou Y, Hasselman D, Raj R. The Effect of Particle Size on the Thermal Conductivity of Zns/Diamond Composites. Acta Metallurgica et Materialia. 1992;40(1):123-9.

[20] Desai A, Haque M. Mechanics of the Interface for Carbon Nanotube–Polymer Composites. Thin-walled Structures. 2005;43(11):1787-803.

[21] Suhr J, Koratkar NA. Energy Dissipation in Carbon Nanotube Composites: A Review. Journal of Materials Science. 2008;43(13):4370-82.

[22] Ogasawara T, Tsuda T, Takeda N. Stress–Strain Behavior of Multi-Walled Carbon Nanotube/Peek Composites. Composites Science and Technology. 2011;71(2):73-8.

[23] Cox H. The Elasticity and Strength of Paper and Other Fibrous Materials. British Journal of Applied Physics. 1952;3(3):72.

[24] Ang KK, Ahmed KS. An Improved Shear-Lag Model for Carbon Nanotube Reinforced Polymer Composites. Composites Part B: Engineering. 2013;50:7-14.

[25] Esteva M, Spanos P. Effective Elastic Properties of Nanotube Reinforced Composites with Slightly Weakened Interfaces. Journal of Mechanics of Materials and Structures. 2009;4(5):887-900.

[26] Cimellaro GP. Simultaneous Stiffness–Damping Optimization of Structures with Respect to Acceleration, Displacement and Base Shear. Engineering Structures. 2007;29(11):2853-70.

[27] Onoda J, Endot T, Tamaoki H, Watanabe N. Vibration Suppression by Variable-Stiffness Members. AIAA Journal. 1991;29(6):977-83.

[28] Smith KE, Maly JR, Johnson CD. Smart Tuned Mass Dampers. Active Materials and Adaptive Structures: Proceedings of the ADPA/AIAA/ASME/SPIE Conference, 1991.

[29] Sierakowski RL, Telitchev IY, Zhupanska OI. On the Impact Response of Electrified Carbon Fiber Polymer Matrix Composites: Effects of Electric Current Intensity and Duration. Composites Science and Technology. 2008;68(3):639-49.

[30] Barakati A, Zhupanska O. Thermal and Mechanical Response of a Carbon Fiber Reinforced Composite to a Transverse Impact and in-Plane Pulsed Electromagnetic Loads. Journal of Engineering Materials and Technology. 2012;134(3):031004.

[31] Balandin AA. Thermal Properties of Graphene and Nanostructured Carbon Materials. Nature Materials. 2011;10(8):569-81.

[32] Hu M, Keblinski P, Schelling PK. Kapitza Conductance of Silicon–Amorphous Polyethylene Interfaces by Molecular Dynamics Simulations. Physical Review B. 2009;79(10):1-7.

[33] Roy AK, Farmer BL, Varshney V, Sihn S, Lee J, Ganguli S. Importance of Interfaces in Governing Thermal Transport in Composite Materials: Modeling and Experimental Perspectives. ACS Applied Materials & Interfaces. 2012;4(2):545-63.

[34] Shenogin S, Xue L, Ozisik R, Keblinski P, Cahill DG. Role of Thermal Boundary Resistance on the Heat Flow in Carbon-Nanotube Composites. Journal of Applied Physics. 2004;95(12):8136-44.

[35] Gardea F, Naraghi M, Lagoudas D. Effect of Thermal Interface on Heat Flow in Carbon Nanofiber Composites. ACS Applied Materials & Interfaces. 2013;6(2):1061-72.

[36] Chandra R, Singh S, Gupta K. Damping Studies in Fiber-Reinforced Composites–a Review. Composite Structures. 1999;46(1):41-51.

[37] Liew K, He X, Wong C. On the Study of Elastic and Plastic Properties of Multi-Walled Carbon Nanotubes under Axial Tension Using Molecular Dynamics Simulation. Acta Materialia. 2004;52(9):2521-7.

[38] Rao A, Jorio A, Pimenta M, Dantas M, Saito R, Dresselhaus G, et al. Polarized Raman Study of Aligned Multiwalled Carbon Nanotubes. Physical Review Letters. 2000;84(8):1820.

[39] Brown S, Jorio A, Dresselhaus M, Dresselhaus G. Observations of the D-Band Feature in the Raman Spectra of Carbon Nanotubes. Physical Review B. 2001;64(7):073403.

[40] Coleman JN, Khan U, Blau WJ, Gun'ko YK. Small but Strong: A Review of the Mechanical Properties of Carbon Nanotube–Polymer Composites. Carbon. 2006;44(9):1624-52.

[41] Hwang S, Gibson R. Micromechanical Modeling of Damping in Discontinuous Fiber Composites Using a Strain Energy/Finite Element Approach. Journal of Engineering Materials and Technology. 1987;109(1):47-52.

[42] Li C, Chou T-W. Multiscale Modeling of Carbon Nanotube Reinforced Polymer Composites. Journal of Nanoscience and Nanotechnology. 2003;3(5):423-30.

[43] Gao X-L, Li K. A Shear-Lag Model for Carbon Nanotube-Reinforced Polymer Composites. International Journal of Solids and Structures. 2005;42(5):1649-67.

[44] Gibson R, Chaturvedi S, Sun C. Complex Moduli of Aligned Discontinuous Fibre-Reinforced Polymer Composites. Journal of Materials Science. 1982;17(12):3499-509.

[45] Suarez S, Gibson R, Sun C, Chaturvedi S. The Influence of Fiber Length and Fiber Orientation on Damping and Stiffness of Polymer Composite Materials. Experimental Mechanics. 1986;26(2):175-84.

[46] Suhr J, Koratkar N, Keblinski P, Ajayan P. Viscoelasticity in Carbon Nanotube Composites. Nature Materials. 2005;4(2):134-7.

[47] Schadler L, Giannaris S, Ajayan P. Load Transfer in Carbon Nanotube Epoxy Composites. Applied Physics Letters. 1998;73(26):3842-4.

[48] Liao K, Li S. Interfacial Characteristics of a Carbon Nanotube–Polystyrene Composite System. Applied Physics Letters. 2001;79(25):4225-7.

[49] Wong M, Paramsothy M, Xu X, Ren Y, Li S, Liao K. Physical Interactions at Carbon Nanotube-Polymer Interface. Polymer. 2003;44(25):7757-64.

[50] Parsegian VA. Van Der Waals Forces: A Handbook for Biologists, Chemists, Engineers, and Physicists. Physical Review Letters. 2013;82(26):5397.

[51] Holmes LA, Kusamizu S, Osaki K, Ferry JD. Dynamic Mechanical Properties of Moderately Concentrated Polystyrene Solutions. Journal of Polymer Science Part A-2: Polymer Physics. 1971;9(11):2009-21.

[52] Du F, Scogna RC, Zhou W, Brand S, Fischer JE, Winey KI. Nanotube Networks in Polymer Nanocomposites: Rheology and Electrical Conductivity. Macromolecules. 2004;37(24):9048-55.

[53] Hadjiev V, Arepalli S, Nikolaev P, Jandl S, Yowell L. Enhanced Raman Microprobe Imaging of Single-Wall Carbon Nanotubes. Nanotechnology. 2004;15(5):562.

[54] Zhao Q, Wagner HD. Raman Spectroscopy of Carbon–Nanotube–Based Composites. Philosophical Transactions of the Royal Society of London Series A: Mathematical, Physical and Engineering Sciences. 2004;362(1824):2407-24.

[55] Wetton R, Marsh R, Van-De-Velde J. Theory and Application of Dynamic Mechanical Thermal Analysis. Thermochimica Acta. 1991;175(1):1-11.

[56] May R. Polyetheretherketones. Encyclopedia Of Polymer Science and Technology. 1988.

[57] Kong Y, Hay J. The Measurement of the Crystallinity of Polymers by Dsc. Polymer. 2002;43(14):3873-8.

[58] Bassett D, Olley R, Al Raheil I. On Crystallization Phenomena in Peek. Polymer. 1988;29(10):1745-54.

[59] Verma R, Marand H, Hsiao B. Morphological Changes During Secondary Crystallization and Subsequent Melting in Poly (Ether Ether Ketone) as Studied by Real Time Small Angle X-Ray Scattering. Macromolecules. 1996;29(24):7767-75.

[60] Lattimer M, Hobbs J, Hill M, Barham P. On the Origin of the Multiple Endotherms in Peek. Polymer. 1992;33(18):3971-3.

[61] Grady BP. Effects of Carbon Nanotubes on Polymer Physics. Journal of Polymer Science Part B: Polymer Physics. 2012;50(9):591-623.

[62] Díez-Pascual AM, Naffakh M, Gómez MA, Marco C, Ellis G, Martínez MT, et al. Development and Characterization of Peek/Carbon Nanotube Composites. Carbon. 2009;47(13):3079-90.

[63] Díez-Pascual AM, Naffakh M, Marco C, Ellis G, Gómez-Fatou MA. High-Performance Nanocomposites Based on Polyetherketones. Progress in Materials Science. 2012;57(7):1106-90.

[64] Sung Y, Kum C, Lee H, Byon N, Yoon H, Kim W. Dynamic Mechanical and Morphological Properties of Polycarbonate/Multi-Walled Carbon Nanotube Composites. Polymer. 2005;46(15):5656-61.

[65] Tsagaropoulos G, Eisenberg A. Dynamic Mechanical Study of the Factors Affecting the Two Glass Transition Behavior of Filled Polymers. Similarities and Differences with Random Ionomers. Macromolecules. 1995;28(18):6067-77.

[66] Eitan A, Fisher F, Andrews R, Brinson L, Schadler L. Reinforcement Mechanisms in Mwcnt-Filled Polycarbonate. Composites Science and Technology. 2006;66(9):1162-73.

[67] Díez-Pascual AM, Martínez G, Martínez MT, Gómez MA. Novel Nanocomposites Reinforced with Hydroxylated Poly (Ether Ether Ketone)-Grafted Carbon Nanotubes. Journal of Materials Chemistry. 2010;20(38):8247-56.

[68] Ma P-C, Mo S-Y, Tang B-Z, Kim J-K. Dispersion, Interfacial Interaction and Re-Agglomeration of Functionalized Carbon Nanotubes in Epoxy Composites. Carbon. 2010;48(6):1824-34.

[69] Wei C. Adhesion and Reinforcement in Carbon Nanotube Polymer Composite. Applied Physics Letters. 2006;88(9):093108.

[70] Liu C, Qin H, Mather P. Review of Progress in Shape-Memory Polymers. Journal of Materials Chemistry. 2007;17(16):1543-58.

[71] Hashin Z. Complex Moduli of Viscoelastic Composites—I. General Theory and Application to Particulate Composites. International Journal of Solids and Structures. 1970;6(5):539-52.

[72] Hong W-T, Tai N-H. Investigations on the Thermal Conductivity of Composites Reinforced with Carbon Nanotubes. Diamond and Related Materials. 2008;17(7):1577-81.

[73] Hong J, Lee J, Hong CK, Shim SE. Effect of Dispersion State of Carbon Nanotube on the Thermal Conductivity of Poly (Dimethyl Siloxane) Composites. Current Applied Physics. 2010;10(1):359-63.

[74] Sui G, Jana S, Zhong W, Fuqua M, Ulven C. Dielectric Properties and Conductivity of Carbon Nanofiber/Semi-Crystalline Polymer Composites. Acta Materialia. 2008;56(10):2381-8.

[75] Cui Y, Liu C, Hu S, Yu X. The Experimental Exploration of Carbon Nanofiber and Carbon Nanotube Additives on Thermal Behavior of Phase Change Materials. Solar Energy Materials and Solar Cells. 2011;95(4):1208-12.

[76] Zhang X, Fujiwara S, Fujii M. Measurements of Thermal Conductivity and Electrical Conductivity of a Single Carbon Fiber. International Journal of Thermophysics. 2000;21(4):965-80.

[77] Macedo F, Ferreira J. Thermal Contact Resistance Evaluation in Polymer-Based Carbon Fiber Composites. Review of Scientific Instruments. 2003;74(1):828-30.

[78] Gojny FH, Wichmann MH, Fiedler B, Kinloch IA, Bauhofer W, Windle AH, et al. Evaluation and Identification of Electrical and Thermal Conduction Mechanisms in Carbon Nanotube/Epoxy Composites. Polymer. 2006;47(6):2036-45.

[79] Yang S, Lozano K, Lomeli A, Foltz HD, Jones R. Electromagnetic Interference Shielding Effectiveness of Carbon Nanofiber/Lcp Composites. Composites Part A: Applied Science and Manufacturing. 2005;36(5):691-7.

[80] Cahill DG, Ford WK, Goodson KE, Mahan GD, Majumdar A, Maris HJ, et al. Nanoscale Thermal Transport. Journal of Applied Physics. 2003;93(2):793-818.

[81] Seidel GD, Lagoudas DC. A Micromechanics Model for the Thermal Conductivity of Nanotube-Polymer Nanocomposites. Journal of Applied Mechanics. 2008;75(4):1-9.

[82] Gardea F, Lagoudas DC. Characterization of Electrical and Thermal Properties of Carbon Nanotube/Epoxy Composites. Composites Part B: Engineering. 2013.

[83] Nan C-W, Birringer R, Clarke DR, Gleiter H. Effective Thermal Conductivity of Particulate Composites with Interfacial Thermal Resistance. Journal of Applied Physics. 1997;81(10):6692-9.

[84] Song YS, Youn JR. Evaluation of Effective Thermal Conductivity for Carbon Nanotube/Polymer Composites Using Control Volume Finite Element Method. Carbon. 2006;44(4):710-7.

[85] Hasselman D, Johnson LF. Effective Thermal Conductivity of Composites with Interfacial Thermal Barrier Resistance. Journal of Composite Materials. 1987;21(6):508-15.

[86] Hatta H, Taya M. Thermal Conductivity of Coated Filler Composites. Journal of Applied Physics. 1986;59(6):1851-60.

[87] Hmina N, Scudeller Y. Thermal Interface Resistance and Subsurface Effusivity of Submicron Metallic Films on Dielectric Substrates: An Experimental Method for Simultaneous Determination. International Journal of Heat and Mass Transfer. 1998;41(18):2781-98.

[88] Log T, Gustafsson S. Transient Plane Source (Tps) Technique for Measuring Thermal Transport Properties of Building Materials. Fire and Materials. 1995;19(1):43-9.

[89] Seidel GD, Lagoudas DC. A Micromechanics Model for the Thermal Conductivity of Nanotube-Polymer Nanocomposites. J Appl Mech. 2008;75(4):041025.

[90] Seidel GD, Lagoudas DC. A Micromechanics Model for the Electrical Conductivity of Nanotube-Polymer Nanocomposites. Journal of Composite Materials. 2009;43(9):917-41.

[91] Hashin Z. Thermoelastic Properties and Conductivity of Carbon/Carbon Fiber Composites. Mechanics of Materials. 1990;8(4):293-308.

[92] Lukes JR, Zhong H. Thermal Conductivity of Individual Single-Wall Carbon Nanotubes. Journal of Heat Transfer. 2007;129(6):705-16.

[93] Hone J, Whitney M, Piskoti C, Zettl A. Thermal Conductivity of Single-Walled Carbon Nanotubes. Physical Review B. 1999;59(4):R2514.

[94] Che J, Cagin T, Goddard Iii WA. Thermal Conductivity of Carbon Nanotubes. Nanotechnology. 2000;11(2):65.

[95] Swartz ET, Pohl RO. Thermal-Boundary Resistance. Reviews of Modern Physics. 1989;61(3):605-68.